

UCLA

UCLA Electronic Theses and Dissertations

Title

Understanding the Kinetics, Stereoselectivity, and Catalysis of Pericyclic Reactions in Chemistry and Biology through Quantum Mechanical Computations

Permalink

<https://escholarship.org/uc/item/06r48353>

Author

Patel, Ashay

Publication Date

2015

Peer reviewed|Thesis/dissertation

UNIVERSITY OF CALIFORNIA

Los Angeles

**Understanding the Kinetics, Stereoselectivity, and Catalysis of Pericyclic Reactions in
Chemistry and Biology through Quantum Mechanical Computations**

A dissertation submitted in partial satisfaction of the requirements for the degree Doctor of
Philosophy in Chemistry

by

Ashay Patel

2015

ABSTRACT OF THE DISSERTATION

Understanding the Kinetics, Selectivity, and Catalysis of Pericyclic Reactions in Chemistry and
Biology through Quantum Mechanical Computations

by

Ashay Patel

Doctor of Chemistry

University of California, Los Angeles, 2015

Professor Kendall N. Houk, Chair

Pericyclic reactions are an important class of chemical reaction because they occur stereospecifically often with a high degree of regio-, stereoselectivity, and atom economy. This dissertation summarizes our efforts – using chemical computations – to better understand how these reactions occur in both biological and abiological settings.

This dissertation is divided into two portions; the first of which describes quantum mechanical studies of biosynthetic and enzyme-catalyzed cycloadditions. Chapter 1, 2, and 3 detail studies of these enzymatic processes. Using state-of-the-art density functional theory, we have determined whether these reactions are feasible biosynthetic transformations, elucidated the

mechanistic subtleties of these reactions, and proposed how enzymes may catalyze such transformations.

Chapter 1 describes a computational study of a strained biosynthetic transannular 1,3-dipolar cycloaddition. Computations reveal that substrate preorganization overrides distortion in the transitions, resulting in a reaction is feasible. Efforts to account for the influence of water – through solvent-solute hydrogen-bonding interactions – were modeled using “microsolventated” reactant and transition states: We conclude that the reaction remains feasible in aqueous media. Strategic hydrogen bonding, according to theory, can accelerate the reaction by 2000-fold.

Chapter 2 summarizes a computational investigation of the Diels-Alder reaction involved in the biosynthesis of spinosyn A. We find that the mechanism of this transannular cycloaddition is “ambimodal”, proceeding through a “bis-pericyclic” transition structure that leads directly two products, the observed Diels-Alder adduct and an unstable [6+4] adduct. This [6+4] adduct can readily and irreversibly rearrange into the Diels-Alder adduct via a Cope rearrangement. Simulations of the reaction mechanism determine that the nonenzymatic cycloaddition occurs predominantly via a mechanism that involves the intermediacy of the [6+4] adduct.

Chapter 3 discusses an ongoing collaboration with the Tang laboratory at UCLA and involves an effort to understand the intramolecular Diels-Alder reaction involved in the biosynthesis of cholesterol-reducing agent, lovastatin. We have modeled the reaction of a related cycloaddition performed experimentally, and computations recapitulate the selectivity observed experimentally for this nonenzymatic process. The stereochemical outcome of the enzymatic reaction diverges from the outcome of its synthetic analogue. Computation of the reactive conformer of the model substrate suggests that substrate preorganization could accelerate the intramolecular Diels-Alder reaction by approximately a 1000-fold.

Theoretical studies of stereoselective electrocyclic reactions are described in Chapters 4, 5, 6, 7, and 8. These reactions have been examined by experimentally by chemists in the laboratory and, subsequently, have been modeled using quantum mechanical computations. From this computational work, we have determined the stereoselectivity of several synthetically relevant electrocyclic reactions, the effect of substituents on the reactivity of the electrocyclization precursors.

In Chapter 4, we summarize our work with Dr. Gregg Barcan and Prof. Ohyun Kwon to elucidate the origins of 1,6-stereoiduction of a triene electrocyclization employed in their total synthesis of reserpine. We determine that conformational transmission of the stereochemical information found at a distal stereocenter is “transmitted” to the forming stereogenic center via $A^{1,3}$ strain. Allylic strain destabilizes the disfavored mode of ring closure. According to both theory and experiment, stereoselectivity is shown to be sensitive to the size of the substituent involved in the $A^{1,3}$ strain.

Chapter 5 outlines a computational investigation of the 8π - 6π electrocyclization cascades of substituted tetraenes, such species are common intermediates in the biosyntheses of many natural products containing bicyclo[4.2.0]-octadiene ring systems. These cascades reaction occur spontaneously in a growing number of natural products. Here we determined the influence terminal substitution on the reactivities, thermodynamics, and stereoselectivities of these reactions. Terminal substituents destabilize the tetraene precursor and the resulting 8π electrocyclization product. Strain relief drives and promotes the subsequent 6π electrocyclization. Where possible, the diastereoselectivity of this cascade is controlled by a steric effect that destabilizes the *endo* mode of electrocyclic ring closure.

Chapter 6 reviews a density functional theory study of a series of torquoselective triene and Nazarov electrocyclizations of bridged bicyclic substrates. We find that the torquoselectivities of highly *exo* selective ring closures are controlled by action of torsional effect that acts in concert with either steric attraction or repulsion. In one case, a Nazarov cyclization, a through space orbital interaction overrides this *exo* selectivity.

Chapter 7 defines a new stereochemical model that rationalizes 1,2-stereoduction observed for a series of electrocyclizations of chiral 1-azatrienes. This model is likely general, in nature, and applies to many other kinds of pericyclic reactions. It invokes stereoelectronic effects the principle stereodeterminants of the *aza*-electrocyclizations. Theory predicts that modification of the substrate (i.e., the replacement of the allylic substituent with a silyl group) reverses the stereochemical outcome of the ring closures. Experiments have verified this prediction.

Chapter 8 describes a continuation to the work discussed in the preceding chapter; the scope of the electrocyclic reactions of α silyl-substituted 1-aza-1E,3Z,5E-trienes was explored. The predicted reversal of stereoselectivity is general. Competing isomerization of a number of substrates via formal [1,7] rearrangement was observed experimentally. Computational work examined several pathways by which isomerization could occur. These results enabled the “educated” proposal of a reaction mechanism.

The dissertation of Ashay Patel is approved.

Jorge Barrio

Yi Tang

Kendall N. Houk, Committee Chair

University of California, Los Angeles

2015

DEDICATION

To friends and family, old and new, near and far.

TABLE OF CONTENTS

ABSTRACT OF THE DISSERTATION	ii
DEDICATION	vii
TABLE OF CONTENTS	viii
ACKNOWLEDGEMENTS	xi
VITA	xvi
CHAPTER 1. Does Nature Click? Theoretical Prediction of an Enzymatic Transannular 1,3-Dipolar Cycloaddition in the Biosynthesis of Lycojaponicumins A and B	1
ABSTRACT	2
INTRODUCTION	3
RESULTS AND DISCUSSION	4
CONCLUSIONS	12
COMPUTATIONAL METHODS	12
AUTHOR CONTRIBUTIONS	14
ACKNOWLEDGMENTS	14
REFERENCES	15
CHAPTER 2. Dynamically complex enzyme-catalyzed [6+4] and [4+2] cycloadditions in the biosynthesis of spinosyn A.	19
ABSTRACT	20
INTRODUCTION	20
RESULTS AND DISCUSSION	23
CONCLUSIONS	30
COMPUTATIONAL METHODS	30
AUTHOR CONTRIBUTIONS	32
ACKNOWLEDGEMENTS	32
REFERENCES	33
CHAPTER 3. Laying Bare the Secrets of Diels-Alder Biocatalysis: A Computational Study of LovB, a Diels-Alderase involved in Lovastatin Biosynthesis	39
ABSTRACT	40
INTRODUCTION	40
RESULTS AND DISCUSSION	41
COMPUTATIONAL METHODS	44
<i>Quantum mechanical computations</i>	44
<i>Conformational Analysis</i>	45
REFERENCES	46
CHAPTER 4. Origins of 1,6-Stereoinduction in Torquoselective 6π Electrocyclizations ...	48
ABSTRACT	49
INTRODUCTION	49
RESULTS AND DISCUSSION	51

<i>Synthesis and Electrocyclization of Trienes</i>	51
<i>Computational Results</i>	55
<i>Origins of Differential Allylic Strain in Electrocyclization Transition States of Trienes 1-6</i>	62
CONCLUSIONS	63
AUTHOR CONTRIBUTIONS	65
ACKNOWLEDGMENTS	65
REFERENCES	66
CHAPTER 5. Terminal Substituent Effects on Reactivity, Thermodynamics, and Stereoselectivity of the 8π-6π Electrocyclization Cascades of 1,3,5,7-Tetraenes	68
ABSTRACT	69
INTRODUCTION	70
RESULTS AND DISCUSSION.....	73
CONCLUSIONS	83
COMPUTATIONAL METHODS	86
AUTHOR CONTRIBUTIONS	87
ACKNOWLEDGMENTS	87
REFERENCES	88
CHAPTER 6. Reactivity and Stereoselectivity of 6π and Nazarov Electrocyclizations of Bridged Bicyclic Trienes and Divinyl Ketones	91
ABSTRACT	92
INTRODUCTION	93
RESULTS AND DISCUSSION.....	95
<i>Reactivities of bridged bicyclic trienes towards 6π electrocyclizations</i>	95
<i>Stereoselectivities of the disrotatory ring closures of bridged bicyclic trienes.</i>	97
<i>Stereoselectivities of the conrotatory ring closures of bridged bicyclic divinyl ketones.</i>	100
CONCLUSIONS	105
COMPUTATIONAL METHODS	105
AUTHOR CONTRIBUTIONS	106
ACKNOWLEDGEMENTS	106
REFERENCES	107
CHAPTER 7. Transition State <i>Gauche</i> Effects Control the Torquoselectivities of the Electrocyclizations of Chiral 1-Azatrienes	112
ABSTRACT	113
INTRODUCTION	114
RESULTS AND DISCUSSION.....	115
CONCLUSIONS	124
COMPUTATIONAL METHODS	125
AUTHOR CONTRIBUTIONS	126
ACKNOWLEDGMENTS.....	126
CHAPTER 8. Highly Torquoselective Electrocyclizations and Competing 1,7-Hydrogen Shifts of 1-Azatrienes with Silyl-Substitution at the Allylic Carbon	131
ABSTRACT	132
INTRODUCTION	132
RESULTS AND DISCUSSION.....	134
CONCLUSIONS	140
COMPUTATIONAL METHODS	141
<i>QM computations</i>	ve 141

<i>Conformational analysis</i>	142
AUTHOR CONTRIBUTIONS	143
ACKNOWLEDGMENTS	143
REFERENCES	144

ACKNOWLEDGEMENTS

First and foremost, I would like to acknowledge my doctoral advisor, Kendall N. Houk, for his patience, wisdom, and judgment. It is only through his mentorship that the work described herein was possible. My years working with him have been the most rewarding fun years of my life. It will be undeniably difficult leaving the auspices of Ken's laboratory: I find it difficult to imagine how the five years to follow could in any way match the five that have preceded them.

It is often said that periods of great suffering can bring people together in ways that rarely in occurs times of happiness. While I can lay little claim to having suffered to any extent during graduate school, I will always recall fondly my interactions with members of my graduate student cohort, especially those involving students who joined Ken's group alongside me. Special mention must be made of Steven Lopez, whose transformation as student, growth as a scientist, and capacity to "grunt and groan" remain breathtaking. His impact on me is undeniable.

Others in the lab must be mentioned not only for their friendship, but their contributions to my development. Of note in my early development is Ryan Pemberton. It was with him that I first learned how to perform the computations reported herein.

Next on the list to embarrass is none other than Dr. Colin Lam. From him I inherited a number of neuroses, including a tendency to overuse the all variations of the word "feature" in my writing. Things could be worse, as I have yet to catch his penchant for drawing "jaundiced" ring conformers. In all seriousness, from Colin I have learned much about how to be rigorous, to be clear, and to frame a scientific story in a compelling manner. And it was as Dr. Lam's teaching assistant for the second quarter of sophomore organic chemistry that I actually "(re-) learnt" the subject. I will always remember what he said about me, especially considering that it runs contrary to my history.

I recall my time with the Germans, Dr. Martin Breugst and Dr. Arne Dieckmann, fondly. Perhaps weren't the "gentlest" scientists, but they were undeniable examples of serious and capable chemists. Martin's obsession with all things typographical, while exhausting in the moment, is much appreciated, especially in hindsight. His example of practicing presentations was not lost on me. Much of the credit in my development as public speaker belongs to him. Arne's directness and insistence that we understand the tools we use to perform computations and keep aware of new developments incited a small, but peaceful rebellion against the established B3LYP/6-31G(d) modality within our group. Arne and Martin, together, challenged many of us to determine not only how to solve a problem, but identify the optimal approach. I will strive to remain a steward of that cause.

I would be remiss if I did not acknowledge a few others. There are the younger students, including Tiffany, Jessie, Brian, Jason, Janice, and Adam. I have probably learned more from them than I could have ever guessed. To those who I have mentored, Cyndi and Peiyuan: I have learned a great deal about the art of mentorship, including the fact that I still have much to learn. Learning about your chemistry was often more rewarding, then exploring my own, a welcome distraction, especially when my research was not working out well. "Teaching" you was my most profound learning experience. And I hope that you have benefited from the experience, as I know I have. I must also acknowledge a few postdoctoral fellows in the group, Buck Taylor, Mareike Holland, and Matt Grayson. They have provided both sound scientific criticism and advice when needed (and sometimes unsolicited) as well as the gift of friendship. They have helped me realized that even "on my way out" I still have a lot to learn about "what I know".

I would like to thank all those involved in our efforts to improve diversity and inclusion in the STEM fields, both at UCLA through the Organization for Cultural Diversity in the

Sciences (OCDS) and nationally through the Alliance for Diversity in Science and Engineering (ADSE), in particular the officers and/or board members of both organizations. The work we have done in service of OCDS and ADSE has served as a reinvigorating tonic of sorts for a sometimes research-weary soul.

I must express my deepest thanks to my parents. These words as well as those to follow could hardly have been written without their love for each other and for me. Their support even when they have not understood my goals and aspirations has always been tremendous. I hope I can one day return the favor. I am equally grateful to my brother. I fear that he has been a better brother to me than I to him; he has challenged me in many ways, often maddeningly, to strive for improvement.

Chapter 1 is a modified version of the publication, “Does Nature Click? Theoretical Prediction of an Enzyme-Catalyzed Transannular 1,3-Dipolar Cycloaddition in the Biosynthesis of Lycojaponicumins A and B”. (Krenske, E. H.; Patel, A.; Houk, K. N. *J. Am. Chem. Soc.*, **2013**, *135*, 17638–17642.) Dr. Elizabeth H. Krenske and I performed the work described in Chapter 1.

Chapter 4 is a modified version of the publication, “Origins of 1,6-Stereinduction in Torquoselective 6π Electrocyclizations”. (Patel, A.; Barcan, G. A.; Kwon, O.; Houk, K. N. *J. Am. Chem. Soc.*, **2013**, *135*, 4878–4883.) Dr. Gregg Barcan performed the experimental work described in the chapter under the Prof. Ohyun Kwon’s supervision. Both Dr. Barcan and I contributed equally to this work.

Chapter 5 is a modified version of the publication, “Terminal Substituent Effects on the Reactivity, Thermodynamics, and Diastereoselectivity of the 8π - 6π Electrocyclization Cascades of 1,3,5,7-Tetraenes”. (Patel, A.; Houk, K. N. *J. Org. Chem.*, **2014**, *79*, 11370-11377.)

Chapter 6 is a modified version of the publication, “Reactivity and Stereoselectivity of 6π and Nazarov Electrocyclizations of Bridged Bicyclic Trienes and Divinylketones.” (Patel, A.; West, F. G.; Houk, K. N. *J. Org. Chem.*, **2015**, *80*, 2790-2795.)

Chapter 7 is a modified version of a submitted manuscript entitled “A Transition State Gauche Effect Controls the Torquoselectivities of the Ring Closures of Chiral 1-Azatrienes”. (Patel, A.; Vella, J. P.; Hsung, R. P.; Houk, K. N. under revision; *J. Org. Chem.*) Joseph R. Vella and I performed the computational work reported in Chapter 7.

Chapter 8 is a modified version of the publication “Highly Torquoselective Electrocyclizations and Competing 1,7-Hydrogen Shifts of 1-Azatrienes with Silyl-Substitution at the Allylic Carbon”. (Ma, Z-X.;* Patel, A.;* Houk, K. N.; and Hsung, R. P.. *Org. Lett*, **2015**, 17, 2138-2141.) Dr. Zhi-Xiong Ma performed the experimental work reported in this chapter under the supervision of Prof. Richard P. Hsung. Both Dr. Ma and I contributed equally to this work.

VITA

Education

University of California, Los Angeles

2010–present

Ph.D. Department of Chemistry. Thesis: Understanding Pericyclic Reactions in Chemistry and Biology Through Quantum Mechanical Computations

Rutgers University

2004–2008

B.A. Chemistry, Summa Cum Laude.

Publications

Published or submitted manuscripts

1. Barcan, G. A.; Patel, A.; Houk, K. N.; Kwon, O. *Org. Lett.*, **2012**, *14*, 5388–5381.
2. Patel, A.;* Barcan, G. A.;* Kwon, O.; Houk, K. N. *J. Am. Chem. Soc.*, **2013**, *135*, 4878–4883.
3. Souris, C.; Frébault, F.; Patel, A.; Audisio, D.; Houk, K. N.; Maulide, N. *Org. Lett.*, **2013**, *15*, 3242–3245.
4. Krenske, E. H.; Patel, A.; Houk, K. N. *J. Am. Chem. Soc.*, **2013**, *135*, 17638–17642.
5. Hu, Y.; Dietrich, D.; Xu, W.; Patel, A.; Thuss, J. A. J.; Wang, J.; Yin, W. B.; Qiao, K.; Houk, K. N. Houk; Vederas, J. C; Tang, Y. *Nat. Chem. Biol.*, **2014**, *10*, 552–554.
6. Patel, A.; Houk, K. N. *J. Org. Chem.*, **2014**, *79*, 11370–11377
7. Patel, A.; West, F. G; Houk, K. N. *J. Org. Chem.*, **2015**, *80*, 2790–2795.
8. Ma, Z-X.;* Patel, A.;* Houk, K. N.; and Hsung, R. P. *Org. Lett.*, **2015**, *17*, 2138–2141.
9. Phillips, E. M.; Mesganaw, T.; Patel, A.; Duttwyler, S.; Mercado, B. Q.; Houk, K. N.; and Ellman, J. A. *Angew. Chem. Int. Ed.*, **2015**, *54*, 12044–12048.
10. Sato, M.; Yagishita, F.; Mino, T.; Uchiyam, N.; Goda, Y.; Noguchi, H.; Patel, A.; Houk, K. N.; Tang, Y.; Hotta, K.; Watanabe, K. *ChemBioChem*, **2015**, *16*, 2294–2298.
11. Yu, P.; Patel, A.; Houk, K. N. *J. Am. Chem. Soc.*, **2015**, *137*, 13518–13523.
12. Patel, A.; Vella, J.; Hsung, R. P.; Houk, K. N. *J. Org. Chem*, **2015**, doi: 10.1021/acs.joc.5b02085
13. He, C.; Chen, T.; Patel, A.; Houk, K. N. *J. Org. Chem.*, **2015**, 10.1021/acs.joc.5b02288

Manuscripts in preparation

1. Chen, Z.;* Patel, A.;* Liu, H. W.; Singleton, D. A.; Houk, K. N. Dynamically Complex Enzyme-Catalyzed [6+4] and [4+2] Cycloadditions in the Biosynthesis of Spinosyn A (submitted; *Nat. Chem.*)

- Lin, H-C.; McMahon, T. C.; Patel, A.; Xu, W.; Corsello, M.; Houk, K. N.; Garg, N. K.; and Tang, Y. A Heterodimeric Indole-Coupling P450 Monooxygenase in Alkaloid Natural Product Biosynthesis (submitted; *J. Am. Chem. Soc.*)
- Patel, A.; Dieckmann, A.; Lebold, T.; Gagello, G.; Viart, H.; Sarpong, R.; Houk, K. N. Thermal and Acid-Promoted Asymmetric Pictet-Spengler Reactions: Computational and Experimental Exploration of Mechanisms and Stereoselectivities.
- Chen, T. Q.;* Yu, P.::* Patel, A.; He, Y.-h., Lam, Y.-h.; Houk, K. N. Double [6+4] Cycloadditions of Tropone and 6,6-Dimethylfulvene: A Computational Study.
- Taylor, B.L.; Petrova, G. P.; Lee, C. W.; Patel, A.; Stoltz, B.; Morokuma, K.; and Houk, K. N. An Unexpected Divinylcyclopropane Rearrangement: A Computational Mechanistic Study.

Presentations

- Patel, A.; Chen, Z.; Singleton, D.; Houk, K. N. Computational Investigation of the Mechanism of an Enzyme-Catalyzed Transannular Diels-Alder Reaction: Is SpnF Really a [6+4]ase? *Oral presentation*. 245th ACS National Meeting & Exposition. New Orleans, LA. April 7-11, 2013.
- Patel, A.; West, F. G; Houk, K. N. Reactivity and Stereoselectivity of 6π and Nazarov Electrocyclizations of Bridged Bicyclic Trienes and Divinylketones. *Oral presentation*. 247th ACS National Meeting & Exposition. Dallas, TX. March 16-21, 2013
- Patel, A.; Houk, K. N. Terminal Substituent Effects on the Reactivity, Thermodynamics, and Diastereoselectivity of the 8π - 6π Electrocyclization Cascades of 1,3,5,7-Tetraenes. *Oral presentation*. 248th ACS National Meeting & Exposition. San Francisco, CA. August 10-14, 2014.
- Patel, A.; Dieckmann, A.; Lebold, T.; Gagello, G.; Viart, H.; Sarpong, R.; Houk, K. N. How Acid Additives Alter the Mechanistic and Stereochemical course of Asymmetric Pictet-Spengler Reactions. *Oral presentation*. 248th ACS National Meeting & Exposition. San Francisco, CA. August 10-14, 2014.
- Patel, A.; Chen, Z.; Singleton, D.; Houk, K. N. Computational Investigation of the Mechanism of an Enzyme-Catalyzed Transannular Diels-Alder Reaction: Is SpnF Really a [6+4]ase? *Oral presentation*. Molecular Biology Institute Retreat. Los Angeles, CA. January 26, 2014.
- Patel, A.; Chen, Z.; Singleton, D.; Houk, K. N. Computational Investigation of the Mechanism of an Enzyme-Catalyzed Transannular Diels-Alder Reaction: Is SpnF Really a [6+4]ase? *Oral presentation*. Chemistry-Biology Interface Training Program Day. Los Angeles, CA. August, 27, 2014.
- Patel, A.; Houk, K. N. Origins of the Stereoselectivities of the Type II 5+2 Cycloadditions of Oxidopyryliums. *Oral presentation* 250th ACS National Meeting & Exposition. Boston, MA. August 16-20, 2015.

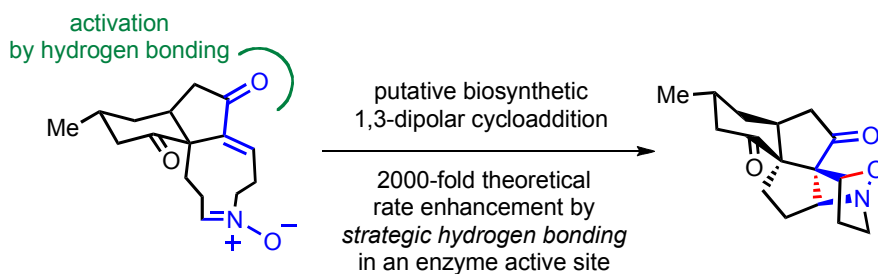
Awards and Fellowships

Chemistry-Biology Interface Training Program Trainee	2011-2014
Dissertation Year Fellowship	2014-2015
Ralph & Charlene Bauer Research Award	2014

Chapter 1

Does Nature Click? Theoretical Prediction of an Enzymatic Transannular 1,3-Dipolar Cycloaddition in the Biosynthesis of Lycojaponicumins A and B

Krenske, E. H.; Patel, A.; Houk, K. N. *J. Am. Chem. Soc.* **2013**, *135*,
17638–17642.



ABSTRACT

Biosynthetic 1,3-dipolar cycloadditions are rare. No enzymes have yet been identified whose function is to catalyze this class of reactions. Recently, however, a 1,3-dipolar cycloaddition was proposed as a key step in the biosynthesis of two *Lycopodium* alkaloids, lycojaponicumins A and B. The lycojaponicumins' fused bicyclic tetrahydroisoxazole ring system was proposed to originate from a transannular 1,3-dipolar cycloaddition between a nitrono and an enone in a nine-membered macrocycle. We have used quantum mechanical calculations to predict whether this cycloaddition could constitute a feasible step in a biosynthetic pathway. Our calculations define a general computational approach for analyzing whether a putative biosynthetic reaction is likely to be enzyme-catalyzed. The quantum mechanically predicted rate of the uncatalyzed reaction in water is compared with the rate enhancement theoretically achievable when the reaction is catalyzed by a theozyme (theoretical enzyme). Density functional theory calculations (M06-2X) predict that the uncatalyzed transannular 1,3-dipolar cycloaddition of the putative lycojaponicumins precursor in water is moderately facile ($\Delta G^\ddagger = 21.5 \text{ kcal mol}^{-1}$, $k = 10^{-3} \text{ s}^{-1}$) and that an enzyme could accelerate the cycloaddition by placing hydrogen bond donors around the enone while maintaining an otherwise non-polar active site. The theoretical enzyme-catalyzed process has $\Delta G^\ddagger \approx 17 \text{ kcal mol}^{-1}$, corresponding to a 2000-fold rate enhancement, and the predicted k_{cat} (2 s^{-1}) is similar to those of known enzymes involved in secondary metabolic

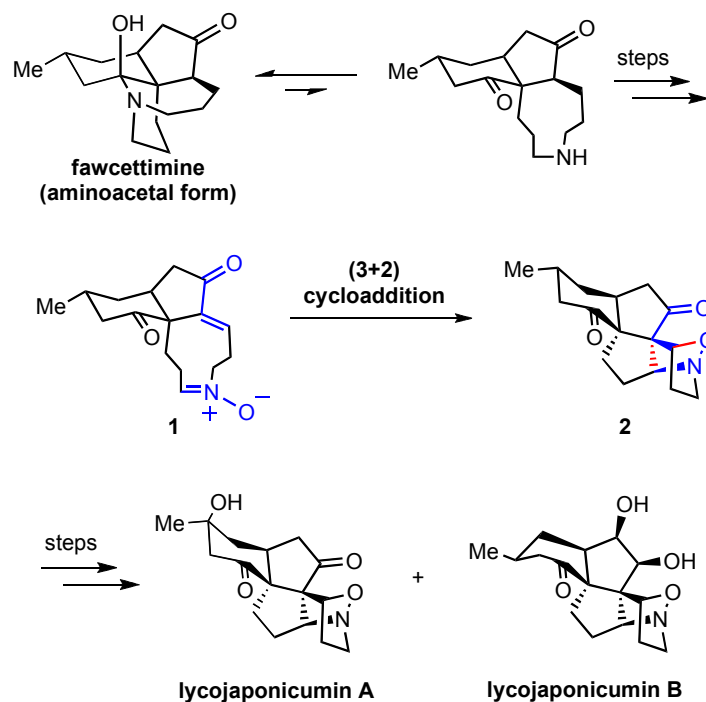
pathways. Thus, theory predicts that the proposed transannular 1,3-dipolar cycloaddition is a plausible step in a biosynthetic pathway leading to the lycojaponicumins and suggests that dipolar cycloadditions can be accelerated by enzyme catalysis.

INTRODUCTION

The 1,3-dipolar cycloaddition is one of the most efficient ways to synthesize heterocycles. Many 1,3-dipolar cycloadditions (including the classic azide–alkyne coupling) have been classified as “click reactions” – clean, high-yielding reactions that assemble products with well-defined stereochemistry from simple precursors in a modular fashion that mimics nature.¹ Considering the utility of click dipolar cycloadditions in organic synthesis, the dearth of 1,3-dipolar cycloadditions in nature is perplexing. Only a handful of natural products have been identified that can be speculatively traced to 1,3-dipolar cycloadditions (involving nitrones,²⁻⁴ oxidopyrylium ions,⁵⁻⁷ or azomethine ylides¹), and little is known about how these reactions might be facilitated in vivo. The scarcity of biological 1,3-dipolar cycloadditions contrasts dramatically with the growing number of known biosynthetic Diels–Alder reactions.⁹⁻¹¹

Recently, Yu and coworkers proposed¹² an intriguing biosynthetic mechanism, featuring a 1,3-dipolar cycloaddition, for the newly-discovered alkaloids, lycojaponicumins A and B (Scheme 1.1). The lycojaponicumins were isolated from the club moss, *Lycopodium japonicum*, and are surmised to derive from fawcettimine. Yu et al. suggested that the unusual bicyclic tetrahydroisoxazole framework of the lycojaponicumins is formed by the transannular nitron–enone 1,3-dipolar cycloaddition **1**→**2**. While the details of the lycojaponicumins biosynthetic pathway still await elucidation, Yu’s proposed mechanism represents an intriguing new lead in the search for the first authentic² 1,3-dipolar cycloaddition-ase. Prompted by the potential significance of such an enzyme’s existence, we have used quantum mechanical calculations to

investigate the feasibility of the proposed biosynthetic 1,3-dipolar cycloaddition of **1**. Our calculations, reported here, represent a general computational approach for analyzing whether a given biosynthetic reaction is likely to require enzymatic catalysis.



Scheme 1.1. Proposed biosynthetic 1,3-dipolar cycloaddition pathway leading to lycojaponicumins A and B, as suggested by Yu and coworkers.¹²

RESULTS AND DISCUSSION

The first stage of our investigation involved prediction of the rate constant for the uncatalyzed transannular 1,3-dipolar cycloaddition **1**→**2**. Computations began with conformational searches of the reactant and transition state at the M06-2X/6-31+G(d,p) level, followed by single-point energy calculations on the important conformers at the M06-2X/def2-TZVPP level. The results of the gas-phase calculations are shown in Figure 1.1. Macrocyclic nitrone **1** was found to have four low-energy conformers (**1a–d**), the most stable of which is **1a**. In three conformers (**1a–c**), the nine-membered ring adopts a tub-like geometry, with the nitrone

moiety poised below the enone C=C bond. These conformers are connected to the cycloaddition transition states **TS1a–c**, respectively. The fourth reactant conformer (**1d**) contains a chair-like nine-membered ring. This conformer is not directly connected to a transition structure, since the nine-membered ring must adopt the tub conformation before the cycloaddition can take place. The chair conformer is 1.1 kcal mol⁻¹ higher in energy than the tub (ΔG). Among the transition states, **TS1a** is lowest in energy in the gas phase, with an activation energy (ΔG^\ddagger) of 21.2 kcal mol⁻¹; **TS1c** is 1 kcal mol⁻¹ higher in energy, and **TS1b** is 3.2 kcal mol⁻¹ higher in energy (than **TS1a**).

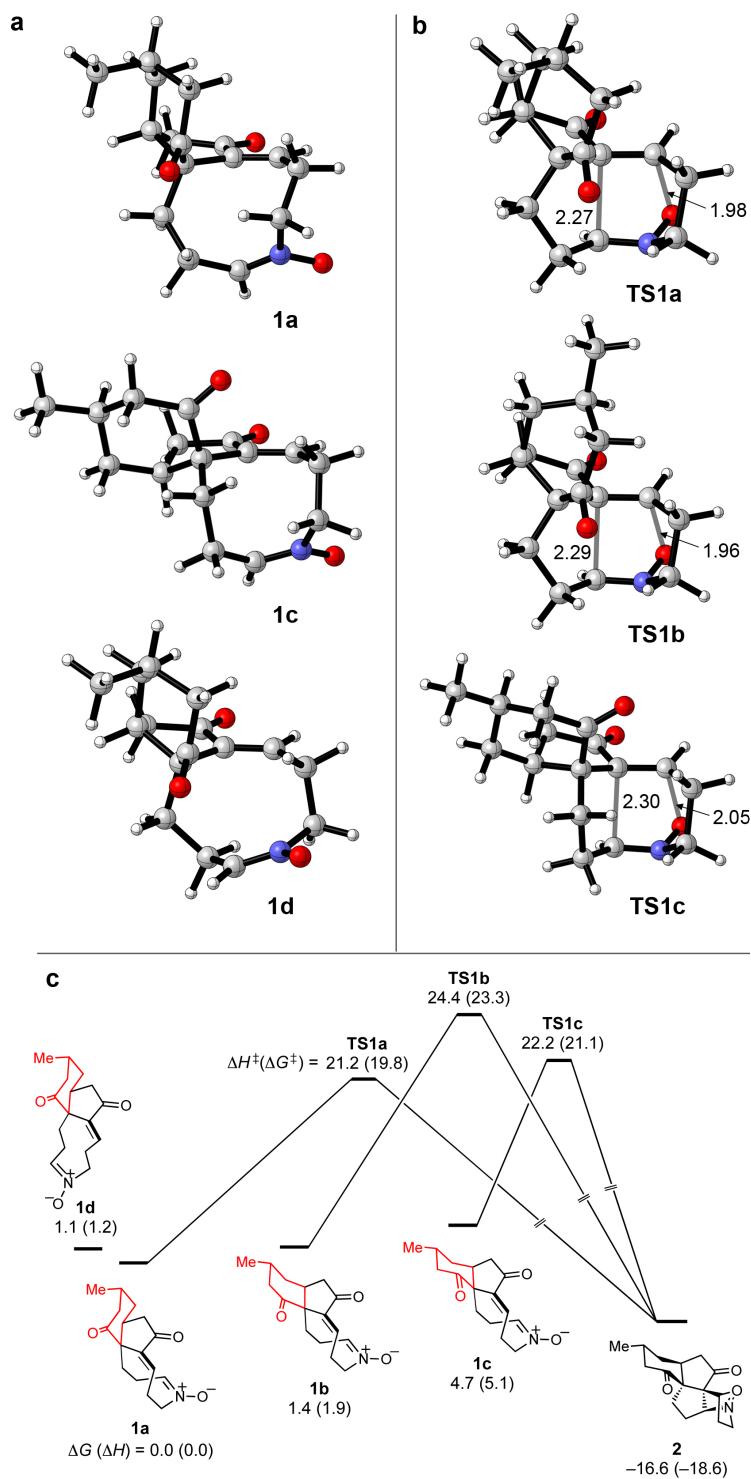


Figure 1.1. Transannular nitron–enone 1,3-dipolar cycloaddition of the putative lycojaponicum precursor **1** in the gas phase. (a) Selected reactant geometries. (b) Transition state geometries. (c) Free energy profiles for the transannular 1,3-dipolar cycloaddition in the gas phase. Free energies (with enthalpies in parentheses) are reported at the M06-2X/def2-TZVPP//M06-2X/6-31+G(d,p) level of theory (kcal mol⁻¹).

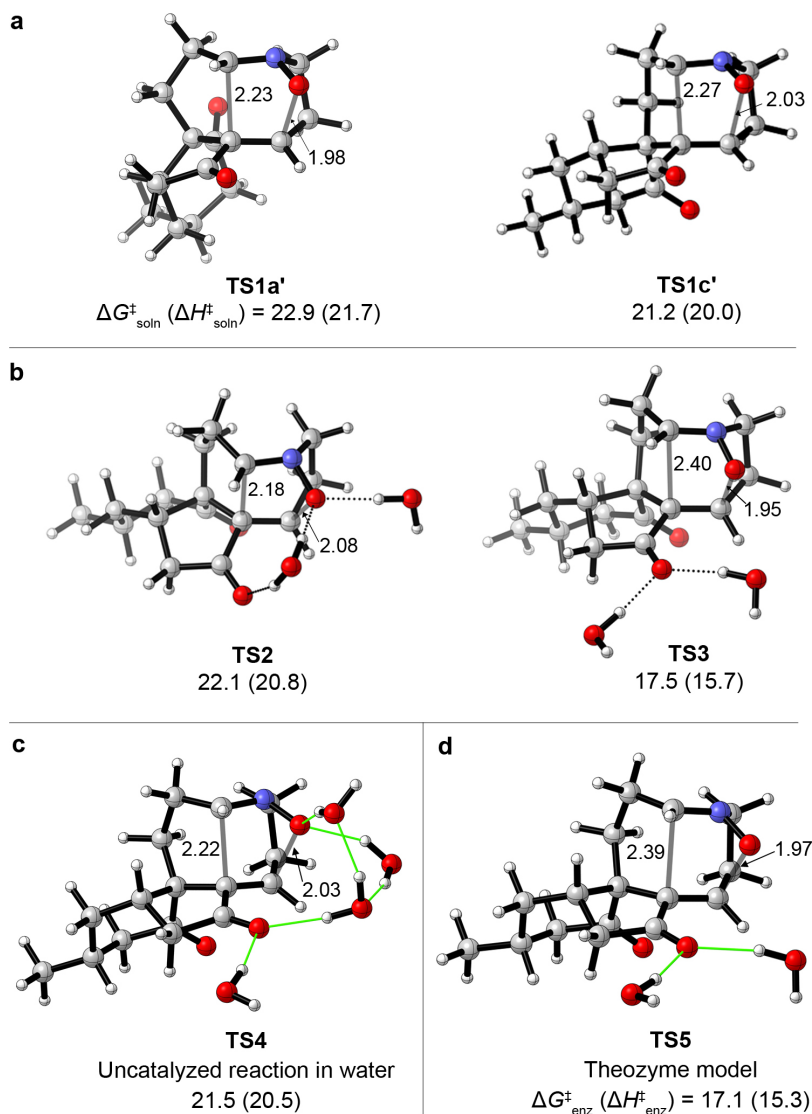


Figure 1.2. Prediction of the rate of the uncatalyzed transannular 1,3-dipolar cycloaddition of **1** and the theoretical enzymatic rate acceleration. (a) Transition states for the transannular 1,3-dipolar cycloaddition of **1** optimized in implicit water without any additional explicit water molecules. (b) Partially microsolvated transition states modeling the effect of hydrogen bonding to the nitron and/or enone. (c) Transition state in which all hydrogen bonds around the nitron and enone oxygens are satisfied, modeling the uncatalyzed reaction in water. (d) Theozyme model comprising strategic hydrogen bonding to the enone within a non-polar active site. All transition states except for **TS5** were optimized in implicit water (IEFPCM) at the M06-2X/6-31+G(d,p) level. **TS5** was optimized in implicit diethyl ether in order to simulate the dielectric constant of the interior of an enzyme. Subsequent single-point calculations at the M06-2X/def2-TZVPP level, in conjunction with the solution-optimized geometries, gave the activation free energies (and enthalpies in parentheses) shown (kcal mol^{-1}). The activation energies for **TS2–TS5** are computed relative to the nearest conformer of the reactant complex, while the activation energies for **TS1a'** and **TS1c'** are computed relative to the most stable conformer of the reactant.

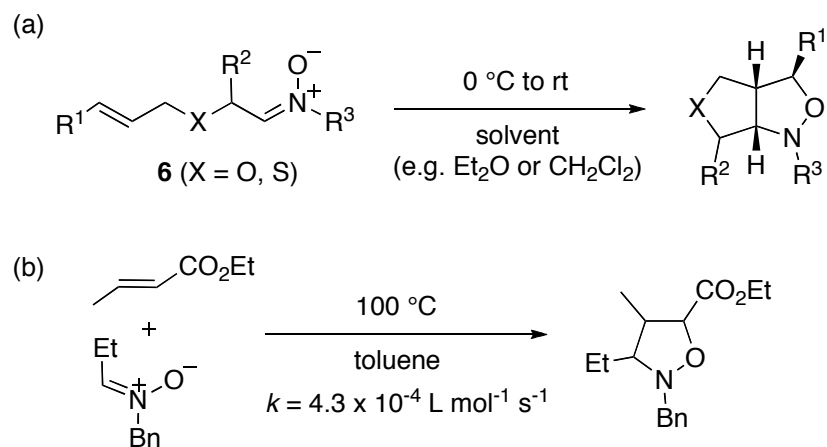
To estimate the activation energy of the uncatalyzed cycloaddition in water, we reoptimized the reactant and transition state in implicit solvent (IEFPCM), both in the absence and presence of additional explicit water molecules (Figure 1.2).¹⁴ Carbonyl groups are well known to accept two strong hydrogen bonds through the oxygen lone pairs;¹⁵ calculations on a nitron–alkene 1,3-dipolar transition state indicate that the nitron oxygen likewise accepts two hydrogen bonds. Thus, the microsolvated transition state **TS4** was constructed with four explicit water molecules satisfying the hydrogen bonds around the nitron and enone.¹⁶

Optimization of the transition states in implicit solvent (**TS1a'**, **TS1c'**) has only a minor effect on the transition state geometries, but does affect the relative stabilities of the transition states, such that **TS1c'** is lowest in energy, 1.7 kcal mol⁻¹ lower than **TS1a'**. The “c” transition-state conformer has a larger dipole moment than the “a” conformer (11.7 D for **TS1c'**, cf. 6.9 D for **TS1a'**), and as a result benefits from a greater free energy of solvation, explaining why **TS1c'** is more stable than **TS1a'** in water. The most stable reactant conformation in solution remains the “a” conformer. Reaction will proceed primarily via the “c” transition state provided that reactants a and c are in rapid equilibrium (via chair–chair interconversion of the cyclohexanone ring). Coordination of two water molecules simultaneously to the nitron and the enone (**TS2**) appears destabilizing, raising ΔG^\ddagger by about 1 kcal mol⁻¹, but coordination of two water molecules to the enone alone (**TS3**) lowers ΔG^\ddagger by up to 3.7 kcal mol⁻¹. Transition state **TS4**, which is the most accurate model for the uncatalyzed cycloaddition in water, has $\Delta G^\ddagger = 21.5$ kcal mol⁻¹, similar to the corresponding transition state with no explicit waters (**TS1c'**). This value of ΔG^\ddagger corresponds to a rate constant of 1×10^{-3} s⁻¹ and a half-life of approximately 10 minutes at room temperature.

Theory therefore predicts that the uncatalyzed transannular 1,3-dipolar cycloaddition of **1** in water is moderately facile. The nitron **1**, being a dialkyl-substituted nitron, is potentially quite susceptible to hydrolysis,¹⁷ but the macrocyclic structure may be expected to suppress any hydrolytic degradation of substrate. In principle, an enzyme could accelerate the cycloaddition of **1** if it could capitalize on the stabilization that can be derived from selective hydrogen bonding to the enone (cf. **TS3**). The rate enhancement available through hydrogen bonding to the enone within a typical dielectric environment of an enzyme active site was modeled by reoptimizing **TS3** in implicit diethyl ether ($\epsilon = 4.24$). The ether-optimized transition state is labeled **TS5** in Figure 1.3. **TS5** represents a theozyme^{18,19} for the cycloaddition of **1**: the two water molecules mimic the role that hydrogen bond donors such as serine, threonine, or tyrosine could play in an actual enzyme. The theozyme-catalyzed cycloaddition of **1** has a predicted ΔG^\ddagger of 17.1 kcal mol⁻¹. This value is 4.4 kcal mol⁻¹ lower than that of the uncatalyzed reaction and corresponds to a k_{cat} of about 2 s⁻¹. Thus, the theozyme calculation suggests that by placing hydrogen-bond donors strategically around the enone, an enzyme could provide a rate enhancement of about 2000-fold, allowing the cycloaddition of **1** to proceed with a half-life of about 0.4 s at 25 °C.

Even in the absence of an enzyme catalyst, the proposed cycloaddition of **1** appears to be a rather low-energy process. In comparison, the known intramolecular (but not transannular) 1,3-dipolar cycloadditions of C-alkenylnitrones **6** (Scheme 1.2a) are reported^{20,21} to occur over periods of hours to days at temperatures between 0 °C and room temperature in Et₂O or CH₂Cl₂. These reactions, studied by Aurich, lead to 5,5-bicyclic ring systems related to the 5,5,5-tricyclic ring system of the lycojaponicumins. Comparable intermolecular nitron-alkene 1,3-dipolar cycloadditions are much more sluggish: for example, the cycloaddition of *N*-benzyl *C*-ethyl

nitronone with ethyl crotonate (Scheme 2b) was reported by Huisgen²² to have a rate constant on the order of $10^{-4} \text{ L mol}^{-1} \text{ s}^{-1}$ at 100°C in toluene.



Scheme 1.2. Related intra- and intermolecular nitronone cycloadditions. (a) Facile intramolecular nitronone–alkene cycloadditions.^{20,21} (b) Sluggish intermolecular nitronone–alkene cycloaddition.²²

The factors leading to high reactivity in the cyclic substrate **1** were analyzed by examination of a series of nitronone cycloadditions involving the model substrates shown in Figure 1.3. Starting with the reference intermolecular cycloaddition of the parent nitronone with *cis*-butene (**TS6**), models of increasing complexity were built up by incorporating, one at a time, the structural features of tricyclic reactant **1**. The intermolecular reference reaction has a ΔG^\ddagger (30.3 kcal mol⁻¹) 9 kcal mol⁻¹ higher than the proposed biogenetic dipolar cycloaddition. The majority of this difference (6 kcal mol⁻¹) is captured in the first step of the series (**TS6**→**TS7**) and is the result of incorporating the cycloaddends into the nine-membered ring. The transannular transition state **TS7** has an activation enthalpy (ΔH^\ddagger) that is 8.5 kcal mol⁻¹ higher than that of the intermolecular transition structure (**TS6**), but it has a small entropic term ($-T\Delta S^\ddagger = 1.7 \text{ kcal mol}^{-1}$), which is 14.3 kcal mol⁻¹ smaller than the $-T\Delta S^\ddagger$ of the intermolecular reaction **TS6** and makes ΔG^\ddagger overall smaller by 5.8 kcal mol⁻¹. This entropy compensation in **TS7** exceeds the typical effect of intramolecularity by a few kcal mol⁻¹. Next, the fusion of the nine-membered ring into a

tricyclic system (**TS7**→**TS8**) lowers ΔG^\ddagger by 1.4 kcal mol⁻¹. This decrease is mostly enthalpic and arises because the tricyclic ring system predisposes the nine-membered ring to adopt a more reactive conformation. As shown in the inset to Figure 1.3, the parent nine-membered cyclic nitrene **7** prefers to adopt a chair-like structure rather than the tub. In **1**, on the other hand, the chair (**1d**, Figure 1.1) is destabilized by electrostatic repulsion between the nitrene and the cyclohexanone carbonyl group. The absence of a low-lying chair form in **1** preorganizes this reactant into a conformation closer to the transition state, reducing the barrier to cycloaddition by about 1 kcal mol⁻¹. Finally, a further 2 kcal mol⁻¹ of activation is derived from the \checkmark -carbonyl substituent on the dipolarophile (**TS8**→**TS1a**).

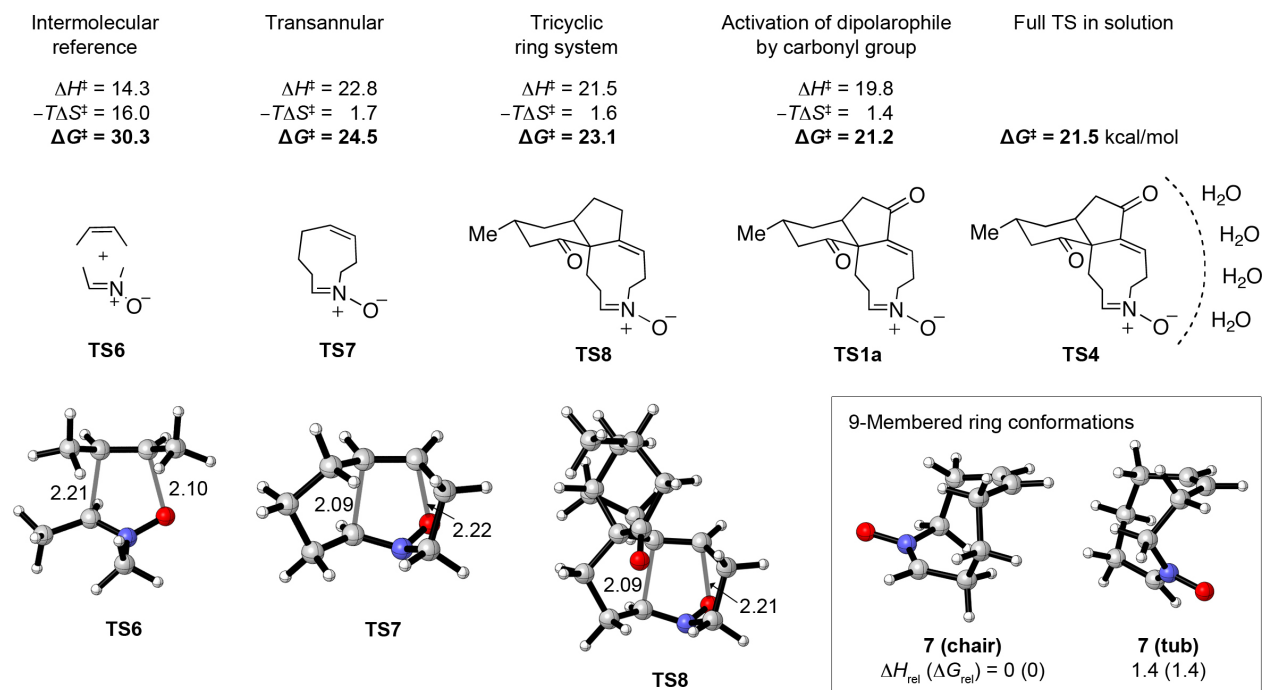


Figure 1.3. Analysis of the factors giving rise to the low barrier for transannular cycloaddition of **1**.

CONCLUSIONS

Does nature click? Although the definitive answer to this question will only come from experiment, our assessment of the rate of the purported 1,3-dipolar cycloaddition of **1** suggests an affirmative answer. Density functional theory calculations predict a k_{uncat} of about 10^{-3} s^{-1} for the uncatalyzed 1,3-dipolar cycloaddition of the putative lycojaponicum precursor **1**, suggesting that the reaction may even occur without the assistance of an enzyme. The predicted k_{cat} for the enzyme-catalyzed cycloaddition of **1**, based on a theozyme model where the transition state is stabilized by coordination of two hydrogen-bond donors to the enone, is about 2 s^{-1} . The predicted k_{cat} is small compared to the catalytic constants of the most efficient known enzymes, which are on the order of 10^3 – 10^7 s^{-1} .²³ However, such large catalytic constants are generally only observed for highly evolved enzymes that are involved in primary metabolism. Enzymes that are involved in secondary metabolic pathways commonly display much smaller k_{cat} values on the order of 0.01^{-1} s^{-1} .²⁴ The predicted k_{cat} for the reaction **1**→**2** falls within this range. Thus, theory predicts that the reaction could be spontaneous, but enzyme catalysis will be necessary to bring the reaction rate into the realm generally occupied by enzyme-catalyzed reactions involved in secondary metabolism.

COMPUTATIONAL METHODS

Quantum Mechanical Calculations. All quantum mechanical calculations were performed using Gaussian 09.²⁵ Geometry optimizations were conducted with the hybrid meta-GGA density functional M06-2X²⁶ and the 6-31+G(d,p) basis set. Normal mode analysis was used to confirm that optimized reactants and products were indeed minima and that transition states were first-order saddle points. Geometry optimizations were followed by M06-2X single point calculations using the triple-zeta def2-TZVPP^{27,28} basis set. The enthalpies and free energies

reported (at 25 °C) were determined by adding the thermal and zero point corrections determined at the M06-2X/6-31+G(d,p) level of theory to the M06-2X/def2-TZVPP single point energies. A standard state of 1 mol L⁻¹ is used. Errors in computed entropies, introduced by the treatment of low frequency modes as harmonic motions, were minimized by use of Truhlar's approximation,²⁹ in which all harmonic frequencies below 100 cm⁻¹ were raised to exactly 100 cm⁻¹ before evaluation of the vibrational component of the thermal contribution to entropy. Several stationary points were also optimized in implicit solvent (water or diethyl ether) using the IEFPCM solvation model.³⁰ Subsequent M06-2X/def2-TZVPP (gas-phase) single-point calculations were used in conjunction with the IEFPCM solvation energy and vibrational corrections to compute the solution-phase activation barriers. The "ultrafine" numerical integration grid of Gaussian 09, consisting of 99 radial shells and 590 angular points per shell, was used throughout.

Conformational Analysis. Conformational analyses of the reacting macrocycles **1** and **7** were performed using the MMFF force field in Macromodel 9.9.³¹ We utilized a newly implemented search methodology that incorporates short molecular dynamics simulations into a low mode/Monte Carlo search protocol optimized for the conformational sampling of macrocycles. A total of 5000 simulation cycles and 5000 Monte Carlo steps were performed, using the GB/SA model to simulate solvation in water. For **1**, the search yielded 15 distinct low-energy conformers within 10 kcal mol⁻¹ of the lowest MMFF energy, while for **7** seven conformers were found. The global minimum among each set of conformers was identified after M06-2X/6-31+G(d,p) reoptimizations of the MMFF structures.

AUTHOR CONTRIBUTIONS

E.H.K and A.P performed the quantum mechanical computations reported herein. E.H.K, and A.P, and K.N.H analyzed the results of these computations and prepared the manuscript.

ACKNOWLEDGMENTS

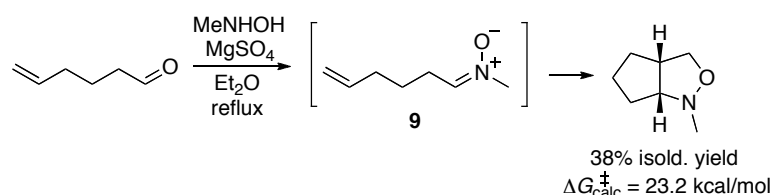
We acknowledge the financial support of the Australian Research Council (FT120100632 to E.H.K.) and the NSF (CHE-1059084 to K.N.H.). A.P. thanks the Chemistry-Biology Interface program (T32 GM 008496) for its support. High-performance computing resources were provided by the Australian National Computational Infrastructure National Facility, the University of Queensland Research Computing Centre, the UCLA Hoffman2 cluster, and the NSF's Extreme Science and Engineering Discovery Environment (TG-CHE040013N).

REFERENCES

1. Kolb, H. C.; Finn, M. G.; Sharpless, K. B. *Angew. Chem. Int. Ed.* **2001**, *40*, 2004–2021.
2. Rao Irlapati, N.; Baldwin, J. E.; Adlington, R. M.; Pritchard, G. J.; Cowley, A. R. *Tetrahedron* **2005**, *61*, 1773–1784.
3. Zhao, B.-X.; Wang, Y.; Zhang, D.-M.; Jiang, R.-W.; Wang, G.-C.; Shi, J.-M.; Huang, X.-J.; Chen, W.-M.; Che, C.-T.; Ye, W.-C. *Org. Lett.* **2011**, *13*, 3888–3891.
4. Zhao, B.-X.; Wang, Y.; Zhang, D.-M.; Huang, X.-J.; Bai, L.-L.; Yan, Y.; Chen, J.-M.; Lu, T.-B.; Wang, Y.-T.; Zhang, Q.-W.; Ye, W.-C. *Org. Lett.* **2012**, *14*, 3096–3099.
5. Tang, B.; Bray, C. D.; Pattenden, G. *Org. Biomol. Chem.* **2009**, *7*, 4448–4457.
6. Sugano, Y.; Kikuchi, F.; Toita, A.; Nakamura, S.; Hashimoto, S. *Chem. Eur. J.*, **2012**, *18*, 9682–9690.
7. Wang, S. C.; Tantillo, D. J. *J. Org. Chem.* **2008**, *73*, 1516–1523.
8. Borowski, T.; de Marothy, S.; Broclawik, E.; Schofield, C. J.; Siegbahn, P. E. M. *Biochemistry* **2007**, *46*, 3682–3691.
9. Stocking, E. M.; Williams, R. M. *Angew. Chem. Int. Ed.* **2003**, *42*, 3078–3115.
10. Oikawa, H. *Bull. Chem. Soc. Jpn.* **2005**, *78*, 537–554.
11. Campbell, C. D.; Vederas, J. C. *Biopolymers* **2010**, *93*, 755–763.
12. Wang, X.-J.; Zhang, G.-J.; Zhuang, P.-Y.; Zhang, Y.; Yu, S.-S.; Bao, X.-Q.; Zhang, D.; Yuan, Y.-H.; Chen, N.-H.; Ma, S.-g.; Qu, J.; Li, Y. *Org. Lett.* **2012**, *14*, 2614–2617.
13. Finn, Sharpless, and coworkers reported that 1,2,3-triazole-containing inhibitors of acetylcholinesterase could be selectively synthesized from a parallel array of azide and alkyne building blocks by 1,3-dipolar cycloaddition in the presence of acetylcholinesterase. In this case the enzyme is not an authentic 1,3-dipolar cycloadditionase but instead accelerates a non-natural

1,3-dipolar cycloaddition. See: Lewis, W. G.; Green, L. G.; Grynszpan, F.; Radić, Z.; Carrier, P. R.; Taylor, P.; Finn, M. G.; Sharpless, K. B. *Angew. Chem. Int. Ed.* **2002**, *41*, 1053–1057.

14. Huisgen (ref. 22) reported rate constants for intermolecular 1,3-dipolar cycloadditions of *C*-phenyl *N*-methylnitron with various alkenes, mostly in non-polar solvents. M06-2X calculations on representative cycloadditions of this nitron with methyl acrylate, ethyl crotonate, maleic anhydride, and dimethyl acetylenedicarboxylate were found to overestimate ΔG^\ddagger , presumably because of difficulties in accurately computing entropies of activation in solution, but much better accuracy is obtained for intramolecular nitron–alkene cycloadditions. For example, LeBel *et al.* reported that the intramolecular cycloaddition of *C*-alkenylnitron **9** gave a 38% isolated yield of cycloadduct over eight hours in refluxing Et₂O, while Aurich's cycloadditions of alkenylnitrones **6** (Scheme 1.2a), which furnish related 5,5-bicyclic ring systems, occur over periods of hours to days at temperatures between 0 °C and room temperature (ref. 20, 21). M06-2X calculations on the cycloaddition of **9** predict a ΔG^\ddagger of 23.2 kcal mol⁻¹ (*t*_{1/2} ≈ 50 min) in refluxing Et₂O, in good agreement with experiment. The experimental study of the cycloaddition of **9** is reported in: LeBel, N. A.; Post, M. E.; Whang, J. J. *J. Am. Chem. Soc.* **1964**, *86*, 3759–3767.



15. *Hydrogen Bonding in Organic Synthesis*, Pihko, P. M., Ed.; Wiley-VCH: Weinheim, 2009.

16. The most stabilizing hydrogen bonding arrangement for two water molecules around a carbonyl group is a planar arrangement. However, based on an analysis of enzyme crystal

structures, Simón and Goodman have shown that the most common hydrogen bonding geometry in oxyanion holes is a “grand jeté” arrangement, where the hydrogen bond donors are positioned approximately perpendicular to the carbonyl plane. Simón and Goodman showed that an in-plane arrangement of hydrogen bond donors stabilizes an oxyanion-like transition state more than a grand jeté arrangement, but the stabilization of the corresponding reactant by in-plane hydrogen bonding is even greater; thus, overall less stabilization is lost on going from reactant to transition structure in the grand jeté arrangement, explaining why the grand jeté arrangement is effective for catalysis. See: (a) Simón, L.; Goodman, J. M. *J. Org. Chem.* **2010**, *75*, 1831–1840. (b) Simón, L.; Goodman, J. M. *Org. Biomol. Chem.* **2012**, *10*, 1905–1913.

16. Hamer, J.; Macaluso, A. *Chem. Rev.* **1964**, *64*, 473–495.
17. Tantillo, D. J.; Chen, J.; Houk, K. N. *Curr. Opin. Chem. Biol.* **1998**, *2*, 743–750.
18. Tantillo, D. J.; Houk, K. N. In: *Stimulating Concepts in Chemistry*, Vögtle, F., Stoddart, J. F., Shibasaki, M., Eds.; Wiley-VCH: Weinheim, 2005.
19. Aurich, H. G.; Ruiz Quintero, J.-L. *Tetrahedron* **1994**, *50*, 3929–3942.
20. Baskaran, S.; Aurich, H. G.; Biesemeier, F.; Harms, K. *J. Chem. Soc., Perkin Trans. 1* **1998**, 3717–3724.
21. Huisgen, R.; Seidl, H.; Brüning, I. *Chem. Ber.* **1969**, *102*, 1102–1116.
22. Fersht, A. *Structure and Mechanism in Protein Science*; W. H. Freeman: New York, 1999; ch 4.
23. Two recent examples of catalytic constants for enzymes involved in secondary metabolism include a k_{cat} of 48.4 min⁻¹ for acyl transfer from α -S-methylbutyryl-LovF to monacolin J catalyzed by LovD, and a k_{cat} of 1.42 min⁻¹ for a geranyl transfer reaction catalyzed by VrtC. See: (a) Xie, X.; Meehan, M. J.; Xu, W.; Dorrestein, P. C.; Tang, Y. *J. Am. Chem. Soc.*

- 2009**, *131*, 8388–8389; (b) Chooi, Y.-H.; Wang, P.; Fang, J.; Li, Y.; Wu, K.; Wang, P.; Tang, Y. *J. Am. Chem. Soc.* **2012**, *134*, 9428–9437.
24. Frisch, M. J.; Trucks, G. W.; Schlegel, H. B.; Scuseria, G. E.; Robb, M. A.; Cheeseman, J. R.; Scalmani, G.; Barone, V.; Mennucci, B.; Petersson, G. A.; Nakatsuji, H.; Caricato, M.; Li, X.; Hratchian, H. P.; Izmaylov, A. F.; Bloino, J.; Zheng, G.; Sonnenberg, J. L.; Hada, M.; Ehara, M.; Toyota, K.; Fukuda, R.; Hasegawa, J.; Ishida, M.; Nakajima, T.; Honda, Y.; Kitao, O.; Nakai, H.; Vreven, T.; Montgomery, J. A.; Peralta, J. E.; Ogliaro, F.; Bearpark, M.; Heyd, J. J.; Brothers, E.; Kudin, K. N.; Staroverov, V. N.; Kobayashi, R.; Normand, J.; Raghavachari, K.; Rendell, A.; Burant, J. C.; Iyengar, S. S.; Tomasi, J.; Cossi, M.; Rega, N.; Millam, J. M.; Klene, M.; Knox, J. E.; Cross, J. B.; Bakken, V.; Adamo, C.; Jaramillo, J.; Gomperts, R.; Stratmann, R. E.; Yazyev, O.; Austin, A. J.; Cammi, R.; Pomelli, C.; Ochterski, J. W.; Martin, R. L.; Morokuma, K.; Zakrzewski, V. G.; Voth, G. A.; Salvador, P.; Dannenberg, J. J.; Dapprich, S.; Daniels, A. D.; Farkas, O.; Foresman, J. B.; Ortiz, J. V.; Cioslowski, J.; Fox, D. J. Gaussian 09, revision C.01; Gaussian, Inc.: Wallingford, CT, 2010.
25. Zhao, Y.; Truhlar, D. G. *Theor. Chem. Acc.*, **2008**, *120*, 215–241.
26. Weigend, F.; Ahlrichs, R. *Phys. Chem. Chem. Phys.* **2005**, *7*, 3297–3305.
27. Schäfer, A.; Huber, C.; Ahlrichs, R. *J. Chem. Phys.* **1994**, *100*, 5829–5835.
28. Zhao, Y.; Truhlar, D. G. *Phys. Chem. Chem. Phys.* **2008**, *10*, 2813–2818.
29. See, for example: Tomasi, J.; Mennucci, B.; Cammi, R. *Chem. Rev.*, **2005**, *105*, 2999–3093 and references cited therein.
30. Macromodel, version 9.9, Schrödinger, LLC, New York, NY, 2012.

Chapter 2

Dynamically complex enzyme-catalyzed [6+4]
and [4+2] cycloadditions in the biosynthesis of
spinosyn A.

Zhuo Chen[‡], Ashay Patel[‡], Osvaldo Gutierrez, Hung-wen Liu, K. N.
Houk^{*} and Daniel A. Singleton^{*}

ABSTRACT

SpnF, an enzyme involved in the biosynthesis of spinosyn A, catalyzes a transannular [4+2] cycloaddition reaction, commonly known as Diels-Alder reaction. Quantum mechanical computations and dynamic simulations now show the remarkable complexity of this reaction. This transannular cycloaddition is not well described as either a concerted or stepwise process, and dynamical effects influence the identity and timing of bond formation. The transition state for the reaction is ambimodal and leads directly to both the observed Diels-Alder and an unobserved [6+4] cycloadduct. The potential energy surface bifurcates and the [6+4] cycloaddition occurs by a dynamically stepwise cycloaddition mode featuring an “entropic intermediate”. A rapid Cope rearrangement converts the [6+4] adduct into the observed [4+2] adduct. Control of nonstatistical dynamical effects may serve as a secondary means by which enzymes control reactions.

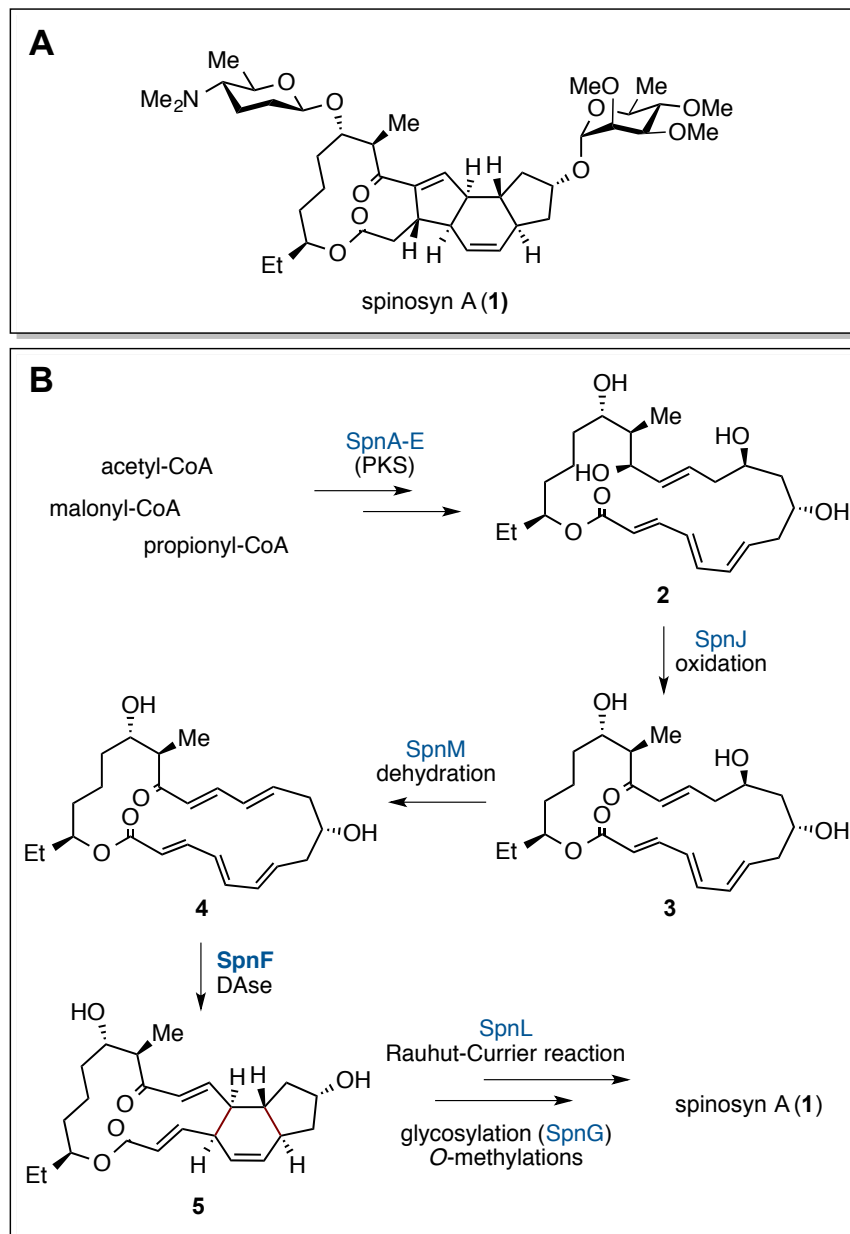
INTRODUCTION

The mechanism of the Diels-Alder reaction has been a topic of scholarly discussion and passionate debate,¹⁻³ since the discovery of this reaction in 1928.⁴ Despite the synthetic utility of this reaction, biological Diels-Alder reactions have only recently been discovered. In fact, some 70 years after Diels and Alder’s initial discovery, the existence of enzyme-catalyzed Diels-Alder reactions still remained in doubt.⁵ However, recent evidence implicates enzymatic Diels-Alder reactions in the biosynthesis of a number of natural products,⁶⁻⁹ but only one enzyme – involved in the biosynthesis of spinosyn A (**1**) – has been shown to catalyze a Diels-Alder reaction. This enzyme, SpnF, – studied experimentally by Liu *et al.* – is the first enzyme for which catalysis of a transannular [4+2]-cycloaddition reaction has been demonstrated to be its sole function.¹⁰

The mechanism of the cycloaddition remains of high interest, since whether SpnF is a

true Diels-Alderase depends on whether it-catalyzed cycloaddition reaction proceeds in a concerted manner. Reported in this paper is a complete description of the mechanism of this cycloaddition using quantum mechanical computations and molecular dynamics simulations. A previous theoretical study of this reaction by Smentek and Hess indicated that the SpnF-catalyzed cycloaddition was “concerted, [but] highly asynchronous”.¹¹ We show that the reaction mechanism is considerably more complex. A previous gas-phase computational study by Smentek and Hess that utilized a simplified model system for the cyclization reaction indicated that a highly asynchronous concerted [4+2]-cycloaddition was possible. Here we show that the reaction coordinate for cyclization of the SpnF substrate may actually be considerably more complicated.

To model the potential energy surface of this reaction we employed both B3LYP-D2/6-3G(d) and B3LYP-D3(BJ)//6-31+G(d,p) computations. Conformational analyses of stationary points were performed using molecular mechanics methods. The 20 or 30 structures of the lowest energy generated in this manner were reoptimized using B3LYP-D3(BJ)/6-31G(d,p) to determine the lowest energy conformations for each stationary point. Additional details and references regarding our computational methodology are provided in the Supporting Information.



Scheme 2.1. Structure and biosynthesis of spinosyn A. A.) Structure of the polycyclic macrolactone Spinosyn A. B.) Established key biosynthetic steps of the natural product. Enzyme(s) responsible for the individual biosynthetic steps are shown in blue.

The mechanism of the cycloaddition remains of high interest, since biocatalysis of Diels-Alder reactions remain poorly understood. Reported in this paper is a complete description of the mechanism of this cycloaddition using quantum mechanical computations and molecular

dynamics simulations. A previous gas-phase computational study by Smentek and Hess that utilized a simplified model system for the cyclization reaction indicated that a highly asynchronous concerted [4+2]-cycloaddition was possible. Here we show that the reaction coordinate for cyclization of the SpnF substrate may actually be considerably more complicated.

RESULTS AND DISCUSSION

To model the potential energy surface of this reaction we employed M06-2X/def2-TZVPP//B3LYP-D2//6-31G(d) computations. Conformational analyses of stationary points were performed using molecular mechanics methods. The 20 or 30 structures of the lowest energy generated in this manner were reoptimized using B3LYP-D2/6-31G(d) to determine the lowest energy conformations for each stationary point.

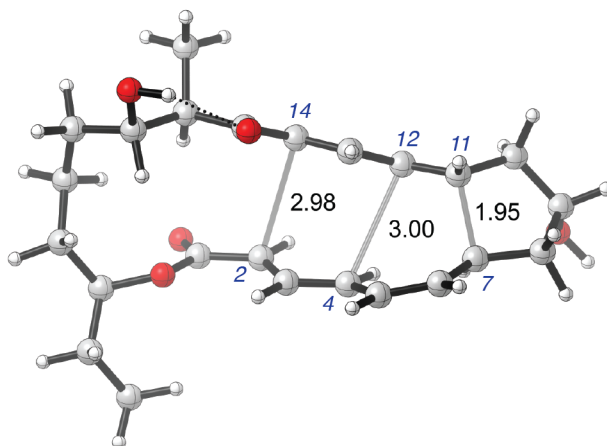


Figure 2. The B3LYP-D3(BJ)/6-31+G(d,p)-optimized bis-pericyclic transition structure **TS7**. The forming-bond distances are shown in Å in grey. Key carbon atoms are numbered in blue.

The lowest energy transition state for the reaction of **4** is **TS7** shown in Figure 2.1. The [4+2] cycloadduct formed via this transition state is the only product observed experimentally; according to theory, transition structures leading to stereoisomers of **5** were at least 3 kcal mol⁻¹ higher in energy. Based on its structure, **TS7** is not a simple asynchronous Diels-Alder transition state, but rather is “bis-pericyclic”,¹²⁻¹⁵ or more generally, ambimodal.¹⁶ A bis-pericyclic

transition state features two sets of stabilizing cyclic aromatic orbital interactions that can give two different pericyclic reaction products. For **TS7**, the two sets of orbital interactions can result in [6+4] and [4+2] cycloadditions;^{17,18} the transition state features *three* partially formed sigma bonds, C⁷-C¹¹, C⁴-C¹², and C²-C¹⁴ with forming bond distances of 1.97 Å, 3.03 Å, and 2.90 Å, respectively. Predicted in 1965,¹⁷ [6+4] cycloadditions were soon detected experimentally^{19,20}; and a variety have been described in the last 50 years.²¹⁻²⁴

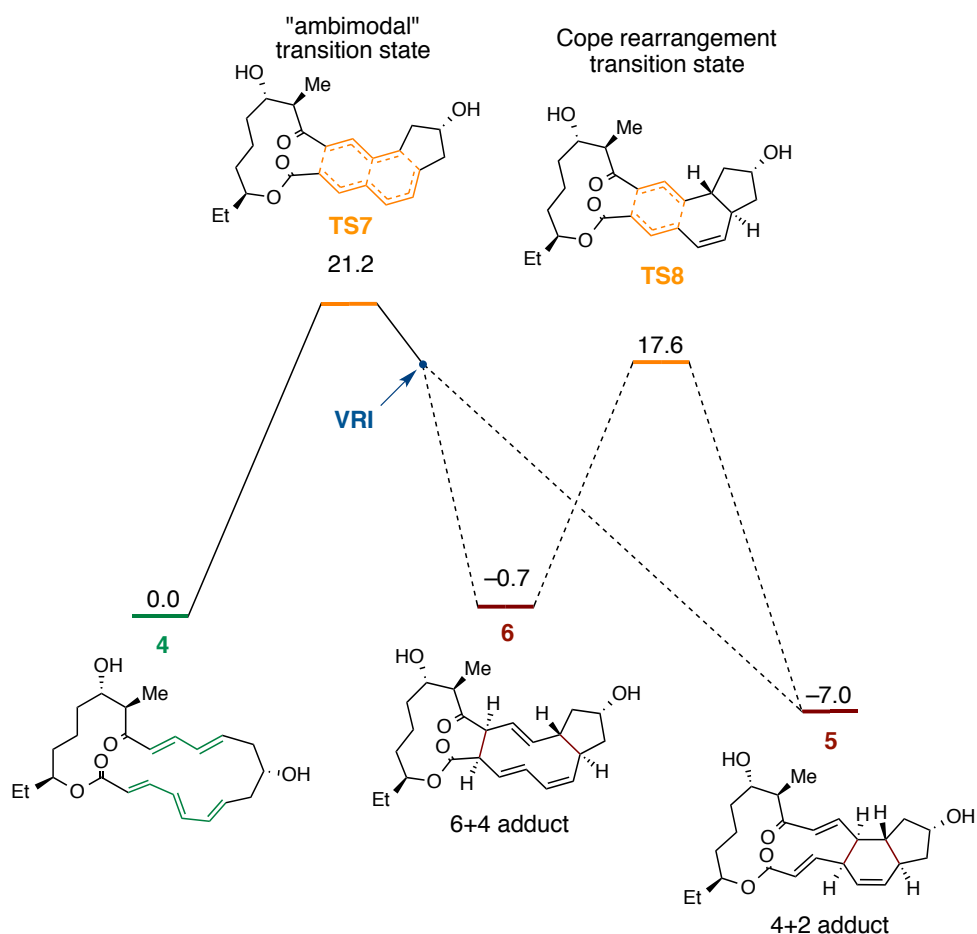


Figure 2.2. Free energy diagram for the cycloaddition of **4**. Gibbs free energies (in kcal mol⁻¹) and geometries determined at the B3LYP-D3(BJ)/6-31+G(d,p) level of theory.

The computed gas-phase mechanism and energetics of the Diels-Alder reaction of macrolactone **4** are illustrated in Figure 2.2. The bis-pericyclic transition state **TS7** is 21 kcal mol⁻¹ higher in energy than the reactant and leads to a valley-ridge inflection (VRI) on the potential energy surface. The reaction path “bifurcates” in two directions with one direction leading to the formation of the expected Diels-Alder adduct **5** and the other leading to the [6+4] cycloadduct **6**. The steepest-descent path from **TS7** along the potential energy surface in mass-weighted coordinates (the minimum energy path or MEP) leads to the [6+4] adduct **6**. Due to strain inherent in 10- and 11-membered rings, the [6+4] adduct **6** is 8 kcal mol⁻¹ less stable than the Diels-Alder product. Intermediate **6** is predicted to undergo a facile Cope rearrangement to afford the Diels-Alder adduct.

The product outcomes of reactions featuring bis-pericyclic transition states and bifurcating potential energy surfaces cannot be predicted with conventional transition state theory, because dynamical effects control the selectivity of the reaction. We performed molecular dynamics trajectory calculations to determine the competition between formation of the [6+4] and [4+2] products. Quasi-classical direct-dynamics simulations²⁵ on a B3LYP-D2/6-31G(d) energy surface were initiated within the region of the potential energy surface near **TS7**, giving each real normal mode in **TS7** its zero-point energy (ZPE) plus a Boltzmann sampling of thermal energy available at 25 °C with a random phase. The trajectories were integrated in time in both the forward and backward directions until either **5** or **6** was formed or reactant **4** was reformed.

Trajectories passing through **TS7** end in one of *three* ways. Out of 353 trajectories simulated, 223 (63%) afforded the [6+4] product **6**, 88 (25%) afford the Diels-Alder adduct **5** and 42 (12%) *recross*, fully forming the C⁷-C¹¹ bond before passing back through the transition

state to re-form the starting material. These simulations predict that [6+4] and [4+2] adducts are initially formed in a 2.5:1 ratio.

The time required for formation of either **5** or **6** is unusually long compared to the time required for the formation of other Diels-Alder adducts. The median times for formation of **5** and **6** starting from the initialization at **TS7**, defined as the time required for both new σ bonds to reach carbon-carbon distances of 1.7 Å, were 171 and 197 fs, respectively. Over 20% of the trajectories require longer than 300 fs to afford **6**. Simple Diels-Alder reactions typically require less than 50 fs to form products from the transition state.²⁶ Another way to determine this time is to assess the time required by trajectories to cross the “transition zone”, which is defined as the set of geometries thermally accessible at the transition state assuming the harmonic frequencies of the transition structure. When this is done, the median times in the transition zone for trajectories leading to **5** and **6** are 130 and 127 fs, respectively, compared to 50-95 fs in other simpler Diels-Alder reactions.²⁶ Finally, the time gap between formation of the first new σ bond in the cycloadduct (the C⁷-C¹¹ bond) and formation of the second new σ bond (either C⁴-C¹² for **5** or C²-C¹⁴ for **6**, defined by interatomic distances <1.7 Å) is exceptionally long, with median times of 173 and 139 fs for **5** and **6**, respectively. For comparison, the Diels-Alder reactions of simple symmetrical reactants (e.g., the reaction of ethylene and butadiene) have median time gaps of shorter than 5 fs while unsymmetrical cycloaddends undergo cycloaddition with longer median time gaps between 10 to 25 fs.²⁶

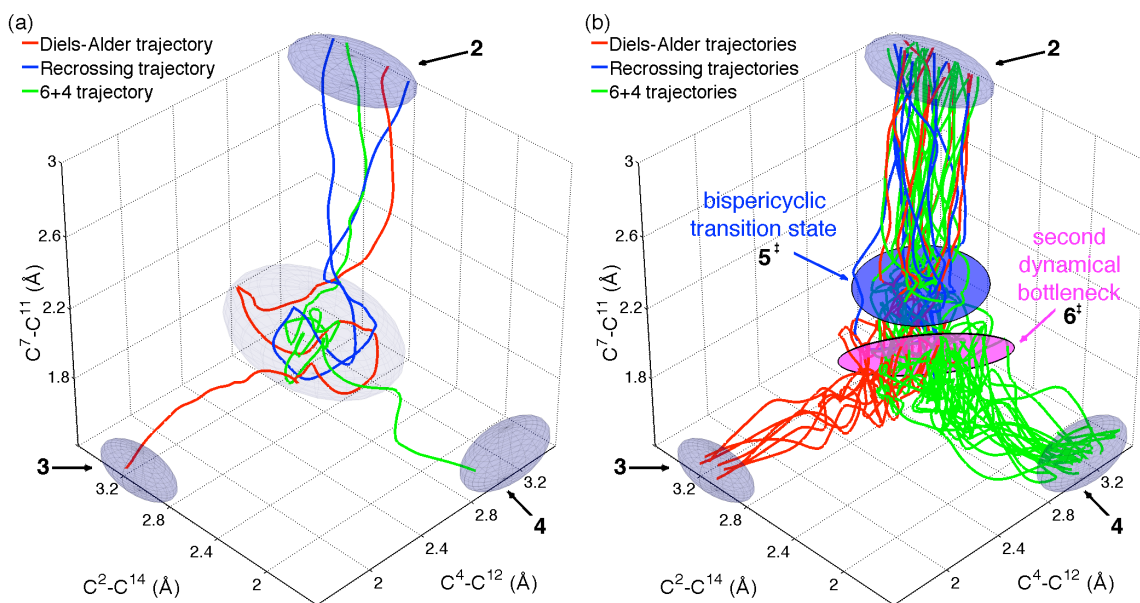


Figure 2.3. Trajectory plots following the C-C interatomic distances. (a). Three selected trajectories. Trajectories pass into an area with a fully formed C⁷-C¹¹ bond, then may form **5** or **6** or recross to **4**. (b). Thirty randomly chosen trajectories.

The simulations illustrate the dynamical nature of the cycloaddition. Figure 2.3a shows a plot of three different types of trajectories in three dimensions, defined by their C⁷-C¹¹, C⁴-C¹², and C²-C¹⁴ interatomic distances, while Figure 4b shows a plot of 30 randomly chosen trajectories. Reactions begin with the approach of C⁷ and C¹¹ towards one another, passing through the cycloaddition transition state when the C⁷-C¹¹ distance is about 1.97 Å, then fully forming the C⁷-C¹¹ bond. The structure that results is loosely delineated by C⁴-C¹² and C²-C¹⁴ distances between 2.8 and 3.2 Å. This family of structures is in the blue ovals in Figure 2.3b. This species tends to persist for a few bond vibrations, and it may undergo three distinguishable reactions, i.e., formation of the Diels-Alder adduct **5**, formation of the [6+4] adduct **6**, or transition state recrossing to the reactant **4**. These properties are suggestive that these structures are best understood as an intermediate, even though there is no potential-energy barrier for the formation of either of the C⁴-C¹² and C²-C¹⁴ bonds from this intermediate. Therefore, the route to

the products must feature a second dynamical bottleneck. In qualitative terms, only when the C⁷-C¹¹ distance is within a limited range can formation of the second bond (either the C⁴-C¹² or C²-C¹⁴ bond) occur, a process that takes the lifetime of a few bond vibrations.

A more quantitative, statistical approach to understanding the nature of the mechanism was pursued by applying canonical variational transition state theory (VTST)²⁷⁻²⁹. In transition state theory, the transition state is defined as a multidimensional hypersurface dividing the starting material from the product, and the properties of the hypersurface are used to calculate the rate constant. In canonical VTST, the position of the transition state hypersurface is varied so as to minimize the rate constant at the reaction temperature. The resulting variational transition states are dynamical bottlenecks and correspond to maxima in the free energy along the minimum energy pathway (MEP) connecting the starting material to the product. Use of VTST to model the reaction of **4** demonstrated that two variational transition states (or dynamical bottlenecks) exist along the MEP. The first (**VTS9**) corresponds closely to the potential-energy saddle point **TS7** but the second, structure **VTS10** (Figure 2.4), occurs after the C⁷-C¹¹ bond is fully formed. The region of the potential energy surface between **VTS9** and **VTS10** is not well defined, but the MEP passing through this area exhibits a shallow minimum in the generalized free energy. This “free energy” minimum can formally be considered an intermediate. From this statistical perspective, the intermediate arises because the formation of either the C⁴-C¹² or C²-C¹⁴ bonds reduces the flexibility of the macrolactone in a way that is entropically unfavorable, and the intermediate is caused by this entropic barrier. The return to starting material **4** requires traversal of a potential-energy barrier, but this process is entropically favorable and competes with the downhill paths to formation of **5** or **6**. Such variational intermediates that only appear

on a free energy surface have been suggested before by Doubleday in his studies of the tetramethylene biradical.³⁰

Quantitatively, there is some difference in the statistical and dynamical predictions. In the harmonic and canonical approximations, the second bottleneck **VTS10** is 2.4 kcal/mol below **6**, so only about 2% reversal would be expected instead of the 12% observed in the trajectory study.

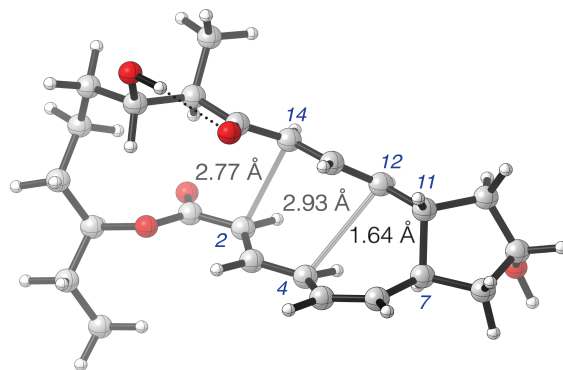


Figure 2.4. Variational transition state (dynamical bottleneck **VTS10**). Once **VTS10** is formed recrossing is no longer observed; however, from **VTS10** either of the two adducts could be formed.

Mechanistic chemistry often divides reactions into concerted versus two-step processes. However, the simple concerted/stepwise ideals are inadequate to describe the complex cycloadditions such as that of **4**. The cycloaddition of **4** involves two cyclic arrays of bonding interactions at its transition state, and one or the other of these arrays is maintained along the paths to the products. There is no opportunity for an “intermediate” to be trapped or lose its stereochemistry; the intermediate itself has no potential-energy minimum and has no parallel in the ions or radicals of ordinary reactive-intermediate chemistry. In contrast to the usual ideal of a concerted Diels-Alder mechanism, the cycloaddition of **4** involves a very shallow free-energy minimum along the reaction pathway. Similar concepts have been proposed by John Bladwin

(bonding stepwise, but energetically concerted)³¹ and by Raymond Firestone (diradical intermediates with lifetimes too short for bond rotation).³² The structure associated with the free energy minimum found here has a significant lifetime and can ultimately evolve along multiple pathways, an indicator of an intermediate. Even the seemingly ordinary stepwise mechanism forming **5** via long-lived **6** occurs through the same initial transition state, and the trajectories that reach **5** do so over a range of 80 to 480 fs.

CONCLUSIONS

The mechanism of the SpnF-catalyzed cycloaddition of **4** is currently unknown, and it need not be identical to the uncatalyzed gas-phase mechanism. When an enzymatic reaction involves a dynamic selection among products on the downhill slope of an energy surface, the enzyme might act by controlling the pitch of the downhill “slalom” course choosing among products. Tantillo *et al.* have demonstrated that this sort of dynamic selection plays a role in terpene biosynthesis.³³ Such possibilities are entirely distinct from the lowering of reaction barriers that is assumed to completely define catalysis, but they are recognizable when the dynamic complexity of real reactions is considered.

COMPUTATIONAL METHODS

The study of the cyclization of **4** to **5** is complicated by the ensemble of conformations that are energetically available to **4** as well as the potential for alternative modes of approach of the cycloaddends that could lead to stereoisomers of **5**. A conformational search of the ground state of **4** was undertaken using an MMFF force field and the low mode / Monte Carlo search protocol optimized for sampling of macrocycles available in MacroModel 9.9^{34,35}. Transition state conformers for each possible cycloaddition mode were obtained by simulated annealing of structures in which the C⁴-C¹² and C⁷-C¹¹ distances were fixed at values typical of Diels-Alder

reactions. Simulated annealing was also used to obtain conformations for the possible cycloadducts. The lowest-energy structures (20 to 30 structures in each case) were then used as the input geometries for full optimizations in density functional theory (DFT) computations. Geometry optimizations and subsequent frequency calculations of all stationary points were initially conducted using B3LYP calculations including Grimme's empirical D2 correction^{36,37} and using a 6-31G(d) basis set. This model chemistry was also employed for direct dynamics trajectory simulations (see below). Stationary points were re-optimized with B3LYP-D3³⁷(BJ)³⁸/6-31+G(d,p) using an ultrafine integration grid consisting of 590 radial shell with each consisting of 99 grid points. Vibrational frequencies were recomputed at this level as well. All thermal corrections were determined using unscaled frequencies assuming a standard state of 298.15 K and 1 atm. Truhlar's quasiharmonic approximation was employed in order to compute the molecular entropies of all stationary points described herein^{39,40}. All DFT computations were performed using *Gaussian 09*.⁴¹ The molecular visualization softwares Gaussview 5⁴² and Avogadro 1.1.1^{43,44} were used. CYLview was used to render the structures shown herein.⁴⁵

AUTHOR CONTRIBUTIONS

Z.C., and O.G., and A.P. performed DFT computations to determine the potential energy surface of cycloaddition; Z.C. performed dynamic simulations and variational transition state theory analysis. H.-w.L., K.N.H., and D.A.S designed the study. Z.C., A.P., K.N.H., and D.A.S. analyzed the computations and wrote the paper. Z.C, A.P, K.N.H., H.-w.L, and D.A.S. discussed the findings and commented on the manuscript. Z.C. and A.P contributed equally.

ACKNOWLEDGEMENTS

K.N.H. and A.P acknowledge the NSF (CHE-1059084 to K.N.H.) and the NIH (1R01GM097200) for funding. A.P thanks the Chemistry-Biology Interface Training Program (T32 GM 008496) grant program for its support and the University of California, Los Angeles for funding. Computations were performed using the UCLA's Hoffman2 Beowulf (to K.N.H.) cluster and the Extreme Science and Engineering Design Environment's (TG CHE 044013N to K.N.H.) Gordon and Trestles supercomputing clusters at the San Diego Supercomputing Center.

REFERENCES

1. Woodward, R. B. The mechanism of the Diels -Alder reaction. *J. Am. Chem. Soc.* **64**, 3058–3059 (1942).
2. Houk, K. N., González, J. & Li, Y. Pericyclic reaction transition states: passions and punctilios, 1935-1995. *Acc. Chem. Res.* **28**, 81–90 (1995).
3. Sauer, J. & Sustmann, R. Mechanistic aspects of Diels-Alder reactions: A critical survey. *Angew. Chem. Int. Ed.* **19**, 779–807 (1980).
4. Diels, O. & Alder, K. Synthesen in der hydroaromatischen Reihe. *Liebigs Ann. Chem.* **460**, 98–122 (1928).
5. Laschat, S. Pericyclic reactions in biological systems—Does nature know about the Diels-Alder reaction? *Angew. Chem. Int. Ed.* **35**, 289–291 (1996).
6. Stocking, E. M. & Williams, R. M. Chemistry and biology of biosynthetic Diels–Alder reactions. *Angew. Chem. Int. Ed.* **42**, 3078–3115 (2003).
7. Oikawa, H. & Tokiwano, T. Enzymatic catalysis of the Diels–Alder reaction in the biosynthesis of natural products. *Nat. Prod. Rep.* **21**, 321–352 (2004).
8. Kelly, W. L. Intramolecular cyclizations of polyketide biosynthesis: mining for a ‘Diels–Alderase’? *Org. Biomol. Chem.* **6**, 4483–4493 (2008).
9. Kim, H. J., Rusczycky, M. W. & Liu, H.-W. Current developments and challenges in the search for a naturally selected Diels-Alderase. *Curr. Opin. Chem. Biol.* **16**, 124–131 (2012).
10. Kim, H. J., Rusczycky, M. W., Choi, S.-H., Liu, Y.-N. & Liu, H.-W. Enzyme-catalysed [4+2] cycloaddition is a key step in the biosynthesis of spinosyn A. *Nature* **473**, 109–112 (2011).

11. Hess, B. A. J. & Smentek, L. Concerted, highly asynchronous, enzyme-catalyzed [4+2] cycloaddition in the biosynthesis of spinosyn A; computational evidence. *Org. Biomol. Chem.* **10**, 7503–7509 (2012).
12. Quadrelli, P., Romano, S., Toma, L. & Caramella, P. A bispericyclic transition structure allows for efficient relief of antiaromaticity enhancing reactivity and endo stereoselectivity in the dimerization of the fleeting cyclopentadienone. *J. Org. Chem.* **68**, 6035–6038 (2003).
13. Thomas, J. B., Waas, J. R., Harmata, M. & Singleton, D. A. Control elements in dynamically determined selectivity on a bifurcating surface. *J. Am. Chem. Soc.* **130**, 14544–14555 (2008).
14. Wang, Z., Hirschi, J. S. & Singleton, D. A. Recrossing and dynamic matching effects on selectivity in a Diels–Alder reaction. *Angew. Chem. Int. Ed.* **48**, 9156–9159 (2009).
15. Caramella, P., Quadrelli, P. & Toma, L. An unexpected bispericyclic transition structure leading to 4+2 and 2+4 cycloadducts in the endo dimerization of cyclopentadiene. *J. Am. Chem. Soc.* **124**, 1130–1131 (2002).
16. Pham, H. V. & Houk, K. N. Diels–Alder Reactions of Allene with Benzene and Butadiene: Concerted, Stepwise, and Ambimodal Transition States. *J. Org. Chem.* 140918111608004 (2014). doi:10.1021/jo502041f
17. Hoffmann, R. & Woodward, R. B. Selection rules for concerted cycloaddition reactions. *J. Am. Chem. Soc.* **87**, 2046–2048 (1965).
18. Woodward, R. B. & Hoffmann, R. The conservation of orbital symmetry. *Angew. Chem. Int. Ed.* **8**, 781–853 (1969).
19. Cookson, R. C., Drake, B. V., Hudec, J. & Morrison, A. The adduct of tropone and

- cyclopentadiene: a new type of cyclic reaction. *Chem. Commun.* 15–16 (1966).
20. Houk, K. N. & Woodward, R. B. Cycloaddition reactions of tropone and 2,5-dimethyl-3,4-diphenylcyclopentadienone. *J. Am. Chem. Soc.* **92**, 4145–4147 (1970).
 21. Mukherjee, D., Dunn, L. C. & Houk, K. N. Efficient guaiazulene and chamazulene syntheses involving [6 + 4] cycloadditions. *J. Am. Chem. Soc.* **101**, 251–252 (1979).
 22. Garst, M. E., Roberts, V. A. & Prussin, C. Fragmentation of bicyclo[4.4.1]undecan-11-ones. *J. Org. Chem.* **47**, 3969–3971 (1982).
 23. Isakovic, L., Ashenurst, J. A. & Gleason, J. L. Application of Lewis Acid Catalyzed Tropone [6+4] Cycloadditions to the synthesis of the core of CP-225,917. *Org. Lett.* **3**, 4189–4192 (2001).
 24. Rigby, J. H. & Fleming, M. Construction of the ingenane core using an Fe(III) or Ti(IV) Lewis acid-catalyzed intramolecular [6+4] cycloaddition. *Tetrahedron Lett.* **43**, 8643–8646 (2002).
 25. Sun, L. & Hase, W. L. Born-Oppenheimer direct dynamics classical trajectory simulations. *Rev. Comput. Chem.* **19**, 79–146 (2003).
 26. Black, K., Liu, P., Xu, L., Doubleday, C. & Houk, K. N. Dynamics, transition states, and timing of bond formation in Diels-Alder reactions. *Proc. Natl. Acad. Sci. U.S.A.* **109**, 12860–12865 (2012).
 27. Truhlar, D. G. & Garrett, B. C. Variational transition-state theory. *Acc. Chem. Res.* **13**, 440–448 (1980).
 28. POLYRATE 2010-A: A Computer Program for the Calculation of Chemical Reaction.
 29. Gaussrate 2009-A.
 30. Doubleday, C. Lifetime of trimethylene calculated by variational unimolecular rate theory.

- Journal of Physical Chemistry* **100**, 3520–3526 (1996).
31. Baldwin, J. E. & Fleming, M. Allene-olefin and allene-allene cycloadditions methylenecyclobutane and 1,2-dimethylenecyclobutane degenerate rearrangements. *Fortsch. Chem. Forschung* **15**, 281–310 (1970).
 32. Firestone, R. A. Mechanism of 1,3-dipolar cycloadditions. *J. Org. Chem.* **33**, 2285–2290 (1968).
 33. Hong, Y. J. & Tantillo, D. J. Biosynthetic consequences of multiple sequential post-transition-state bifurcations. *Nature Chem* **6**, 104–111 (2014).
 34. Schrödinger Release 2013-3: MacroModel, version 10.2, Schrödinger, LLC, New York, NY, 2013.
 35. Schrödinger Release 2013-3: Maestro, version 9.6, Schrödinger, LLC, New York, NY, 2013.
 36. Grimme, S. Semiempirical GGA-type density functional constructed with a long-range dispersion correction. *J. Comput. Chem.* **27**, 1787–1799 (2006).
 37. Grimme, S., Antony, J., Ehrlich, S. & Krieg, H. A consistent and accurate ab initio parametrization of density functional dispersion correction (DFT-D) for the 94 elements H-Pu. *J. Chem. Phys.* **132**, 154104 (2010).
 38. Grimme, S., Ehrlich, S. & Goerigk, L. Effect of the damping function in dispersion corrected density functional theory. *J. Comp. Chem.* **32**, 1456–1465 (2011)
 39. Zhao, Y. & Truhlar, D. G. Computational characterization and modeling of buckyball tweezers: density functional study of concave-convex $\pi\cdots\pi$ interactions. *Phys. Chem. Chem. Phys.* **10**, 2813–2818 (2008).

40. Ribeiro, R. F. R., Marenich, A. V. A., Cramer, C. J. C. & Truhlar, D. G. D. Use of solution-phase vibrational frequencies in continuum models for the free energy of solvation. *J Phys Chem B* **115**, 14556–14562 (2011).
41. Gaussian 09, Revision **D.01**, Frisch, M. J., Trucks, G. W., Schlegel, H. B., Scuseria, G. E., Robb, M. A., Cheeseman, J. R., Scalmani, G., Barone, V., Mennucci, B., Petersson, G. A., Nakatsuji, H., Caricato, M., Li, X., Hratchian, H. P., Izmaylov, A. F., Bloino, J., Zheng, G., Sonnenberg, J. L., Hada, M., Ehara, M., Toyota, K., Fukuda, R., Hasegawa, J., Ishida, M., Nakajima, T., Honda, Y., Kitao, O., Nakai, H., Vreven, T., Montgomery, J. A., Jr., Peralta, J. E., Ogliaro, F., Bearpark, M., Heyd, J. J., Brothers, E., Kudin, K. N., Staroverov, V. N., Kobayashi, R., Normand, J., Raghavachari, K., Rendell, A., Burant, J. C., Iyengar, S. S., Tomasi, J., Cossi, M., Rega, N., Millam, J. M., Klene, M., Knox, J. E., Cross, J. B., Bakken, V., Adamo, C., Jaramillo, J., Gomperts, R., Stratmann, R. E., Yazyev, O., Austin, A. J., Cammi, R., Pomelli, C., Ochterski, J. W., Martin, R. L., Morokuma, K., Zakrzewski, V. G., Voth, G. A., Salvador, P., Dannenberg, J. J., Dapprich, S., Daniels, A. D., Farkas, Ö., Foresman, J. B., Ortiz, J. V., Cioslowski, J. & Fox, D. J. Gaussian, Inc., Wallingford CT, 2009.
42. GaussView, Version 5, Dennington, Roy; Keith, Todd; Millam, John. Semichem Inc., Shawnee Mission, KS, 2009.
43. Hanwell, M. D., Curtis, D. E., Lonie, D. C., Vandermeersch, T., Zurek, E. & Hutchison, G. R. Avogadro: an advanced semantic chemical editor, visualization, and analysis platform. *J Cheminform.* **4**, 1-17 (2012).
44. Avogadro: an open-source molecular builder and visualization tool, version 1.1.1; <http://avogadro.openmolecules.net/>.

45. CYLview, 1.0b; Legault, C. Y., Université de Sherbrooke, 2009
(<http://www.cylview.org>).

Chapter 3

Laying Bare the Secrets of Diels-Alder
Biocatalysis: A Computational Study of LovB, a
Diels-Alderase involved in Lovastatin
Biosynthesis

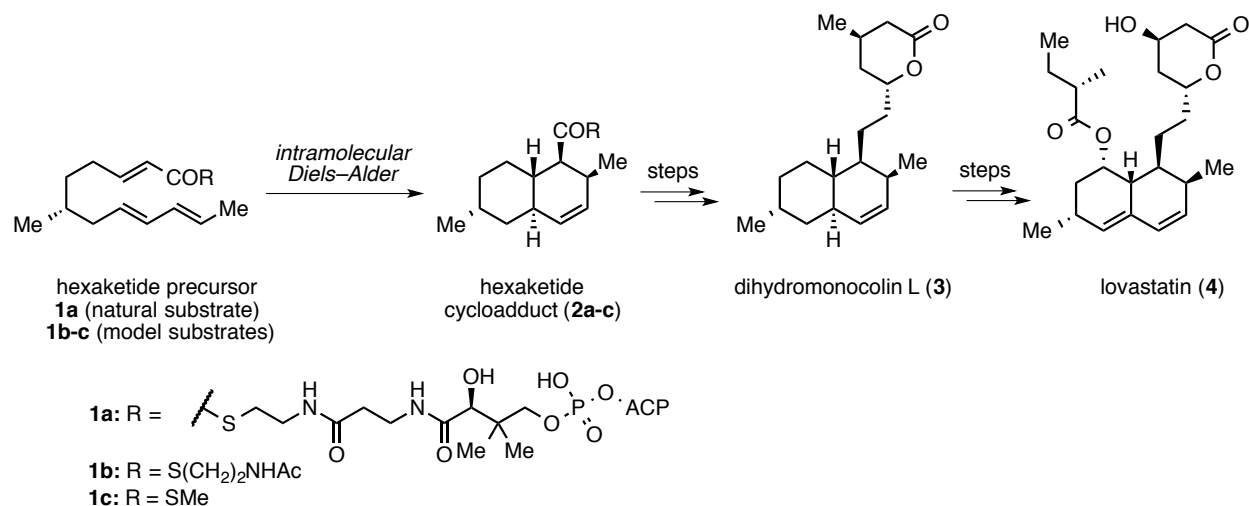
ABSTRACT

We computationally modeled various aspects of the enzymatic intramolecular Diels-Alder reaction involved in the biosynthesis of lovastatin using the M06-2X/6-31+G(d,p) level of theory. These computations quantitatively reproduce the experimental selectivity of a model intramolecular Diels-Alder reaction used to demonstrate the existence of a Diels-Alderase for this process. According to theory, a proposed 1,3-diaxial interaction at the transition state is, indeed, responsible for the intrinsic stereoselectivity of the cycloaddition. The reactive conformer of substrate leading to the product of the enzymatic cycloaddition is 5 kcal mol⁻¹ higher in free energy than the most stable conformer of the hexaketide precursor modeled computationally. Therefore, the con domain by preorganizing the substrate in this geometry could accelerate the reaction by at least ~10³-fold.

INTRODUCTION

The biosyntheses of a growing number of natural products are now known or speculated to involve Diels-Alder cycloadditions. In many cases, these transformations are known or believed to be enzyme-catalyzed.¹⁻⁴ Delineating the mechanisms of these reactions and the mode of enzyme catalysis is of significant interest to chemists seeking to design biomimetic catalysts. Vederas and Tang have reported that an enzymatic intramolecular Diels-Alder reaction forms of the decalin moiety of lovastatin. The enzyme responsible for catalysis is lovastatin nonaketide synthase (LNKS or LovB), a polyketide (mega)synthase. LovB possesses a condensation (con) domain that has been demonstrated as necessary for catalysis of the observed intramolecular Diels-Alder cycloaddition.⁵⁻⁷ Little is known about the molecular basis of the *con* domain's Diels-Alderase activity, although mutational evidence gathered by our collaborator, Dr. Yi Tang (UCLA), suggests a conserved sequence (a HXXGH motif) of residues of may be important for

catalyst. A crystal structure of the *apo* form of the con domain confirms that these residues are found within a cavity.⁸ We report density functional theory (DFT) computations performed – u



sing the M06-2X/6-31+G(d,p) model chemistry – to determine the mechanism, energetics, and transition structures of a thermal cycloaddition closely related to the biosynthetic process.

Scheme 3.1. Enzymatic intramolecular Diels-Alder reaction involved in lovastatin biosynthesis.

RESULTS AND DISCUSSION

Vederas *et al.* have determined that the uncatalyzed thermal cycloaddition an analogue of the enzymatic substrate, **1b**, is has an outcome that is stereodivergent from the enzymatic reaction. To determine the structures and energies of these transition states, we modeled the Diels-Alder reaction of truncated hexaketide **1c** using the M06-2X/6-31+G(d,p) model chemistry. The results of this work are summarized in Figure 3.1. The lowest energy modes of [4+2] cycloaddition, proceeding through **TS6c_{endo2}** and **TS7c_{exo2}**, both have almost identical free energies of activation (ca. 23 kcal mol⁻¹). These transition states correspond to modes of cycloaddition that lead to the observed stereoproducts of the reaction of **1b**, namely adducts **6b** and **7b**. The stereoselectivity of the thermal Diels-Alder reaction is controlled by the disposition

of the C6 methyl group found on the aliphatic tethers of **TS6c_{endo1}** and **TS7c_{exo1}**. These tethers preferentially adopt a chair-like arrangement in the computed transition structures, disposing the C6 methyl substituent in either a pseudoequatorial or a pseudoaxial position. **TS2c_{endo1}** and **TS5c_{exo1}** feature this methyl substituent in a pseudoaxial position, which introduces destabilizing a 1,3-diaxial-like interaction in these transition structures (see Figure 3.1). This clash – occurring between a methyl and methylene group – is most severe in **TS5c_{exo1}**, explaining why this transition state is the least stable.

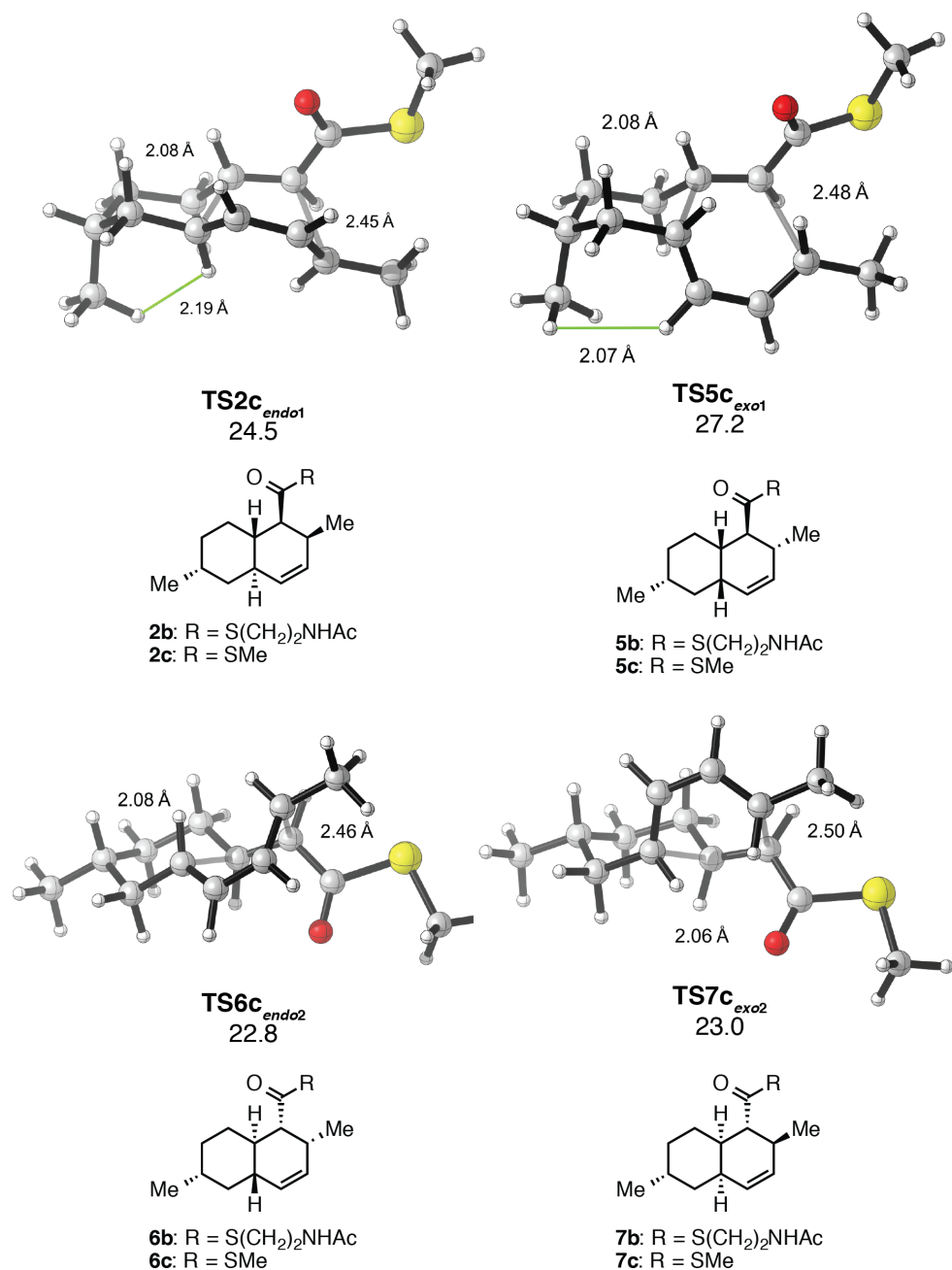


Figure 3.1. QM-optimized transition structures and ΔG^\ddagger of Diels-Alder reaction of **1c**. Energies in kcal mol⁻¹. Products **6b** and **7b** are the observed product of the nonenzymatic (thermal) Diels-Alder reaction of **1c**. The enzymatic product features the same stereochemistry as adducts **2b** and **2c**.

We have determined the electronic structure and energy of the reactive conformer of **1c** (shown as **1c-rc** in Figure 3.2) that leads to product of the enzyme-catalyzed Diels-Alder reaction. This conformer is 5.4 kcal mol⁻¹ less stable than the global minimum conformer. Based on this value, we can estimate that the con domain could enhance the rate of reaction by approximately a 1000-fold (at 298.15 K) by simply pre-organizing the substrate in the conformation shown in Figure 3.2. Based on the computed energetics of the nonenzymatic cycloaddition, the reaction free energy barrier would be reduced from 21.1 kcal mol⁻¹ (as shown in Figure 3.1) to 15.7 kcal mol⁻¹, corresponding to a $t_{1/2}$ of 0.4 s⁻¹.

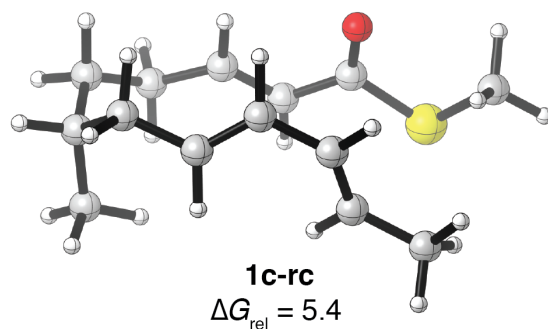


Figure 3.1. QM-optimized structure of the reactive conformer leading to the *endo* product of the enzymatic cycloaddition and its free energy relative to that of the most state substrate conformer. Energies in kcal mol⁻¹.

COMPUTATIONAL METHODS

Quantum mechanical computations

Quantum mechanical computations were performed using the M06-2X⁹ density functional and the 6-31+G(d,p) basis set using *Gaussian09*.¹⁰ Geometry optimizations of all stationary points were followed by frequency calculations. Normal mode analysis of calculated vibrations were used to confirm stationary points as minima or first-order saddle points. For all

geometry optimization and frequency calculations, the default integration grid consisting of 75 radial shells and 99 angular points per shell was used. Thermal corrections were determined using unscaled M06-2X/6-31+G(d,p) frequencies assuming a standard state of 1 atm and 298.15 K. Errors in the computed vibrational entropies were “corrected” using Truhlar’s quasiharmonic approximation.^{11,12} The electronic energies of the M06-2X/6-31+G(d,p) stationary points were recomputed using M06-2X/def2-TZVPP^{13,14} single point energy calculations. These single point energy calculations were performed using an ultrafine integration grid, having 99 radial shells each with 590 angular grid points. The free energy values reported herein were determined by adding the M06-2X/6-31+G(d,p) zero-point energy and thermal corrections to the /M06-2X/def2-TZVPP electronic energies. Images were made using CYLView.¹⁵ Input files were prepared using Gaussview 5¹⁶ and Avogadro V1.1.^{17,18}

Conformational Analysis

The conformers of **1c** were sampled using the following protocol. Conformers of these structures were initially sampled using mixed low-mode/molecular mechanics Monte Carlo (LM/MMMC) simulations.^{19,20} These simulations were performed using Macromodel (V 10.6)²¹ and Maestro software (V 10.0.013).²² For all simulations, 14,000 Monte Carlo steps were performed; minimizations were performed using the Polak-Ribiere conjugate gradient (PRNG) minimization scheme²³ (5000 cycles) with a gradient-based convergence criterion of 0.0012 kcal mol⁻¹ Å⁻¹ (0.005 kJ mol⁻¹ Å⁻¹). Conformers differing in maximum atomic deviation by at least 0.5 Å were considered unique. Unique structures with energies within 25 kcal mol⁻¹ of the global minimum were included in the conformer library. The 20 lowest energy structures were re-optimized at the M06-2X/6-31+G(d,p) level. Subsequently, thermal corrections for these minima were determined by performing M06-2X/6-31+G(d,p) frequency computations.

REFERENCES

- (1) Stocking, E. M.; Williams, R. M. *Angew. Chem. Int. Ed.* **2003**, *42*, 3078–3115.
- (2) Oikawa, H. *Bull. Chem. Soc. Jpn.* **2005**, *78*, 537–554.
- (3) Kelly, W. L. *Org. Biomol. Chem.* **2008**, *6*, 4483–4493.
- (4) Kim, H. J.; Ruzsyczky, M. W.; Liu, H.-W. *Curr. Opin. Chem. Biol.* **2012**, *16*, 124–131.
- (5) Witter, D. J.; Vederas, J. C. *J. Org. Chem.* **1996**, *61*, 2613–2623.
- (6) Auclair, K.; Sutherland, A.; Kennedy, J.; Witter, D. J.; Van den Heever, J. P.; Hutchinson, C. R.; Vederas, J. C. *J. Am. Chem. Soc.* **2000**, *122*, 11519–11520.
- (7) Ma, S. M.; Li, J. W. H.; Choi, J. W.; Zhou, H.; Lee, K. K. M.; Moorthie, V. A.; Xie, X.; Kealey, J. T.; Da Silva, N. A.; Vederas, J. C.; Tang, Y. *Science*. **2009**, *326*, 589–592.
- (8) Tang, Y.; et al. unpublished data.
- (9) Zhao, Y.; Truhlar, D. G. *Theor. Chem. Acc.* **2008**, *120*, 525–525.
- (10) Gaussian 09, Revision D.01, Frisch, M. J.; Trucks, G. W.; Schlegel, H. B.; Scuseria, G. E.; Robb, M. A.; Cheeseman, J. R.; Scalmani, G.; Barone, V.; Mennucci, B.; Petersson, G. A.; Nakatsuji, H.; Caricato, M.; Li, X.; Hratchian, H. P.; Izmaylov, A. F.; Bloino, J.; Zheng, G.; Sonnenberg, J. L.; Hada, M.; Ehara, M.; Toyota, K.; Fukuda, R.; Hasegawa, J.; Ishida, M.; Nakajima, T.; Honda, Y.; Kitao, O.; Nakai, H.; Vreven, T.; Montgomery, J. A., Jr.; Peralta, J. E.; Ogliaro, F.; Bearpark, M.; Heyd, J. J.; Brothers, E.; Kudin, K. N.; Staroverov, V. N.; Kobayashi, R.; Normand, J.; Raghavachari, K.; Rendell, A.; Burant, J. C.; Iyengar, S. S.; Tomasi, J.; Cossi, M.; Rega, N.; Millam, J. M.; Klene, M.; Knox, J. E.; Cross, J. B.; Bakken, V.; Adamo, C.; Jaramillo, J.; Gomperts, R.; Stratmann, R. E.; Yazyev, O.; Austin, A. J.; Cammi, R.; Pomelli, C.; Ochterski, J. W.; Martin, R. L.; Morokuma, K.; Zakrzewski, V. G.; Voth, G. A.; Salvador, P.;

Dannenberg, J. J.; Dapprich, S.; Daniels, A. D.; Farkas, Ö.; Foresman, J. B.; Ortiz, J. V.; Cioslowski, J.; Fox, D. J. Gaussian, Inc., Wallingford CT, 2009.

(11) Zhao, Y.; Truhlar, D. G. *Phys. Chem. Chem. Phys.* **2008**, *10*, 2813–2818.

(12) Ribeiro, R. F.; Marenich, A. V.; Cramer, C. J.; Truhlar, D. G. *J. Phys. Chem. B.* **2011**, *115*, 14556–14562.

(13) Weigend, F.; Ahlrichs, R. *Phys. Chem. Chem. Phys.* **2005**, *7*, 3297–3305.

(14) Weigend, F. *Phys. Chem. Chem. Phys.* **2006**, *8*, 1057–1065.

(15) CYLview, 1.0b; Legault, C. Y., Université de Sherbrooke, 2009
(<http://www.cylview.org>)

(16) GaussView, Version 5, Dennington, R.; Keith, T.; Millam, J. Semichem Inc., Shawnee Mission KS, 2009.

(17) Hanwell, M. D.; Curtis, D. E.; Lonie, D. C.; Vandermeersch, T.; Zurek, E.; Hutchinson, G. R. *J. Cheminform.* **2012**, *4*, 1–17.

(18) Avogadro: an open-source molecular builder and visualization tool. Version 1.0.1.
<http://avogadro.openmolecules.net/>.

(19) Kolossvary, I.; Guida, W. C. *J. Am. Chem. Soc.* **1996**, *118*, 5011–5019.

(20) Kolossvary, I.; Guida, W. C. *J. Comput. Chem.* **1999**, *20*, 1671–1684.

(21) Schrödinger Release 2014-4: MacroModel, version 10.6, Schrödinger, LLC, New York, NY, **2014**.

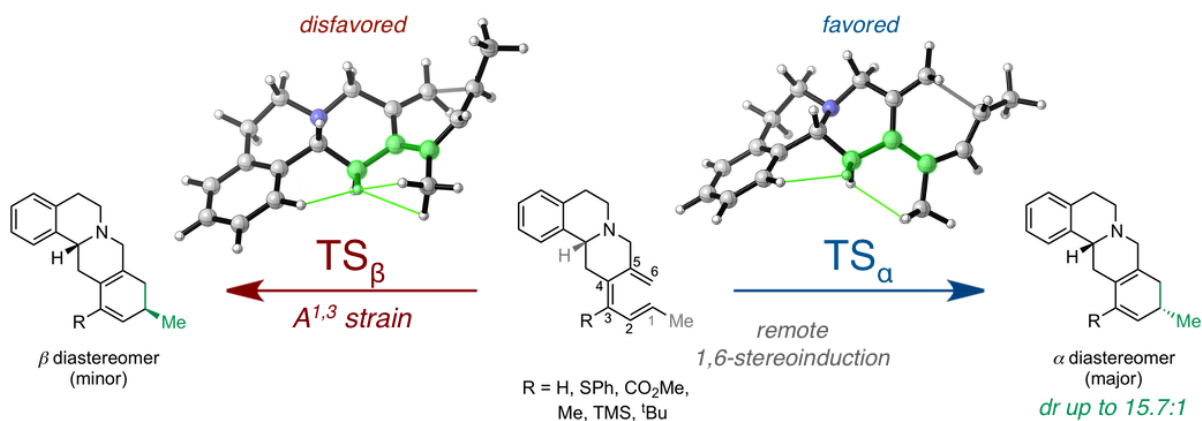
(22) Schrödinger Release 2014-4: Maestro, version 10.0.013, Schrödinger, LLC, New York, NY, **2014**.

(23) Polak, E.; Ribiere, G. *Francaise Informat. Recherche Operationnelle, Serie Rouge.* **1969**, *16*, 35.

Chapter 4

Origins of 1,6-Stereoinduction in Torquoselective 6π Electrocyclizations

Patel, A.; Barcan, G. A.; Kwon, O.; Houk, K. N. *J. Am. Chem. Soc.*
2013, *135*, 4878–4883.



ABSTRACT

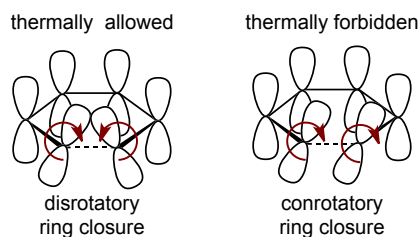
A novel stereoselective electrocyclic ring closure developed for the total synthesis of reserpine has been explored by both experiment and computation. A stereocenter 6 atoms away from the newly forming chiral center is responsible for the diastereoselectivity of this ring closure. This stereogenic center – lying at the junction of two 6-membered rings – defines the conformation of the substrates' fused ring skeleton that ultimately distinguishes between the two allowed, disrotatory triene geometries at the transition state. The presence of allylic strain in the disfavored transition state results in a torquoselective ring closure (d.r. up to 15.7:1).

INTRODUCTION

The 6π electrocyclizations of hexatrienes were an impetus for the formulation of the ground-breaking orbital symmetry rules formulated by Woodward and Hoffmann.¹ The orbital symmetry rules predict that the thermal 6π electrocyclic ring closure is disrotatory, while the photochemical process is conrotatory. (Scheme 4.1).²

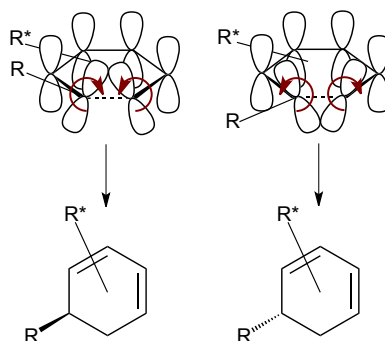
Two modes of disrotation exist for all thermal 6π electrocyclizations. For a chiral substrate, these two disrotatory modes of electrocyclic ring closure yield diastereomeric products. If one

diastereomer is formed preferentially, such a ring closure is said to be torquoselective (Scheme 4.2).^{3,4}



Scheme 4.1. Disrotatory and conrotatory modes for the electrocyclic ring closure of 1,3,5-hexatriene.

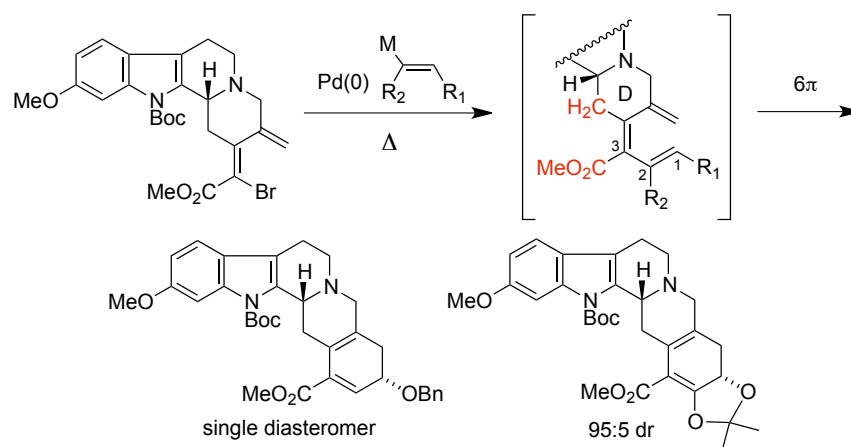
While the orbital symmetry rules clearly explain that thermal 6π electrocyclizations must occur through disrotation, it is less clear what specific factors control the preference for one disrotatory mode of 6π electrocyclic ring closure over the other. Examples of the torquoselective thermal 6π electrocyclization of hexatrienes date back to 1963,⁵ and many examples have been reported since then.⁶⁻¹³ However, in many cases the origins of stereoselectivities in these examples remain unclear.



Scheme 4.2. The two disrotatory modes of electrocyclization of a chiral hexatriene.

We recently reported an approach to the reserpine alkaloids based upon a highly torquoselective thermal 6π electrocyclization.¹⁴ Pentacyclic structures were prepared with

extremely high levels of selectivity by employing a tandem cross-coupling/electrocyclization protocol that relied on a remote stereocenter to induce a diastereoselective ring closure (Scheme 4.3). Intrigued by the high levels of selectivity observed in these reactions, we explored the scope of this chemistry computationally. Initial results suggested that the methyl ester at the 3-position of the triene could be engaged in allylic strain with the adjacent D-ring methylene. We proposed that varying the steric bulk of groups at the 3-position would have a significant impact on the diastereoselectivity of the electrocyclization. Herein, we report our experimental and computational efforts toward determining the origins of this remote 1,6-stereinduction.



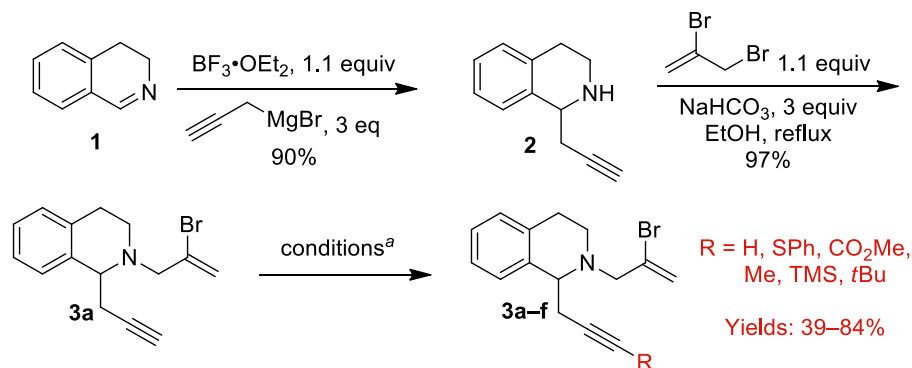
Scheme 4.3. 1,6 stereinduction in a 6 π electrocyclization approach to reserpine alkaloids.

RESULTS AND DISCUSSION

Synthesis and Electrocyclization of Trienes

In order to assess the effect of substituent size on the electrocyclization reaction, we envisioned an expedient route to several trienes with variations in the size of the functional groups at the 3-position. Our synthetic plan began with the addition of propenylmagnesium bromide to the BF₃-complexed dihydroisoquinoline **1** (Scheme 4.4). Alkylation of amine **2**

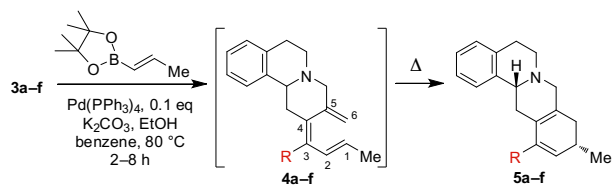
provided enyne **3a** that was functionalized at the alkyne terminus with groups of varying steric requirement. We then prepared and studied the electrocyclization of six distinct trienes derived from the tandem carbopalladation/cross-coupling of enynes **3a–f** (Table 4.1).



Scheme 4.4. Synthesis of key enynes **3a–f**.

The tandem carbopalladation/Suzuki coupling sequence generated the corresponding trienes, which upon heating provided the 6π electrocyclization products. Table 1 provides experimental diastereoselectivities and the A-values of the C3 substituent, as a measure of size, for each triene examined. All of the electrocyclizations took place at 120 °C in xylenes, except for R = CO₂Me and R = TMS which underwent cyclization in the cross-coupling reaction at 80 °C. Starting with the smallest substituent, R = H (Table 4.1), we observed an increase in the diastereomeric ratio from 3.5:1 to 6.7:1 for R = SPh and then to 15.7:1 and 13.3:1 for R = CO₂Me and R = Me respectively. The diastereomeric ratio is greater for the reaction of triene **4c** (R = CO₂Me) compared to the ring closure of **4d** (R = Me) due to differences in reaction temperature; however, the experimentally determined $\Delta\Delta G^\ddagger$ is larger for the triene **4d** than **4c**. (*vide infra*). The observation that trienes bearing larger substituents provide greater levels of diastereoselectivity than trienes with smaller substituent is intuitive. Surprisingly, with the larger

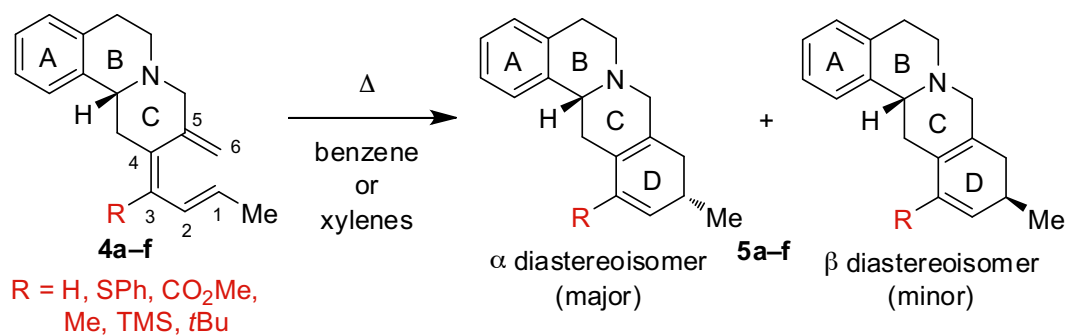
R = TMS and R = *t*Bu substituents, we observe that the diastereomeric ratio decreases to 4.3:1 and 3.2:1, respectively.



enyne (R)	A-value (kcal mol)	6π product (dr) ^{a,b,c}
3a (H)	0	 5a (3.5:1)
3b (SPh)	0.8	 5b (6.7:1)
3c (CO ₂ Me)	1.3	 5c (15.7:1)
3d (Me)	1.7	 5d (13.3:1)
3e (TMS)	2.4	 5c (4.3:1)
3f (<i>t</i> Bu)	>4.5	 5f (3.2:1)

Table 4.1. Synthesis of trienes and experimental diastereoselectivities of electrocyclizations. ^aFor entries 3 and 5 the electrocyclization product was isolated directly from the cross-coupling reaction without isolation of the triene. All other products were generated by subsequent heating of the isolated triene at 120 °C in xylenes. ^bDiastereomeric ratios determined by ¹H NMR. ^cRelative configuration of the new stereogenic center assigned by analogy to a crystal structure of a pentacyclic reserpine precursor (see SI).¹⁴

Computational Results



Scheme 4.5. The six model systems examined computationally.

The electrocyclizations of trienes **4a–f** are all highly exergonic with ΔG_{rxn} ranging from –18 kcal mol⁻¹ for the reaction of triene **4a** to –27 kcal mol⁻¹ for the reaction of triene **4f**. Consequently, the stereoselectivity observed experimentally is due to differences in the energies of the two electrocyclic transition states. The activation energies for this series of electrocyclization reactions are approximately 30 kcal mol⁻¹ and is consistent with the elevated temperatures required experimentally for efficient ring closure. However, the barriers of the electrocyclic ring closures of trienes **4e** and **4f** are lower ($\Delta G^\ddagger = 26$ kcal mol⁻¹) than those for the electrocyclizations of **4a–d**. The computed and experimentally determined energy differences between the lowest energy conformers of the α and β transition states for electrocyclization of **4a–f** are listed in Table 4.2.

triene (R)	A Value (kcal mol ⁻¹)	Comp. ^a $\Delta\Delta H^\ddagger$ ($\Delta\Delta G^\ddagger$) (kcal mol ⁻¹)	Comp. ^b $\Delta\Delta H^\ddagger$ ($\Delta\Delta G^\ddagger$) (kcal mol ⁻¹)	Expt. $\Delta\Delta G^\ddagger$ (kcal mol ⁻¹)
4a (H)	0	0.8 (0.8)	1.0 (1.0)	1.0
4b (SPh)	0.8	-0.3 (0.1)	0.3 (0.8)	1.5
4c (CO ₂ Me)	1.2	1.6 (1.4)	1.6 (1.4)	1.9
4d (Me)	1.7	2.3 (2.4)	2.4 (2.5)	2.0
4e (TMS)	2.4	1.2 (1.3)	1.5 (1.6)	1.0
4f (<i>t</i> Bu)	>4.5	-0.2 (-0.7)	-0.1 (-0.7)	0.9

Table 4.2. A-values of C3 substituents, computed $\Delta\Delta H^\ddagger$ and $\Delta\Delta G^\ddagger$, and experimental $\Delta\Delta G^\ddagger$ values. ^aGas phase M06-2X/6-31+G(d,p) energies. ^b Gas phase M06-2X/def2-TZVPP//M06-2X/6-31+G(d,p) energies.

In general, computed selectivities for this series of electrocyclic reactions are in reasonable agreement with experiment, although we are not able to reproduce the experimental selectivity of the reaction of triene **4f** (R = *t*Bu). As shown in Table 4.2, computations overestimate the diastereoselectivity of the electrocyclizations of trienes **4c**, **4d**, and **4e** and underestimate the selectivities of the electrocyclic reactions of **4b** and **4f**. The mean absolute deviation (MAD) between the computed $\Delta\Delta G^\ddagger$ and corresponding experimental values is 0.6 kcal mol⁻¹ for this series of electrocyclizations.

For the reactions of **4a**, **4c**, and **4d** a simple relationship between the steric bulkiness of the C3 substituent, as measured by A-values, and selectivity exists. Triene **4a**, bearing only a hydrogen atom at C3, undergoes ring closure with little diastereoselectivity ($\Delta\Delta G^\ddagger = 1.0$ kcal mol⁻¹). Trienes **4c** and **4d** with ester and methyl substituents, respectively, yield more highly selective electrocyclizations ($\Delta\Delta G^\ddagger = 1.5$ - 1.9 kcal mol⁻¹). Despite the relative bulkiness of TMS

and *t*Bu, the electrocyclization of trienes **4e** and **4f** are not very selective, according to experiment and suggests that the neither the α nor the β transition state can effectively accommodate the extremely bulky C3 substituents like TMS or *t*Bu.

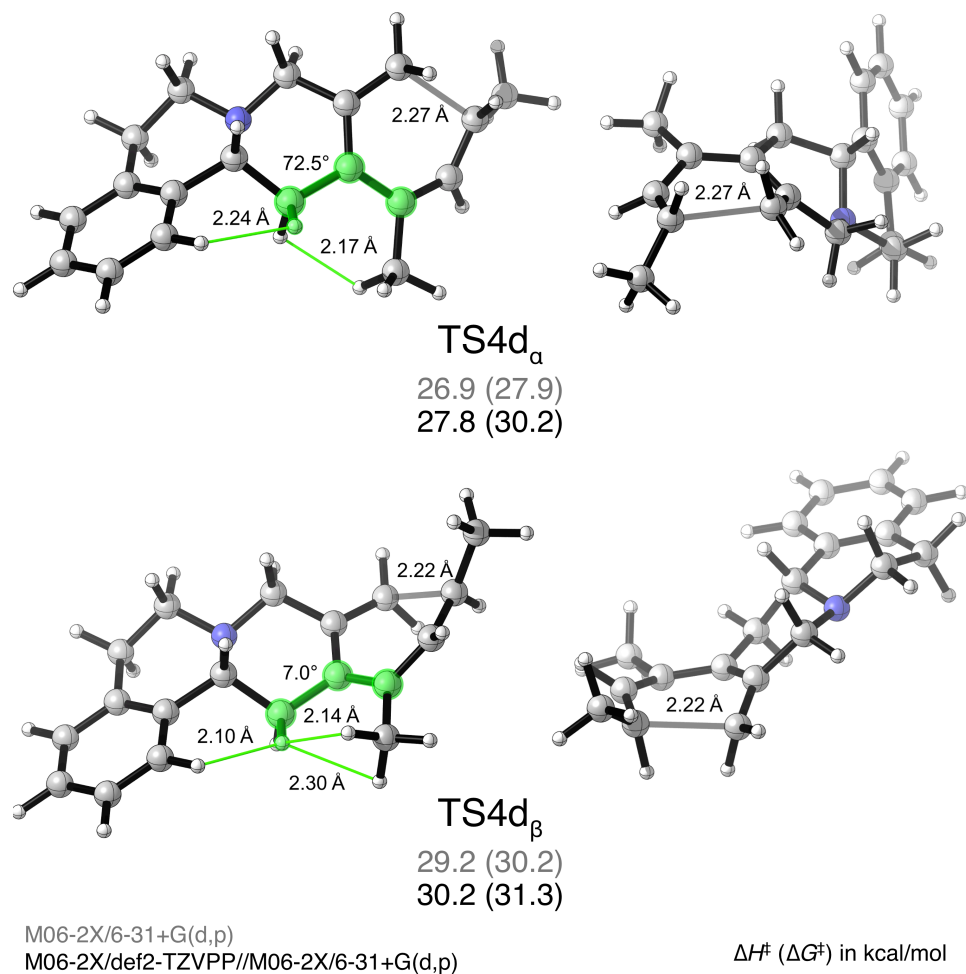


Figure 4.1. Top and front views of the α and β disrotatory transition states of the electrocyclic reactions of triene **4**, optimized using M06-2X/6-31+G(d,p) *in vacuo*.

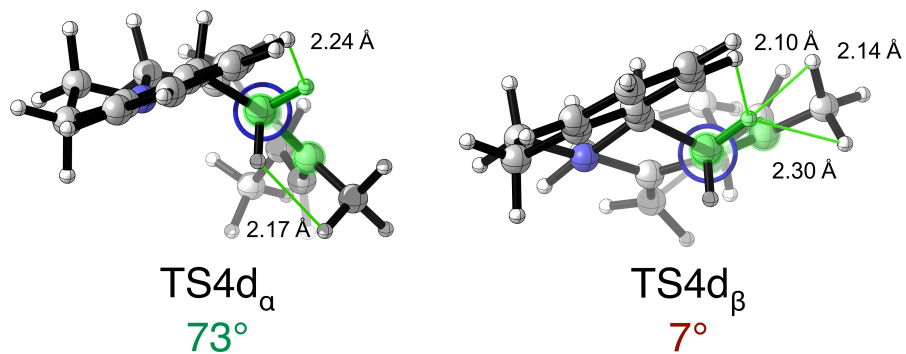


Figure 4.2. Newman projections of TS4d_α and TS4d_β , highlighting the allylic strain present in the disfavored transition state.

Transition states TS4d_α and TS4d_β of the electrocyclozation of triene **4d** are shown in Figure 4.2. The triene adopts a boat-like geometry in the disrotatory transition structures, and the two modes of ring closure can be viewed on the right side of Figure 4.1. In the favored TS4d_α , the C-terminal methyl group rotates downward through a “concave down” boat geometry. The key difference between the two transition states can be found in the dihedral highlighted in green in Figure 4.2. This dihedral angle is nearly planar (7°) in the disfavored transition structure (TS4d_β), and more staggered (73°) in the lower-energy TS4d_α . The Newman projections of TS4d_α and TS4d_β in Figure 4.2 show more clearly this difference between the two transition structures. The planar arrangement in TS4d_β introduces allylic strain in this transition state between the C3 substituent and the methylene hydrogens of the piperidine (highlighted). This effect includes contributions from steric clashes between the piperidine hydrogen (highlighted) and the methyl group as well as torsional strain between the two coplanar bonds.

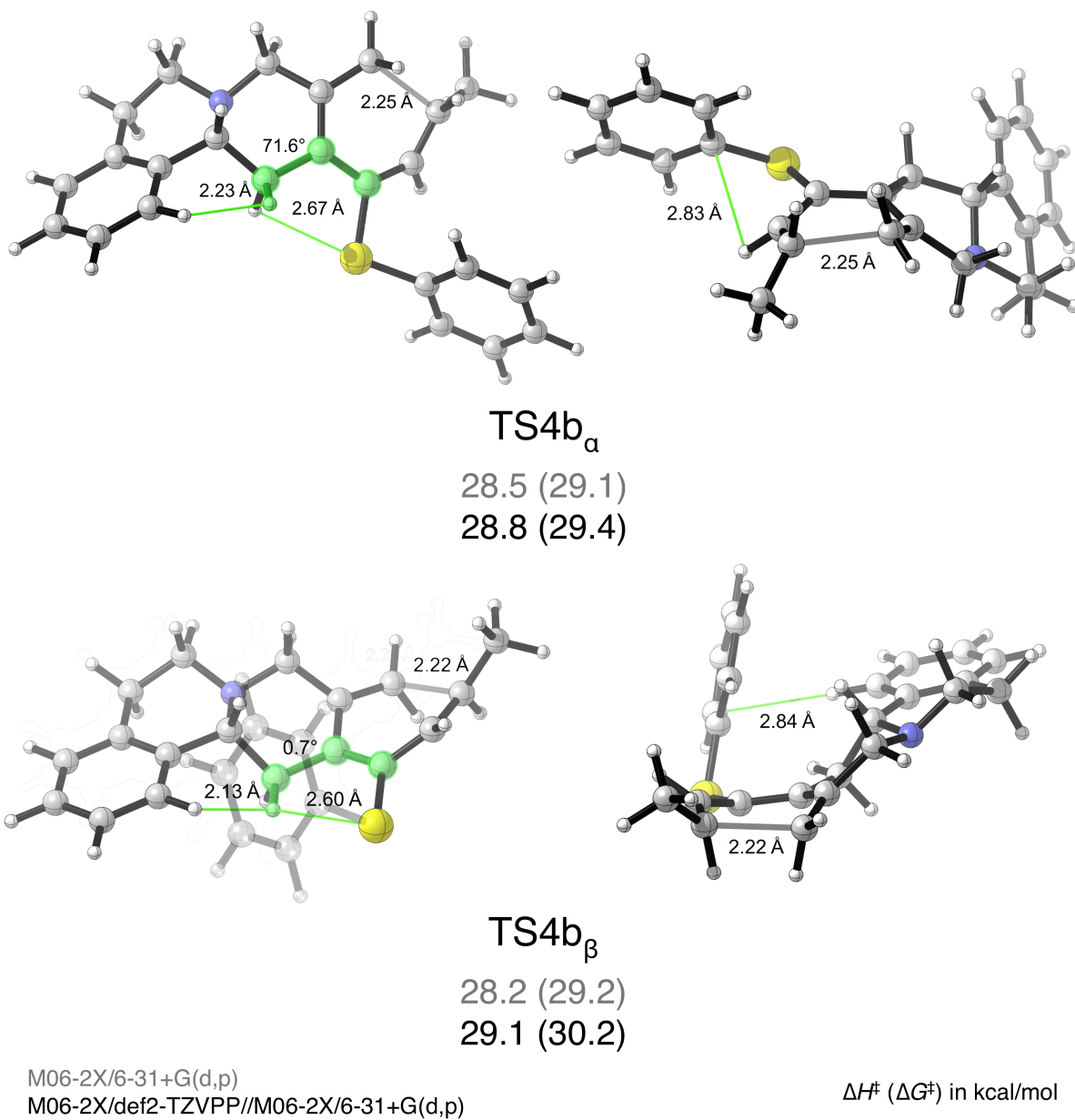


Figure 4.3. Top and front views of the α and β disrotatory transition states of the electrocyclic reaction of triene **4b** optimized using M06-2X/6-31+G(d,p) *in vacuo*. Note the *S*-phenyl group is made transparent for clarity where necessary.

The electrocyclic reactions of tricyclic trienes **4b** and **4f** merit further discussion, as factors beside allylic strain are also important in explaining the torquoselectivity of these ring closings. Triene **4b** possesses a flexible thiophenyl substituent at the C3 position of the triene,

introducing the possibility that several rotameric α and β transition states exist. The lowest energy transition state rotamers leading to the α and β diastereomers, **TS4b _{α}** and **TS4b _{β}** , respectively, are shown in Figure 4.3. **TS4b _{α}** is 0.8 kcal mol⁻¹ lower in free energy than **TS4b _{β}** according to the large basis set calculations. This $\Delta\Delta G^\ddagger$ is smaller than 1.5 kcal mol⁻¹ value observed experimentally. The difference in the corresponding H-C-C-C dihedral between **TS4b _{α}** and **TS4b _{β}** is even larger than that of **TS4d _{α}** and **TS4d _{β}** , as the dihedral angle in **TS4b _{β}** is 0.7° presumably because thiophenyl substituent is conjugated with the triene in this structure. Allylic strain in **TS4b _{β}** may, however, be attenuated by electrostatic attraction between the electronegative sulfur atom and the positively charged hydrogen atom; however, torsional strain will still destabilize **TS4b _{β}** relative to **TS4b _{α}** .

TS4b _{α} and **TS4b _{β}** are both stabilized by intramolecular C-H π interactions that could provide stabilization by dispersion. In **TS4b _{α}** the C-H interaction occurs between the *S*-phenyl group and the C2 hydrogen of the triene (2.85 Å). A similar interaction occurs in **TS4b _{β}** between *S*-phenyl group and an aromatic hydrogen of the aromatic A ring (2.84 Å). Because the reactions are performed in xylenes, the solvent may be competing with the *S*-phenyl group for these weak interactions in such way that the two transition states may not be differentially stabilized. In order to estimate the selectivity that would exist in the absence of these intramolecular dispersion interactions, we replaced the phenyl group with a hydrogen atom or methyl group and performed single point energy calculations on these structures. $\Delta\Delta E$ between these model trienes are 5.9 and 4.9 kcal mol⁻¹, respectively, favoring the formation of the α -diastereomer.

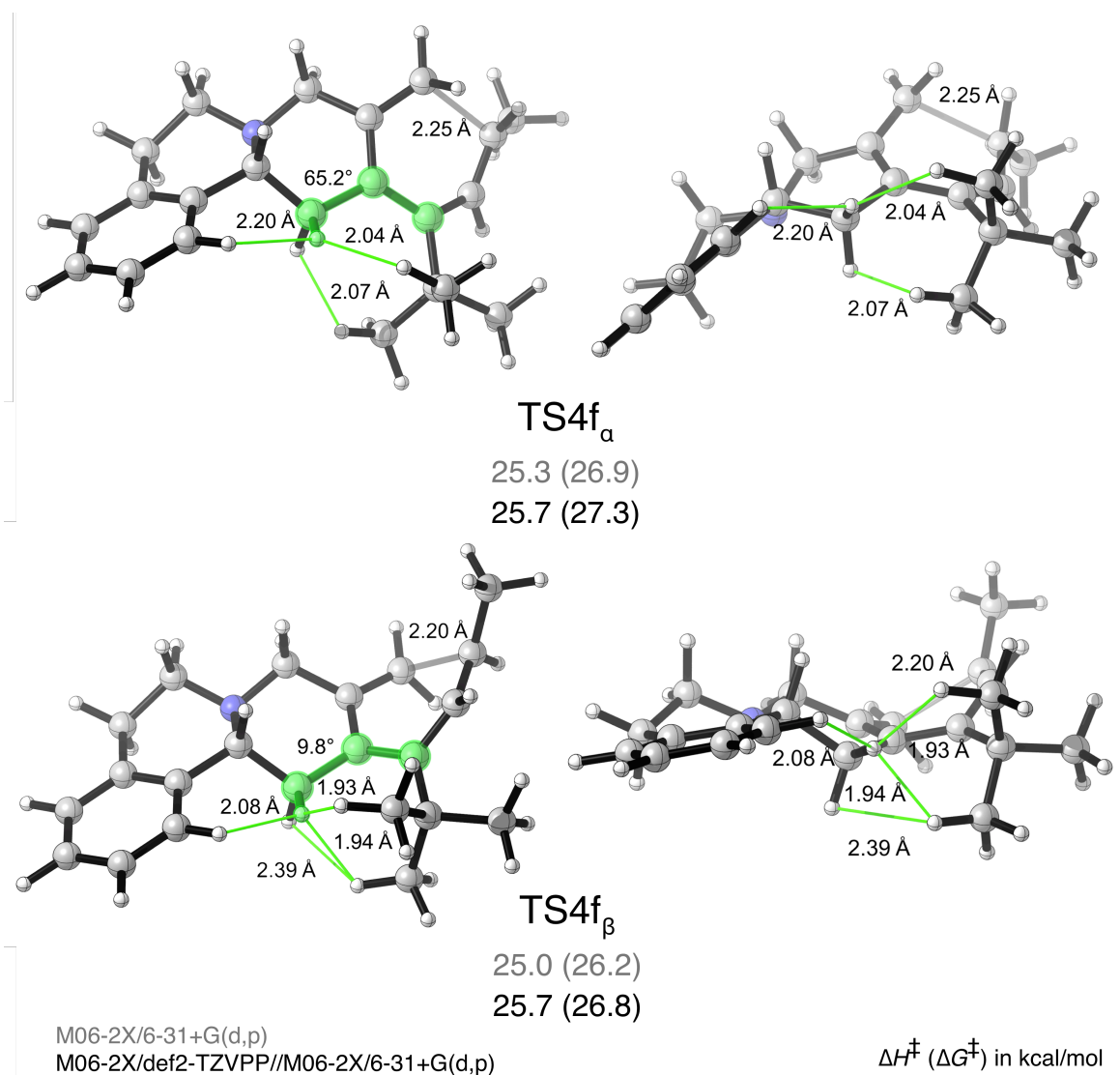


Figure 4.4. Top and back views of the α and β disrotatory transition states of the electrocyclic reaction of triene **4d** optimized using M06-2X/6-31+G(d,p) *in vacuo*.

According to computations, the reaction of **4f** proceeds with a ΔG^\ddagger of 25 kcal mol⁻¹ and a ΔG_{rxn} of -27 kcal mol⁻¹. These values are similar to corresponding values determined for the reaction of **4e**. In comparison to the electrocyclizations of trienes **4a–d**, **4e** and **4f** undergo ring closures with a 3–5 kcal mol⁻¹ lower barrier and are also 3–7 kcal mol⁻¹ more exergonic. The lower barrier and the increased exergonicity of the electrocyclizations of both **4e** and **4f** is due to a decrease in steric demand for the *t*Bu group as the reactant progresses along the reaction

coordinate toward the product. Computations also indicate that the electrocyclic reaction of triene **4f** (R = *t*Bu) is essentially nonselective, with a slight preference for β stereoisomer (minor product). Illustrated in Figure 4.4 are the α and β transition states for this electrocyclization. Both **TS4f $_{\alpha}$** and **TS4f $_{\beta}$** suffer from a number of steric clashes, some of which are quite severe and range in terms of interatomic (H–H) distances from 1.94 Å to 2.07 Å. The introduction of additional steric clashes in the α transition state of **4f** leads to the erosion of selectivity.

Origins of Differential Allylic Strain in Electrocyclization Transition States of Trienes 1-6

The piperidine ring (C-ring, Scheme 4.5) directly fused to the triene discriminates between the two modes of disrotation. This ring prefers to adopt a half-chair conformation, which places the hydrogen at the stereocenter in an axial position. Overlaying the piperidine rings (heavy atoms only) of the α and β transition structures (**TS4 $_{\alpha}$** and **TS4 $_{\beta}$**) reveals the conformations of this heterocycle in either transition state are nearly identical (RMSD 0.17 Å).

How does this piperidine ring cause the two disrotatory modes to have different energies? In the α transition states, the triene adopts "concave-down" boat geometry. This arrangement places the C3 substituent (see Figure 4.1 and 4.2) between the pseudoaxial and pseudoequatorial hydrogens of the piperidine ring. Eclipsing strain is avoided as the C3–C4 bond of the triene also lies between these hydrogens. In the β transition states, the triene features a "concave-up" boat that forces the C3–C4 bond into the plane of pseudoequatorial C–H bond (Figure 4.1 and 4.2), introducing eclipsing strain as well as allylic strain between the C3 substituent and the pseudoequatorial hydrogen.

Remote stereoiduction in this manifold is only possible because the triene adopts one of two well-defined, clearly distinguishable boat-like geometries (i.e., "concave up" or "concave down") at the transition state. These boat-like transition states are relatively rigid due to the strict

orbital requirements at the transition state.¹⁸ Overlays of the triene portions of **TS4a_β** – **TS4f_β** confirm this recalcitrance towards distortion as the triene geometries are conserved throughout the series of trienes, even for **TS4e_β** (R= TMS) and **TS4f_β** (R = *t*Bu).

CONCLUSIONS

We have explored the torquoselective 6π electrocyclizations of a series of isoquinoline-derived trienes featuring varying functionality at the 3-position of the triene experimentally and computationally. For the electrocyclic ring closures of the six trienes examined, there is a qualitative agreement between the computation and experiment. The observed diastereoselectivities for this series of trienes is sensitive to substitution at the C3 position of the triene. Trienes bearing moderately bulky substituents like methyl or methyl ester at this position undergo the 6π electrocyclization reaction with the greatest levels of diastereoselectivity, whereas trienes with more bulky C3 substituents like R = TMS or R = *t*Bu undergo a much less stereoselective ring closing. Our results also illustrate that the conformation of the piperidine ring (C-ring) in conjunction with the strict geometric requirements of the triene at the transition state are responsible for the relay of stereochemical information from a distal stereogenic center six atoms away from the forming stereocenter. Allylic strain in the β transition states explains the observed preference for the α diastereomer in this series of electrocyclizations.

COMPUTATIONAL METHODS

All structures examined computationally were initially prepared using Avogadro, a freely-available molecular editor/builder program that includes a constrained force field optimization feature useful in generating reasonable starting geometries for QM optimization.¹⁵ Quantum mechanical calculations were performed using *Gaussian09*.¹⁶ Geometries were initially optimized *in vacuo* using the meta-hybrid density functional M06-2X with the 6-31+G(d,p) basis

set. Normal-mode analysis confirmed that all optimized reactants, intermediates, and products were, indeed, minima, and that all transition states located were first order saddle points. Activation barriers (ΔH^\ddagger and ΔG^\ddagger) were also determined using M06-2X/def2-TZVPP//M06-2X/6-31+G(d,p) single points with thermal corrections determined at the M06-2X/6-31+G(d,p) level of theory; whereas reaction energies (ΔH_{rxn} and ΔG_{rxn}) were only calculated at the M06-2X/6-31+G(d,p) level of theory. All QM calculations were performed using an “ultrafine” numerical integration grid, consisting of 99 radial shells and 590 angular points per shell. Errors in computed entropies introduced by the treatment of low frequency modes as the harmonic motions were corrected by raising all harmonic frequencies below 100 cm^{-1} to exactly 100 cm^{-1} as described by Truhlar.¹⁷ The discussion of stereoselectivity is restricted to only the lowest energy transition state conformers.

AUTHOR CONTRIBUTIONS

A.P. performed the computational work; G.A.B. carried out the experimental work under the supervision of O.K. A.P. and K.N.H analyzed the computational results. All authors contributed to the preparation of this manuscript. All authors have given approval to the final version of the manuscript. [#]These authors (A.P. and G.A.B.) contributed equally.

ACKNOWLEDGMENTS

A.P. and K.N.H. acknowledge the financial support of the NIH (GM-36700 to KNH). A.P. thanks the Chemical-Biology Interface Training Program for its support. The following computational resources were used in this study: the Hoffman2 cluster at UCLA and the Extreme Science and Engineering Discovery Environment (XSEDE) supported by the NSF (OCI-1053575). O.K. and G.A.B. acknowledge funding from the NIH (R01GM071779 and P41GM081282) and the NSF (Equipment Grant CHE-1048804).

REFERENCES

- (1) Woodward, R. B.; Hoffmann, R. *J. Am. Chem. Soc.* **1965**, *87*, 395–397.
- (2) Woodward, R. B.; Hoffmann, R. *Angew. Chem. Int. Ed.* **1969**, *8*, 781–932.
- (3) Rondan, N. G.; Houk, K. N. *J. Am. Chem. Soc.* **1985**, *107*, 2099–2111.
- (4) Kirmse, H.; Rondan, N. G.; Houk, K. N. *J. Am. Chem. Soc.* **1984**, *106*, 7989–7991.
- (5) Corey, E. J.; Hortmann, A. G. *J. Am. Chem. Soc.* **1963**, *85*, 4033–4034.
- (6) Okamura, H. H.; Peter, R.; Reischl, H. *J. Am. Chem. Soc.* **1985**, *107*, 1034–1041.
- (7) Bamba, M.; Nishikawa, T.; Isobe, M. *Tetrahedron Lett* **1996**, *37*, 8199–8202.
- (8) Bamba, M.; Nishikawa, T.; Isobe, M. *Tetrahedron* **1998**, *54*, 6639.
- (9) Tanaka, K.; Katsumura, S. *J. Am. Chem. Soc.* **2002**, *124*, 9660.
- (10) Whitesell, J. K.; Minton, M. A. *J. Am. Chem. Soc.* **1987**, *109*, 6403–6408.
- (11) Benson, C. L. C.; West, F. G. F. *Org. Lett.* **2007**, *9*, 2545–2548.
- (12) E, J. M.; Min, S.-J. *Tetrahedron* **2007**, *63*, 3682–3701.
- (13) Feltenberger, J. B.; Hsung, R. P. *Org. Lett.* **2011**, *13*, 3114–3117.
- (14) Barcan, G. A.; Patel, A.; Houk, K. N.; Kwon, O. *Org. Lett.* **2012**, *14*, 5388–5391.
- (15) Hanwell, M. D.; Curtis, D. E.; Lonie, D. C.; Vandermeersch, T.; Zurek, E.; Hutchison, G. *R. J. Cheminf* **2012**, *4*, 17.
- (16) Frisch, M. J.; Trucks, G. H.; Schlegel, H. B.; Scuseria, G. E.; Robb, M. A.; Cheeseman, J. R.; Scalmani, G.; Barone, V.; Mennucci, B.; Petersson, G. A.; Nakatsuji, H.; Caricato, M.; Li, X.; Hratchian, H. P.; Izmaylov, A. F.; Bloino, J.; Zheng, G.; Sonnenberg, J. L.; Hada, M.; Ehara, M.; Toyota, K.; Fukuda, R.; Hasegawa, J.; Ishida, M.; Nakajima, T.; Honda, H.; Kitao, O.; Nakai, H.; Vreven, T.; Montgomery, J. A.; Peralta, J. E.; Ogliaro, F.; Bearpark, M.; Heyd, J. J.; Brothers, E.; Kudin, K. N.; Staroverov, V. N.; Kobayashi, R.; Normand, J.; Raghavachari, K.;

Rendell, A.; Burant, J. C.; Iyengar, S. S.; Tomasi, J.; Cossi, M.; Rega, N.; Millam, J. M.; Klene, M.; Knox, J. E.; Cross, J. B.; Bakken, V.; Adamo, C.; Jaramillo, J.; Gomperts, R.; Stratmann, R. E.; Yazyev, O.; Austin, A. J.; Cammi, R.; Pomelli, C.; Ochterski, J. H.; Martin, R. L.; Morokuma, K.; Zakrzewski, V. G.; Voth, G. A.; Salvador, P.; Dannenberg, J. J.; Dapprich, S.; Daniels, A. D.; Farkas; Foresman, J. B.; Ortiz, J. V.; Cioslowski, J.; Fox, D. J. *Gaussian 09, Revision C.01* **2009**.

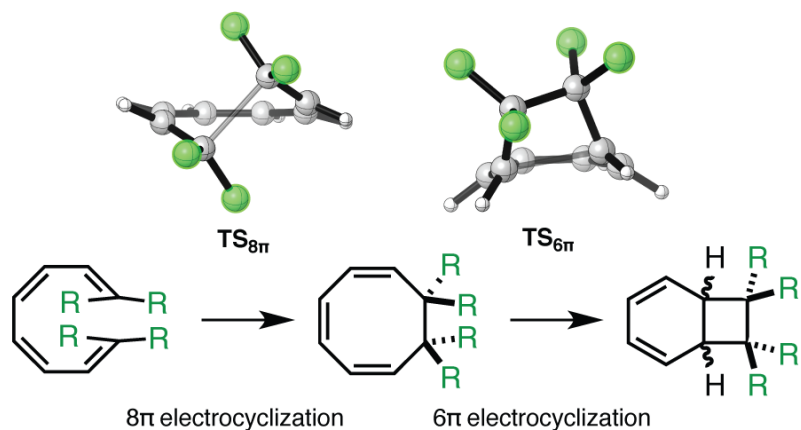
(17) Ribeiro, R. F.; Marenich, A. V.; Cramer, C. J.; Truhlar, D. G. *J. Phys. Chem. B* **2011**, *115*, 14556–14562.

(18) Houk, K. N.; Li, H.; Evanseck, J. D. *Angew. Chem. Int. Ed. Engl.* **1992**, *31*, 682–708.

Chapter 5

Terminal Substituent Effects on Reactivity, Thermodynamics, and Stereoselectivity of the 8π - 6π Electrocyclization Cascades of 1,3,5,7- Tetraenes

Patel, A.; Houk, K. N. *J. Org. Chem.* **2014**, *79*, 11370–11377.



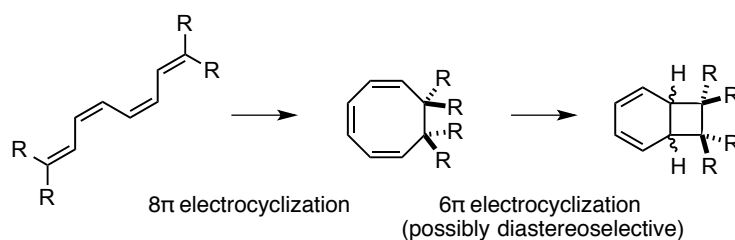
ABSTRACT

M06-2X/6-31+G(d,p) computations are reported for the 8π - 6π electrocyclic cascades of 1,3,5,7-tetraenes. The rate-determining step for these cascades is typically the second (6π) ring closure. According to experiment and theory, un- and monosubstituted tetraenes readily undergo 8π electrocyclic ring closure to form 1,3,5-cyclooctatrienes; however, the 6π electrocyclizations of these cyclooctatriene intermediates are slow and reversible, and mixtures of monocyclic and bicyclic products are formed. Computations indicate that di- and trisubstituted tetraenes undergo facile but less exergonic 8π electrocyclic ring closure due to a steric clash that destabilizes the 1,3,5-cyclooctatriene intermediates. Relief of this steric clash ensures the subsequent 6π ring closures of these intermediates are both kinetically facile and thermodynamically favorable, and only the bicyclic products are observed for the cascade reactions of naturally occurring tri- and tetra-substituted tetraenes (in agreement with computations). The 6π electrocyclic ring closure step of these cascade electrocyclizations is also potentially diastereoselective, and di- and trisubstituted tetraenes often undergo cascade reactions with high diastereoselectivities. The *exo* mode of ring closure is favored for these 6π electrocyclizations due to a steric interaction that destabilizes the *endo* transition state. Thus,

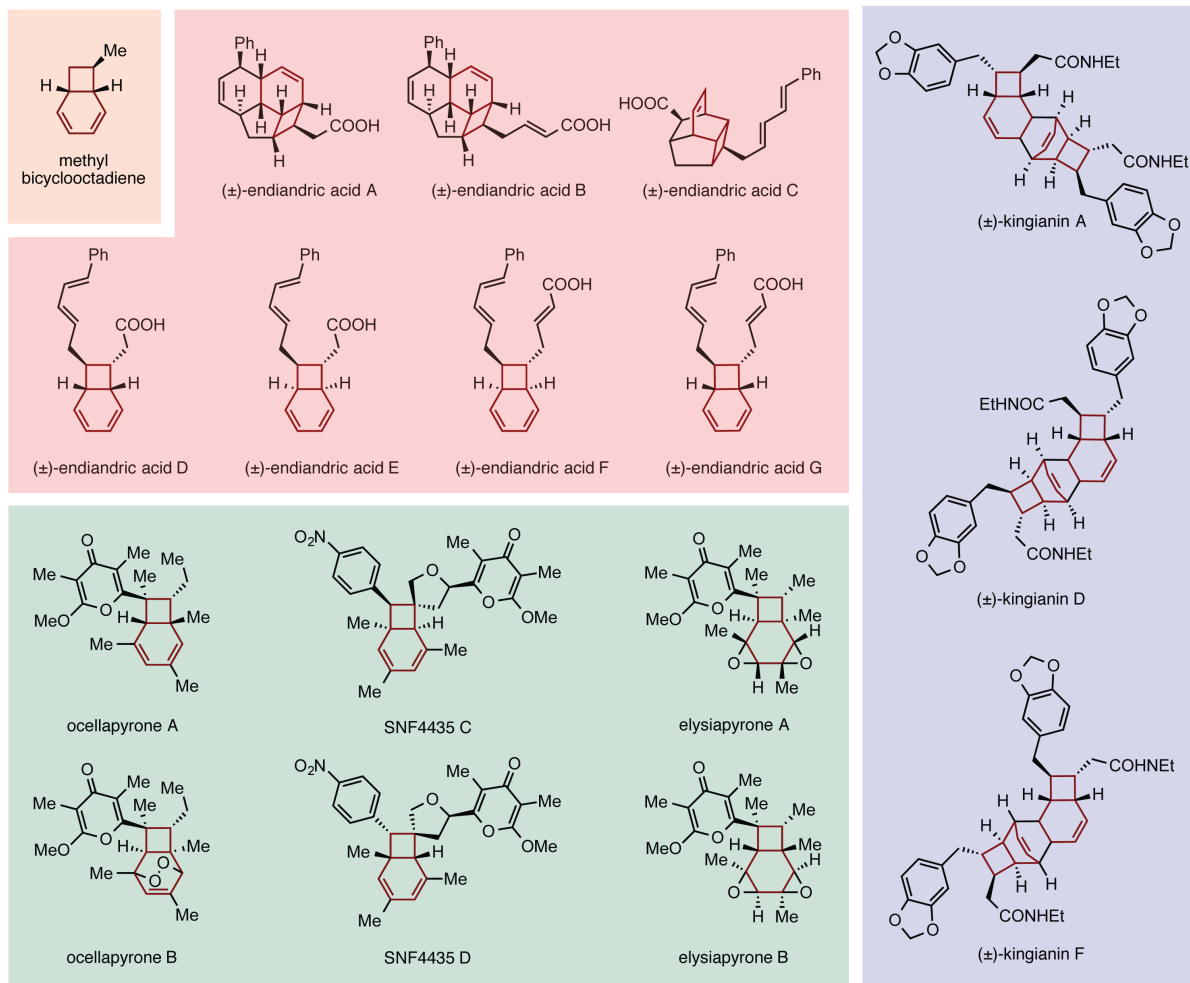
theory explains both the recalcitrance of the unsubstituted 1,3,5,7-octatetraene and 1-substituted tetraenes towards formation of the bicyclo[4.2.0]octa-2,4-diene products, as well as the ease and the stereoselectivity with which terminal di- and trisubstituted tetraenes are known to react biosynthetically.

INTRODUCTION

The 8π - 6π electrocyclic cascade of the 1,3,5,7-tetraene shown in Scheme 5.1 is an important transformation in biosynthesis and chemical synthesis. A selection of natural products formed by such cascades is shown in Scheme 5.2. Black and colleagues' original proposal¹ that the endiandric acids are biosynthesized via nonenzymatic 8π - 6π electrocyclizations prompted Nicolaou et al.²⁻⁵ to develop a biomimetic synthetic strategy to access members of this family of natural products. Their studies validated Black and coworkers' biosynthetic proposal. Since the initial isolation of the endiandric acids, a number of additional metabolites arising from this pericyclic cascade have emerged (see Scheme 5.2).⁶⁻¹⁰ Subsequent biomimetic syntheses of those molecules by Trauner¹¹⁻¹⁴, Baldwin¹⁵⁻¹⁹, Parker²⁰, and Sherburn²¹ have demonstrated the generality of this electrocyclic cascade. With the exception of the elysiapyrones²², most of these natural products exist as racemates, suggesting that the cascade reactions can readily occur without catalysis by an enzyme.



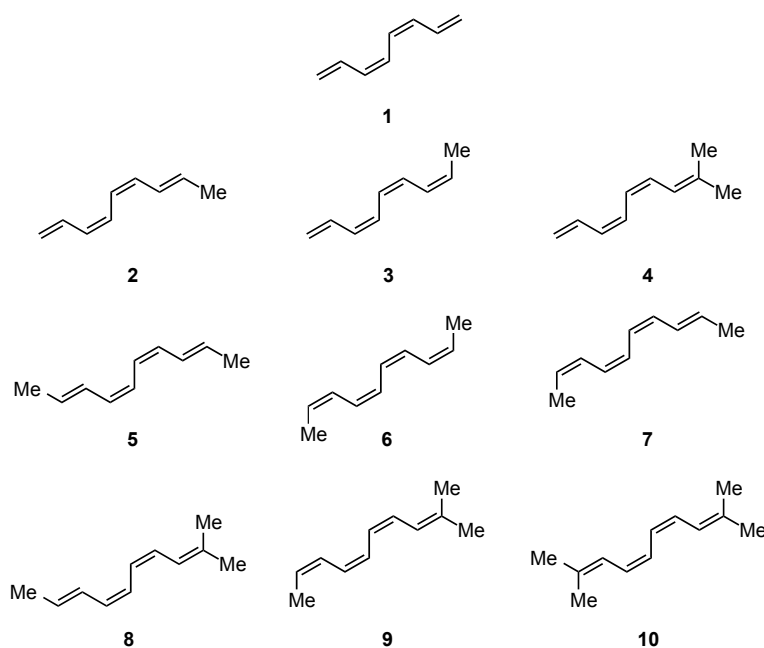
Scheme 5.1. The 8π - 6π electrocyclic cascade.



Scheme 5.2. Examples of natural products formed by biosynthetic and biomimetic 8π - 6π electrocyclization cascades.

Terminal substitution of the tetraene reactants has been shown to strongly influence the chemistry of these 8π - 6π electrocyclization cascades. These substituents affect, in particular, the kinetics, thermodynamics, and diastereoselectivity of the 6π electrocyclization step of the cascade.²³⁻²⁷ Despite the importance of this electrocyclization cascade in biosynthesis and the attention it has received from the synthetic community, no systematic investigation of the influence of terminal substitution on the cascade reaction has been reported. We performed a

density functional theory (M06-2X) study to address this problem. The data from this study reveal that terminal substitution reduces the exothermicity of the 8π electrocyclization step of the cascade and that the second ring closure is both kinetically and thermodynamically more favorable. For those substrates that undergo 8π ring closure to form chiral 1,3,5-cyclooctatrienes, our work shows that the observed diastereoselectivity of the transannular 6π ring closure arises from the steric destabilization of the *endo* mode of 6π ring closure. We anticipate that these findings will inform the design of synthetic strategies for the stereoselective formation of new bicyclo[4.2.0]octa-2,4-diene scaffolds.



Scheme 5.3. The set of 1,3,5,7-octatetraenes (**1-10**) examined in this study.

The tetraenes examined herein are shown in Scheme 5.3. The kinetics and thermodynamics of the electrocyclic reactions of **1**, **2**, **5**, **6**, and **7** have been experimentally studied previously.^{24,28,29} Tetraenes **5** and **6** possess substitution patterns similar to those of the tetraenes used in the synthesis of the endiandric acids and kinganian natural products, whereas trisubstituted tetraenes **8** and **9** resemble the starting materials used for the preparation of the

pyrone-containing natural products (green box in Scheme 5.1).¹¹⁻²¹ The electrocyclization cascades of **4** and **10** have not been studied experimentally, and metabolites arising from tetraenes possessing the same substitution patterns as **4** and **10** have not been isolated. The 8π ring closure of **4**, **5**, **6**, and **10** yield achiral 1,3,5-cyclooctatrienes; thus, the 6π electrocyclization of these cyclooctatrienes cannot be diastereoselective.

RESULTS AND DISCUSSION

The energetics and the transition states for the 8π - 6π electrocyclization cascade of **1** are shown in Figure 5.1. Goldfarb and Lindqvist reported that 1,3,5,7-octatetraene undergoes 8π ring closure with an activation enthalpy of about 17 kcal mol^{-1} ;²⁸ Pohnert and Boland have expressed concern that this value may be an overestimate, as they have determined that the 8π electrocyclization of tetraene **2**, which shows reactivity similar to that of substrate **1**, has an $\Delta H^\ddagger_{298.15 \text{ K}}$ of $13.6 \text{ kcal mol}^{-1}$.²⁹ Our computed ΔH^\ddagger value (*ca* $14.5 \text{ kcal mol}^{-1}$) is in closer agreement with Pohnert and Boland's experimental data and constitutes a significant improvement in accuracy compared with previously reported Hartree-Fock or MP2 data.³⁰ The half-life of the 8π ring closure is 0.5 s ($\Delta G^\ddagger = 17 \text{ kcal mol}^{-1}$). The formation of 1,3,5-cyclooctatriene (**1COT**) is exergonic by 9 kcal mol^{-1} .

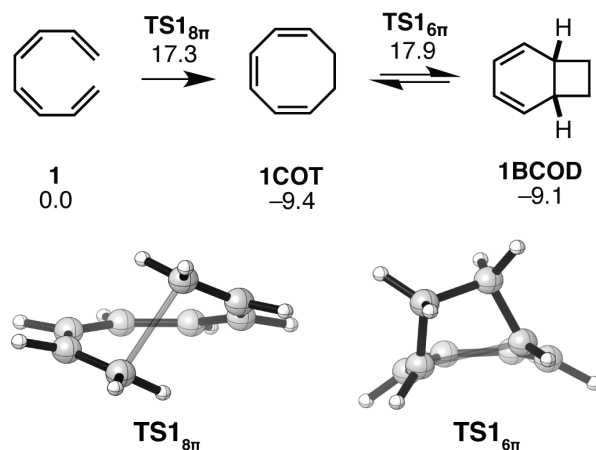


Figure 5.1. Gibbs free energy profile and transition structures for the 8π - 6π ring closure cascade of unsubstituted tetraene **1**. Structures and free energies (in kcal mol⁻¹) determined using M06-2X/6-31+G(d,p) level of theory.

Experimentally, the thermal isomerization of **1** does not yield bicyclo[4.2.0]2,4-octadiene **1BCOD** unless performed at elevated temperatures. Computations can explain this observation: The 8π and 6π electrocyclization transition states of **1** are nearly isoenergetic; however, the cyclooctatriene **1COT** is significantly more stable than its tetraene precursor. It is for this reason that the rate-determining step for the cascade reaction of compound **1** is the 6π electrocyclization with a Gibbs free energy of activation of 27 kcal mol⁻¹, corresponding to a reaction half-life of approximately 130 days at room temperature. The 8π product **1COT** and the cascade product **1BCOD** are isoenergetic and are predicted to be observed in almost equal amounts if the cascade reaction is under thermodynamic control.

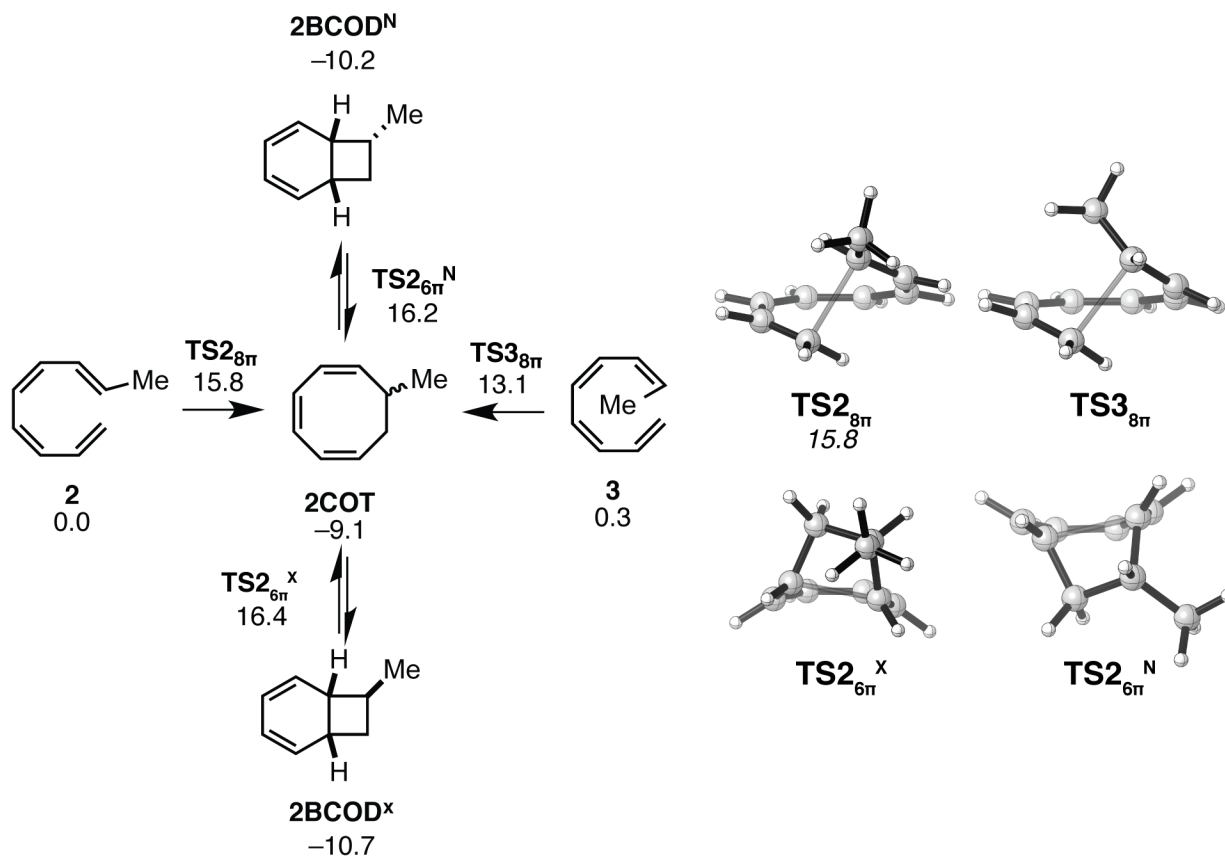


Figure 5.2. Gibbs free energy profile and transition structures for the 8π - 6π ring closure cascade of monosubstituted tetraenes **2** and **3**. Structures and free energies (in kcal mol⁻¹) determined using M06-2X/6-31+G(d,p) level of theory.

The energy profiles for the cascade reactions of the monosubstituted tetraenes **2** and **3** are qualitatively similar to that for **1**; the initial 8π electrocyclizations are facile and exothermic, while the subsequent 6π ring closures are significantly more sluggish (see Figure 5.2 for ΔG_{rxn} and ΔG^\ddagger values). The monosubstituted *Z*-tetraene (**3**) is approximately 100-fold more reactive (at room temperature) toward 8π ring closure than the *E*-tetraene (**2**). Presumably, the *Z* isomer is more reactive toward 8π ring closure due to greater strain relief that occurs upon pyramidalization of the substituted carbon at the transition state. The computed ΔH^\ddagger value of

13.6 kcal mol⁻¹ for the 8 π electrocyclization of **2** is in excellent agreement with the experimental $\Delta H^\ddagger_{298.15\text{ K}}$ value of 13.4 kcal mol⁻¹ as determined by Pohnert and Boland.²⁹

Experimentally, only at high temperatures are **2BCOD^X** and **2BCOD^N**, the products of the 6 π ring closure of intermediate **2COT**, observed,²⁹ and then only as minor products in relation to the cyclooctatriene **2COT**. Our computations indicate that the bicyclic species, **2BCOD^X** and **2BCOD^N**, are slightly more stable than **2COT**. This preference is small, and the deviation between theory and experiment are well within the computational error of our method. Because the 1,3,5-cyclooctatriene **2COT** formed from **2** and **3** is chiral, the ensuing 6 π ring closure can produce diastereomeric products. According to computations, this ring closure is nonselective, in agreement with experiment. The *exo* and *endo* transition states **TS2_{6 π} ^X** and **TS2_{6 π} ^N** are shown in Figure 5.2. A single terminal methyl substituent alone does not exert a strong influence on the stereochemical course of the second ring closure because it can occupy a sterically uncongested position in both transition states.

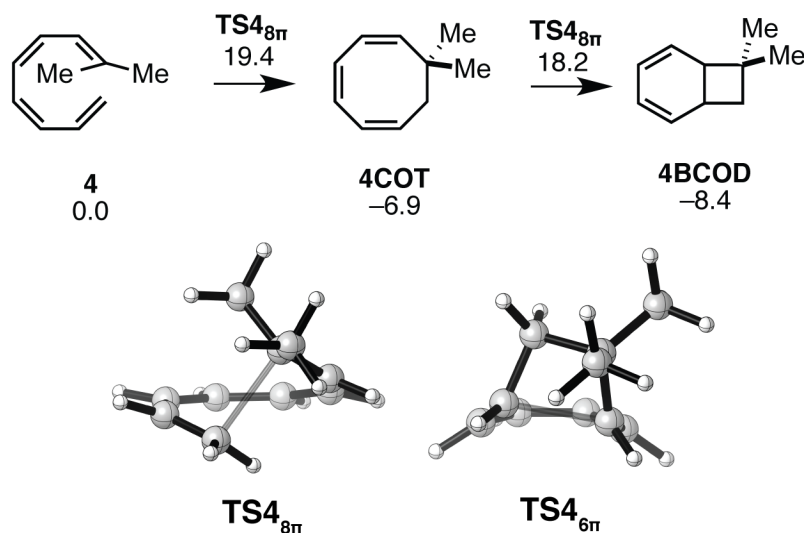


Figure 5.3. Gibbs free energy profile and transition structures for the 8π - 6π ring closure cascade of gem-disubstituted tetraene **4**. Structures and free energies (in kcal mol⁻¹) determined using M06-2X/6-31+G(d,p) level of theory.

The reactivity of **4** resembles the reactivities of model substrates **1-3**; because the 8π electrocyclization of **4** results in the formation of an achiral 1,3,5-cyclooctatriene (**4COT**), the subsequent 6π electrocyclization cannot be stereoselective. Still, the 8π ring closure of **4** is predicted to be a facile means of generating a quaternary center in a medium-sized ring (see Fig. 5.3).

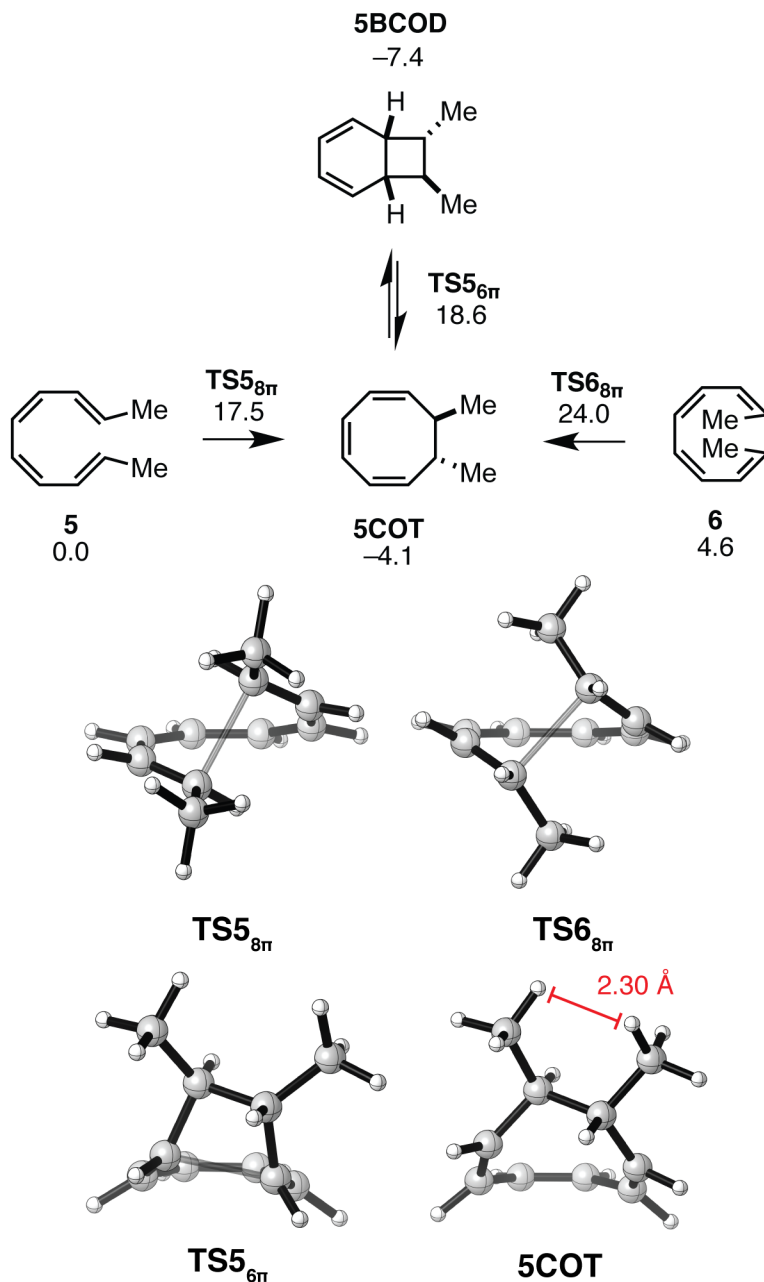


Figure 5.4. Gibbs free energy profile and transition structures for the 8π - 6π ring closure cascade of disubstituted tetraenes **5** and **6**. Structures and free energies (in kcal mol⁻¹) determined using M06-2X/6-31+G(d,p) level of theory.

Huisgen and coworkers have studied the kinetics of the thermal isomerizations of tetraenes **5-7** experimentally.²³⁻²⁵ The computed data are shown in Figures 5.4 and 5.5. The

reactions of substrates **5** and **6** correspond to the reactions involved in the biosyntheses of the endiandric acid and kinginian families of natural products. The 8π electrocyclization of tetraene **5** proceeds with a $\Delta H^\ddagger_{298.15\text{ K}}$ of $15.1\text{ kcal mol}^{-1}$,²⁴ similar to the computed value of $14.4\text{ kcal mol}^{-1}$ (Figure 5.4). In the case of the 8π electrocyclization of **6**, the computed value of $\Delta H^\ddagger_{298.15\text{ K}}$ of $17.6\text{ kcal mol}^{-1}$ deviates from the experimental value²⁴ of $21.8\text{ kcal mol}^{-1}$ by approximately 4 kcal mol^{-1} . The thermodynamic product of the 8π - 6π electrocyclization of **5** and **6** is **5BCOD**, although computations overestimate the stability of bicyclic product.²⁵

The 8π ring closures of tetraenes **5** and **6** are approximately 5 kcal mol^{-1} less exergonic than those of **1-3** ($\Delta G_{\text{rxn}} = -4$ and -9 kcal mol^{-1} respectively) because the product, **5COT**, is destabilized by steric repulsion between vicinal methyl groups at the 7 and 8 positions of the cyclooctatriene (shown in Figure 5.4, H–H distance of 2.30 \AA). The ΔG^\ddagger of 6π electrocyclization of **5COT** is 23 kcal mol^{-1} and **5BCOD** is 3 kcal mol^{-1} more stable than its cyclooctatriene precursor. The increased reactivity of **5COT** relative to **1COT** ($\Delta\Delta G^\ddagger_{6\pi} = 4\text{ kcal mol}^{-1}$) as well as the increased stability of the bicyclo[4.2.0]octadiene resulting from the ring closure of **5COT** is due to relief of the steric clash found in **5COT**. Neither **TS5_{6 π}** nor **5BCOD** feature a clash between the vicinal methyl groups. What prevents the C7 and C8 methyl substituents from clashing with one another in **TS5_{6 π}** and **5BCOD**? Formation of a strained 4-membered ring leads to compression of the C5-C6-C7 and C1-C7-C6 angles from approximately 110° to 90° . Compression of these internal angles of the cyclobutane is accompanied by a widening of the external angles of the ring, which alleviates the clash between the vicinal methyl groups.

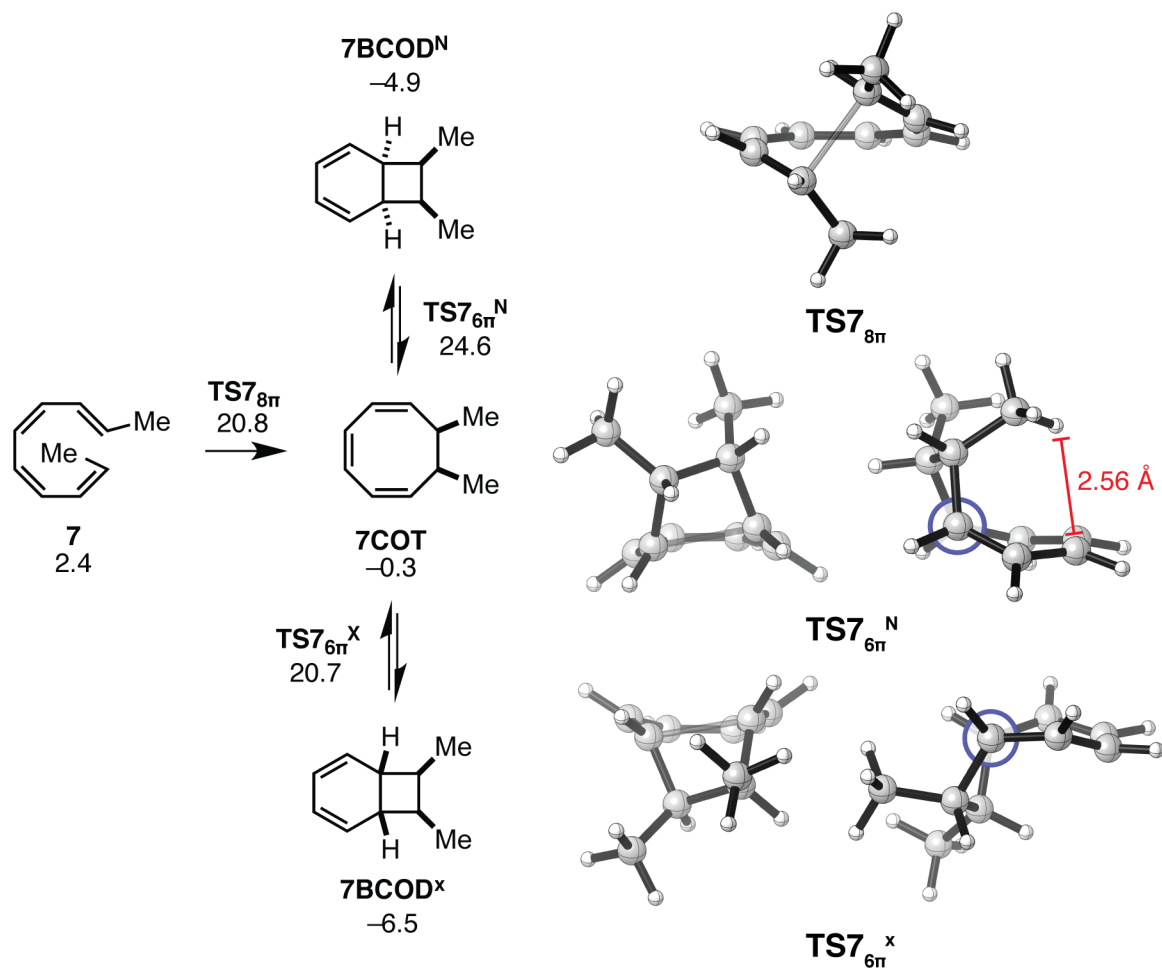


Figure 5.5. Gibbs free energy profile and transition structures for the 8π-6π ring closure cascade of tetraene **7**. Structures and free energies (in kcal mol⁻¹) determined using M06-2X/6-31+G(d,p) level of theory. Both a front view and a side view (Newman projection along the forming bond also shown) of TS7_{6π}^N and TS7_{6π}^X are provided. Note the energies shown above are relative to the most stable 1,8-dimethyl tetraene, **5**.

The activation free energy (ca. 21 kcal mol⁻¹) for the first step of the cascade process for the electrocyclization of **7** is similar to those of tetraenes **5** and **6**, differing by only 4 and 2 kcal mol⁻¹, respectively. The computed $\Delta H_{298.15\text{ K}}^\ddagger$ for the conversion of **7** into 7COT is 1.4 kcal mol⁻¹ lower than the experimental value of 17.8 kcal mol⁻¹. The 8π electrocyclic reaction of **7** is 1 kcal mol⁻¹ less exergonic than those of **5** and **6**. Like intermediate 5COT, 7COT is destabilized by steric repulsion between the C7 and C8 methyl groups. In fact, the steric clash between the *syn*

methyl groups of **7COT** is more severe than the clash present in **5COT**. As found for the 6π electrocyclization of **5COT**, relief of steric strain explains the favorable kinetics and thermodynamics for the second ring closure.

According to computations, the second step of the cascade, the 6π electrocyclization, occurs with exclusive selectivity for the *exo* diastereomer, **7BCOD^X**. The transition states for the 6π ring closure of **7COT** are shown in Figure 5.5. A destabilizing steric clash in the *endo* transition state (**TS7_{6 π} ^N**) (also present in the product) is responsible for this preference. Natural products featuring a *cis* arrangement of the C7 and C8 substituents (as in **7BCOD^X**) have not been reported.

The 8π - 6π electrocyclic reactions of trisubstituted tetraenes **8** and **9**, which resemble reactions used by nature to synthesize the γ -pyrone-containing metabolites (see the green box in Scheme 5.2), are both facile and selective. Both electrocyclic reactions have similar ΔG^\ddagger values, and the rate-determining step of the cascades is now the 8π electrocyclization. The formation of **8BCOD** is exergonic. Figure 5.6 shows the 8π and 6π electrocyclization transition states of substrates **8** and **9**. The formation of intermediate **8COT** is endergonic by 2 kcal mol⁻¹. Steric repulsion is more severe in **8COT** than in **6COT** or **7COT** due to the presence of a third methyl substituent in **8COT**, which introduces a second steric clash. Relief of both clashes by the geometric changes occurring during formation of the cyclobutane ring of **8BCOD** explains the high reactivity of **8COT**. The ring closure of intermediate **8COT** is also highly diastereoselective ($\Delta\Delta G^\ddagger = 4.7$ kcal mol⁻¹), exclusively forming **8BCOD^X**. In fact, our computations overestimate the diastereoselectivity of this ring closure based on the biomimetic tandem electrocyclizations used to synthesize the elysiapyrones and SNF4435 C and D.^{11-13,15,16,18,20,22} Structural differences between the substrates studied computationally and those used by nature to construct these

natural products, including the presence of additional substituents, may be responsible for this lack of quantitative agreement. Qualitatively, the diastereoselectivity of this ring closure can be rationalized using the same argument made to explain the selectivity of the 6π electrocyclicization of the disubstituted cyclooctatriene **7COT**. A steric effect destabilizes the *endo* transition state. This effect is responsible for increased closed shell repulsion and and geometric distortion of $\text{TS8}_{6\pi}^{\text{N}}$.

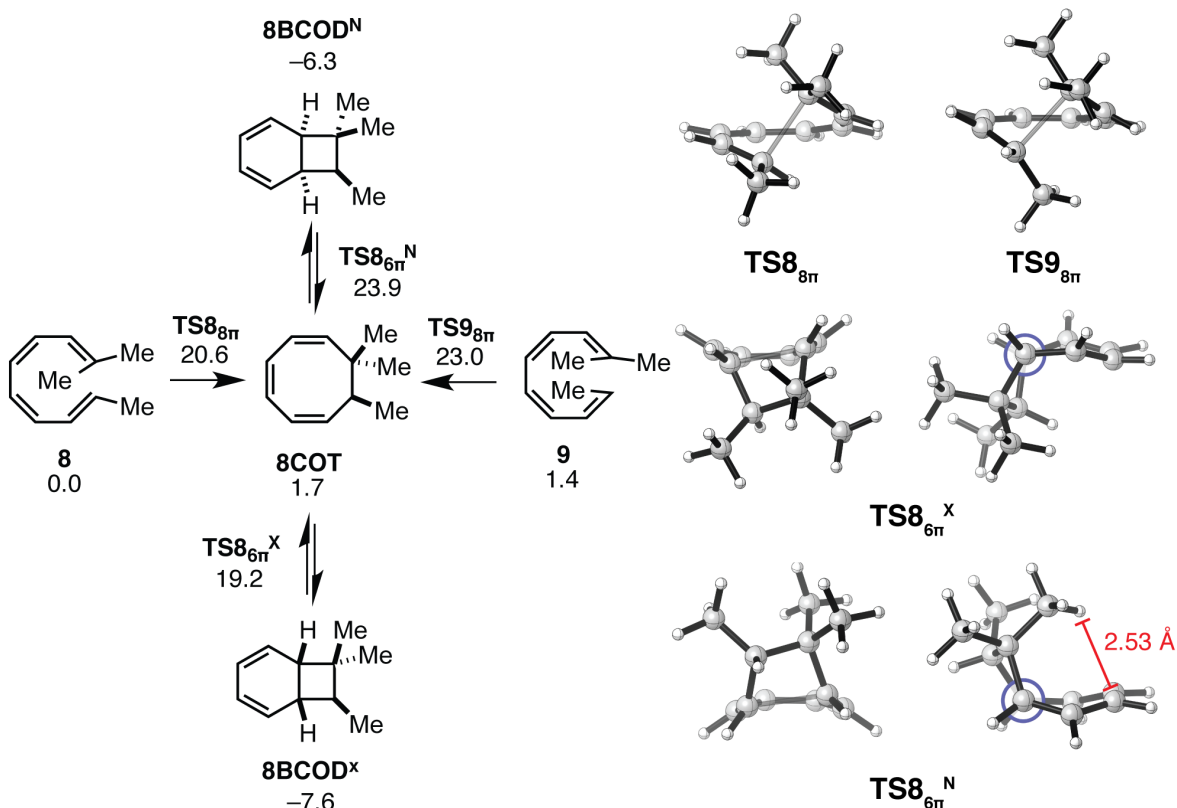


Figure 5.6. Gibbs free energy profile and transition structures for the 8π - 6π ring closure cascade of trisubstituted tetraenes **8** and **9**. Structures and free energies (in kcal mol⁻¹) determined using M06-2X/6-31+G(d,p) level of theory. Both a front view and a side view (Newman projection) of $\text{TS8}_{6\pi}^{\text{N}}$ and $\text{TS8}_{6\pi}^{\text{X}}$ are provided.

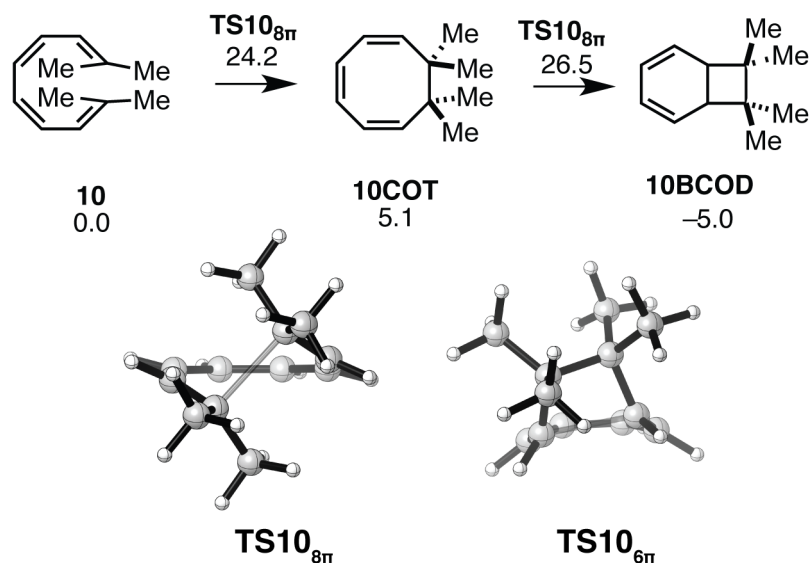


Figure 5.7. Gibbs free energy profile and transition structures for the 8π - 6π ring closure cascade of tetrasubstituted tetraene **10**. Structures and free energies (in kcal mol^{-1}) determined using M06-2X/6-31+G(d,p) level of theory.

The reaction of the tetrasubstituted tetraene **10** has a $\Delta G^\ddagger = 24.2 \text{ kcal mol}^{-1}$ (see Figure 5.7). Tetrasubstitution destabilizes the cyclooctatriene intermediate such that the initial 8π electrocyclization is endergonic. Thermodynamically, the formation of the bicyclic product **10BCOD** remains favorable. Although tetrasubstituted tetraenes like **10** are not known in nature, these results suggest that the formation of two vicinal quaternary centers via an 8π - 6π electrocyclization cascade is possible.

CONCLUSIONS

Table 5.1 summarizes the results of our computational investigation of tetraenes **1-10**. While **1-4** only undergo 8π electrocyclization, **5-10** readily undergo both steps of the 8π - 6π electrocyclization cascade. Destabilization of the 1,3,5-cyclooctatriene intermediates by steric repulsion of vicinal groups at the 7 and 8 positions of cyclooctatrienes **5BCOD**, **7BCOD**, **8BCOD**, and **10BCOD** reduces the barriers of the 6π ring closures of these intermediates,

explaining why the cascade reactions of **5-10** are so efficient. Tetraenes **7-9** yield chiral 1,3,5-cyclooctatrienes that are predicted to undergo highly diastereoselective 6π ring closures, favoring the formation of the *exo* mode of disrotatory ring closure. The diastereoselectivities in these cases are attributed to a destabilizing steric clash in the *endo* transition state. Lastly, computations of the cascade electrocyclizations of tetraene **10**, we demonstrate a potential means of generating vicinal quaternary centers in a single chemical step.

Tetraene	$\Delta G_{8\pi}^\ddagger$ ^a	$\Delta G_{8\pi}$ ^b	$\Delta G_{6\pi}^\ddagger$ ^a	$\Delta G_{6\pi}$ ^{b,c}	$\Delta\Delta G_{6\pi}^\ddagger$ ^d
1	17	-9	18	-9	N/A
2	16	-9	16	-11 (<i>exo</i>)	0
3	13	-9	16	-10 (<i>exo</i>)	0
4	19	-7	18	-8	N/A
5	18	-4	19	-7	N/A
6	19	-9	14	-12	N/A
7	18	-3	18	-9 (<i>exo</i>)	4
8	21	2	19	-8 (<i>exo</i>)	5
9	22	0	18	-10 (<i>exo</i>)	5
10	24	5	27	-5	N/A

Table 5.1. Summary of M06-2X/6-31+G(d,p) computed activation and reaction free energies for cascade ring closures of tetraenes **1-10**. All Gibbs free energies are reported in kcal mol⁻¹ and were calculated using the tetraene precursor as the point of reference. ^a $\Delta G_{8\pi}^\ddagger$ and $\Delta G_{6\pi}^\ddagger$ are the free energies of activation for 8 π and 6 π ring closure of the indicated tetraene, respectively. ^bThe reaction energies for the 8 π and 6 π electrocyclizations are, respectively, $\Delta G_{8\pi}$ and $\Delta G_{6\pi}$. ^cThe *endo* and *exo* designations indicate which of the two stereoproducts is more stable (where relevant). ^dFree energy difference between the *endo* and *exo* 6 π ring closure transition states.

COMPUTATIONAL METHODS

All computations were performed using *Gaussian09* (Revision D.01).³¹ Geometry optimizations and frequency calculations were carried out using the M06-2X³² meta-hybrid functional with the 6-31+G(d,p) basis set. The M06-2X functional was chosen for its accuracy in modeling main group chemistry.³³ The B3LYP/6-31G(d) model chemistry was also tested; however, it was inferior in terms of accuracy to the M06-2X/6-31+G(d,p) level of theory. The details of the B3LYP/6-31G(d) computations are presented in the Supporting Information. The structures described herein are the lowest energy M06-2X/6-31+G(d,p)-optimized conformers. For the M06-2X/6-31+G(d,p) computations, a numerical integration grid consisting of 99 radial shells and 590 angular points per shell was employed. All stationary points were characterized as minima or transition states on the basis of normal vibrational mode analysis. Thermal corrections were computed from unscaled frequencies, assuming a standard state of 298.15 K and 1 atm. The vibrational partition functions used to calculate the entropic contributions of the Gibbs free energies were evaluated using Truhlar's quasiharmonic approximation, in which all vibrational modes with frequencies below than 100 cm⁻¹ were raised to 100 cm⁻¹, to reduce errors arising from the treatment of low modes as harmonic oscillations.^{34,35} The computed structures were rendered using the CYLview software.³⁶ Gaussview³⁷ and Avogadro^{38,39} were used to generate input geometries and visualize output structures.

AUTHOR CONTRIBUTIONS

AP performed the computations. A.P. and K.N.H. analyzed the computational data and wrote the manuscript.

ACKNOWLEDGMENTS

We are grateful to the NSF (CHE 1059084 to K.N.H.) for financial support of this research. A.P. thanks the Chemistry-Biology Interface Training Program (National Institute of Health T32 GM 008496) for support. Computations were performed using UCLA's Hoffman2 cluster as well as the Extreme Science and Engineering Design Environment's (TG CHE 040013N) Gordon and Trestles supercomputers at the San Diego Supercomputing Center.

REFERENCES

- (1) Bandaranayake, W. M.; Banfield, J. E.; Black, D. S. C. *J. Chem. Soc., Chem. Commun.* **1980**, 902-903.
- (2) Nicolaou, K. C.; Zipkin, R. E.; Petasis, N. A. *J. Am. Chem. Soc.* **1982**, *104*, 5555-5557.
- (3) Nicolaou, K. C.; Zipkin, R. E.; Petasis, N. A. *J. Am. Chem. Soc.* **1982**, *104*, 5557-5558.
- (4) Nicolaou, K. C.; Petasis, N. A.; Zipkin, R. E. *J. Am. Chem. Soc.* **1982**, *104*, 5558-5560.
- (5) Nicolaou, K. C.; Petasis, N. A.; Zipkin, R. E. *J. Am. Chem. Soc.* **1982**, *104*, 5560-5562.
- (6) Kurosawa, K.; Takahashi, K.; Tsuda, E. *J. Antibiot (Tokyo)* **2001**, *54*, 541-547.
- (7) Takahashi, K.; Tsuda, E.; Kurosawa, K. *J. Antibiot (Tokyo)* **2001**, *54*, 548-553.
- (8) Manzo, E.; Ciavatta, M. L.; Gavagnin, M.; Mollo, E.; Wahidulla, S.; Cimino, G. *Tetrahedron Lett.* **2005**, *46*, 465-468.
- (9) Leverrier, A.; Dau, M. E. T. H.; Retailleau, P.; Awang, K.; Guéritte, F.; Litaudon, M. *Org. Lett.* **2010**, *12*, 3638-3641.
- (10) Leverrier, A.; Awang, K.; Guéritte, F.; Litaudon, M. *Phytochemistry* **2011**, *72*, 1443-1452.
- (11) Beaudry, C. M.; Trauner, D. *Org. Lett.* **2002**, *4*, 2221-2224.
- (12) Beaudry, C. M.; Trauner, D. *Org. Lett.* **2005**, *7*, 4475-4477.
- (13) Barbarow, J. E.; Miller, A. K.; Trauner, D. *Org. Lett.* **2005**, *7*, 2901-2903.
- (14) Miller, A. K.; Trauner, D. *Angew. Chem. Int. Ed.* **2005**, *44*, 4602-4606.
- (15) Moses, J. E.; Baldwin, J. E.; Marquez, R.; Adlington, R. M. *Org. Lett.* **2002**, *4*, 3731-3743.

- (16) Jacobsen, M. F.; Moses, J. E.; Adlington, R. M.; Baldwin, J. E. *Org. Lett.* **2005**, *7*, 2473-2476.
- (17) Moses, J. E.; Adlington, R. M.; Rodriguez, R.; Eade, S. J.; Baldwin, J. E. *Chem. Commun.* **2005**, 1687-1689.
- (18) Jacobsen, M. F.; Moses, J. E.; Adlington, R. M.; Baldwin, J. E. *Tetrahedron* **2006**, *62*, 1675-1689.
- (19) Eade, S. J.; Walter, M. W.; Byrne, C.; Odell, B.; Rodriguez, R.; Baldwin, J. E.; Adlington, R. M.; Moses, J. E. *J. Org. Chem.* **2008**, *73*, 4830-4839.
- (20) Parker, K. A.; Lim, Y.-H. *J. Am. Chem. Soc.* **2004**, *126*, 15968-15969.
- (21) Drew, S. L.; Lawrence, A. L.; Sherburn, M. S. *Angew. Chem. Int. Ed.* **2013**, *52*, 4221-4224.
- (22) Cueto, M.; D'Croz, L.; Maté, J. L.; San-Martín, A.; Darias, J. *Org. Lett.* **2005**, *7*, 415-418.
- (23) Huisgen, R.; Dahmen, A.; Huber, H. *J. Am. Chem. Soc.* **1967**, *89*, 7130-7131.
- (24) Huisgen, R.; Dahmen, A.; Huber, H. *Tetrahedron Lett.* **1969**, *10*, 1461-1464.
- (25) Dahmen, A.; Huisgen, R. *Tetrahedron Lett.* **1969**, *10*, 1465-1469.
- (26) Marvell, E. N.; Seubert, J. *J. Am. Chem. Soc.* **1967**, *89*, 3377-3378.
- (27) Marvell, E. N.; Seubert, J. *Tetrahedron Lett.* **1969**, *10*, 1333-1336.
- (28) Goldfarb, T. D.; Lindqvist, L. *J. Am. Chem. Soc.* **1967**, *89*, 4588-4592.
- (29) Pohnert, G.; Boland, W. *Tetrahedron* **1994**, *50*, 10235-10244.
- (30) Thomas, B. E., IV; Evanseck, J. D.; Houk, K. N. *J. Am. Chem. Soc.* **1993**, *115*, 4165-4169.
- (31) Frisch, M. J.; Trucks, G. W.; Schlegel, H. B.; Scuseria, G. E.; Robb, M. A.; Cheeseman, J. R.; Scalmani, G.; Barone, V.; Mennucci, B.; Petersson, G. A.; Nakatsuji, H.; Caricato, M.; Li,

X.; Hratchian, H. P.; Izmaylov, A. F.; Bloino, J.; Zheng, G.; Sonnenberg, J. L.; Hada, M.; Ehara, M.; Toyota, K.; Fukuda, R.; Hasegawa, J.; Ishida, M.; Nakajima, T.; Honda, Y.; Kitao, O.; Nakai, H.; Vreven, T.; J A Montgomery, J.; Peralta, J. E.; Ogliaro, F.; Bearpark, M.; Heyd, J. J.; Brothers, E.; Kudin, K. N.; Staroverov, V. N.; Kobayashi, R.; Normand, J.; Raghavachari, K.; Rendell, A.; Burant, J. C.; Iyengar, S. S.; Tomasi, J.; Cossi, M.; Rega, N.; Millam, J. M.; Klene, M.; Knox, J. E.; Cross, J. B.; Bakken, V.; Adamo, C.; Jaramillo, J.; Gomperts, R.; Stratmann, R. E.; Yazyev, O.; Austin, A. J.; Cammi, R.; Pomelli, C.; Ochterski, J. W.; Martin, R. L.; Morokuma, K.; Zakrzewski, V. G.; Voth, G. A.; Salvador, P.; Dannenberg, J. J.; Dapprich, S.; Daniels, A. D.; Farka, Ö.; Foresman, J. B.; Ortiz, J. V.; Cioslowski, J. Gaussian 09, Revision D.01. Gaussian, Inc., Wallingford CT, 2014.

(32) Zhao, Y.; Truhlar, D. G. *Theor. Chem. Acc.* **2008**, *120*, 215-241.

(33) Zhao, Y.; Truhlar, D. G. *Acc. Chem. Res.* **2008**, *41*, 157-167.

(34) Zhao, Y.; Truhlar, D. G. *Phys. Chem. Chem. Phys.* **2008**, *10*, 2813-2818.

(35) Ribeiro, R. F.; Marenich, A. V.; Cramer, C. J.; Truhlar, D. G. *J. Phys. Chem. B* **2011**, *115*, 14556-14562.

(36) CYLview, 1.0b; Legault, C. Y., Université de Sherbrooke, 2009.

(37) GaussView, Version 5, Dennington, R.; Keith, T.; Millam, J. Semichem Inc., Shawnee Mission, KS, **2009**.

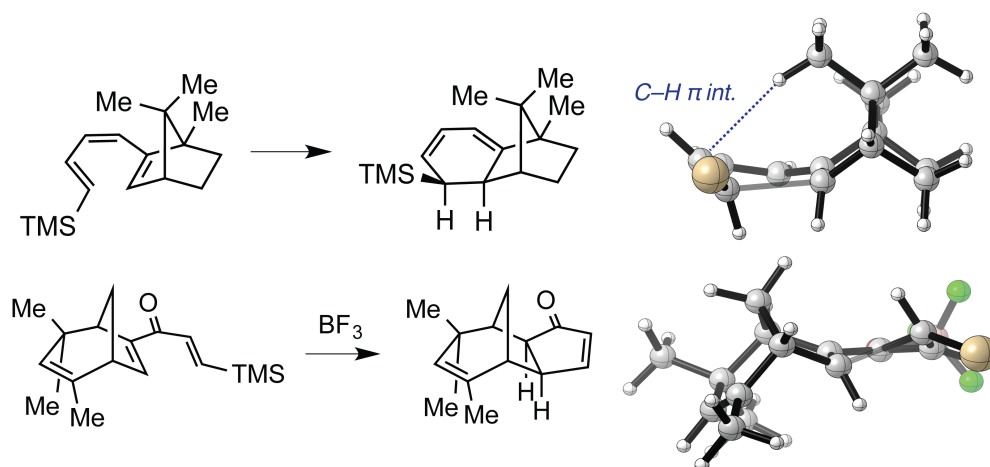
(38) Avogadro: an open-source molecular builder and visualization tool. Version 1.1.1. <http://avogadro.openmolecules.net/>.

(39) Hanwell, M. D.; Curtis, D. E.; Lonie, D. C.; Vandermeersch, T.; Zurek, E.; Hutchison, G. *R. J. Cheminform.* **2012**, *4*, 17.

Chapter 6

Reactivity and Stereoselectivity of 6π and Nazarov Electrocyclizations of Bridged Bicyclic Trienes and Divinyl Ketones

Patel, A.; West, F. G.; Houk, K. N. *J. Org. Chem.* **2015**, *80*, 2790–2795.

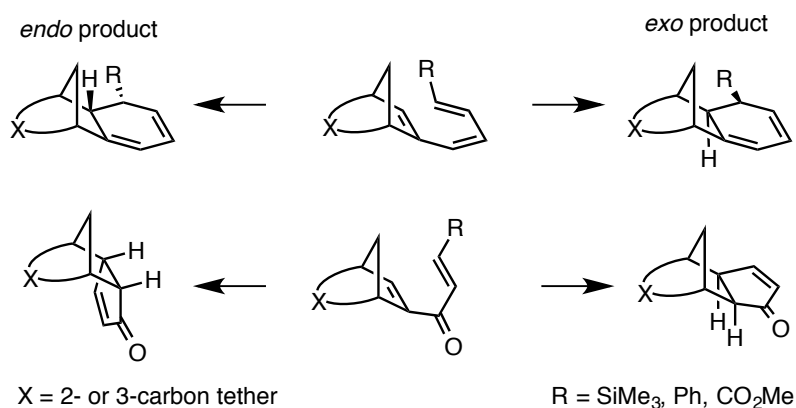


ABSTRACT

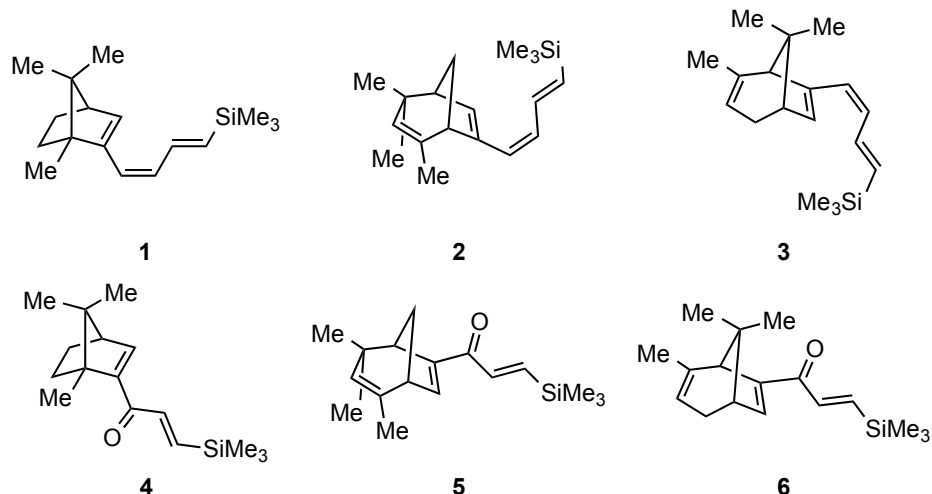
The 6π electrocyclizations and Nazarov cyclizations of a series of bridged bicyclic substrates were modeled with the M06-2X density functional and the def2-TZVPP basis set, and the factors responsible for the reactivities of these substrates and the stereoselectivities of their ring closures were identified. The ring closures of these bridged bicyclic trienes are up to a million-fold faster ($\Delta\Delta G^\ddagger = 10 \text{ kcal mol}^{-1}$) than that of 1,3,5-hexatriene, despite the absence of any activating groups. Three effects – preorganization, predistortion, and a CH π interaction – are responsible for this sizable difference in reactivity. Stereoselectivity is partially controlled by torsional effects, but for highly *exo* selective electrocyclizations is reinforced by a second effect (either a CH π interaction or a steric clash). The absence of this second effect in the ring closures of several divinyl ketones explains the reduced selectivity of these ring closures. In one case, a divinyl ketone (ketone **6**) undergoes Nazarov cyclization to yield the *endo* product preferentially. For this example, through space interaction of a nonconjugated alkene with the divinyl ketone π system in the *endo* transition state and a steric effect override the intrinsic *exo* selectivity.

INTRODUCTION

West *et al.* have prepared a series of bridged bicyclic trienes¹ and divinyl ketones^{2,3} that undergo highly stereoselective triene (6π) electrocyclizations and Nazarov cyclizations. These are shown in Scheme 6.1. Carbatriene^{4,9} and Nazarov electrocyclizations¹⁰⁻²⁵ have been the subject of prior computational studies, but the ring closures of bridged bicyclic substrates like those shown in Scheme 6.2 have yet to be examined computationally. The electrocyclic reactions of these bridged bicyclic trienes and divinyl ketones merit computational study because: 1) the bridged bicyclic trienes react with surprising ease when compared to their acyclic counterpart, 1,3,5-hexatriene; 2) these bridged bicyclic trienes and divinylketones undergo ring closure with (often high) *exo* selectivity.



Scheme 6.1. 6π and Nazarov electrocyclizations of bridged bicyclic trienes and divinyl ketones.



Scheme 6.2. Experimental substrates examined computationally in this study.

We have discovered that the enhanced reactivity of these bicyclic trienes toward disrotatory ring closure is due to three factors: substrate preorganization, predistortion, and a CH π interaction. Each of these effects individually has a modest impact on the rate of reaction; but taken together these effects are – according to computations – responsible for up to a $\sim 10^6$ -fold (at 298.15 K) increase in the rate of ring closure relative to that of 1,3,5-hexatriene. This explains why the triene precursor – generated *in situ* – is never observed experimentally. The *exo* selectivities of both the Nazarov and triene ring closures are consistent with the observed stereoselectivity of (cyclo)additions involving bridged bicyclic alkenes, including norbornene,²⁶⁻³² and are controlled by torsional effects.³³⁻³⁷ However, no investigation of the role of such effects on electrocyclization stereoselectivities has been reported. Our results suggest that, unlike (cyclo)additions to bicyclic substrates, high *exo* selectivity in the electrocyclizations of bridged bicyclic substrates **1-6** requires more than torsional effects. In the examples reported here, either a CH π interaction or steric repulsion can also promote *exo* stereoselectivity. By contrast, divinyl ketone **6** reacts to form the *endo* product, because participation of a nonconjugated alkene stabilizes the *endo* transition state overcoming the intrinsic preference for the *exo* product.

RESULTS AND DISCUSSION

Reactivities of bridged bicyclic trienes towards 6π electrocyclizations.

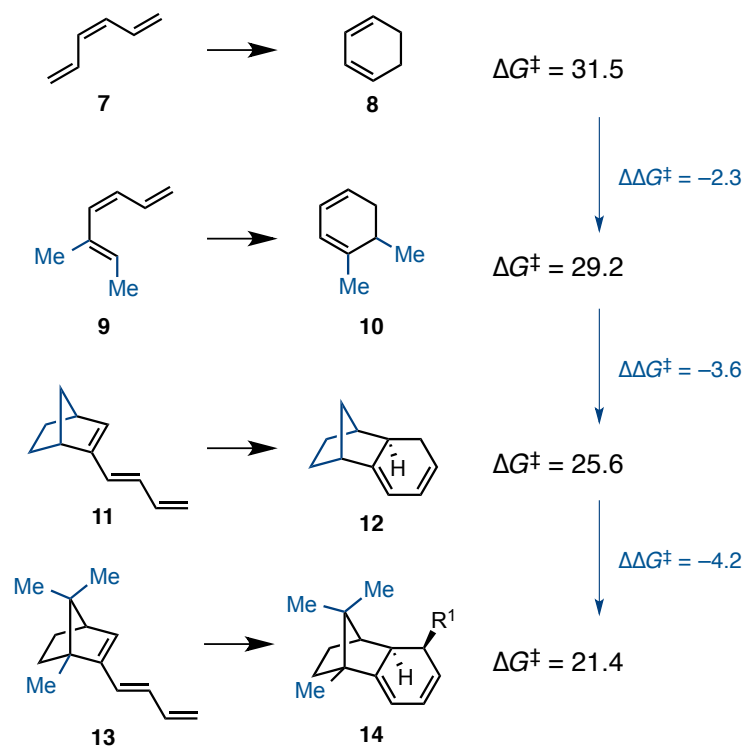


Figure 6.1. ΔG^\ddagger of the electrocyclizations of model trienes **7**, **9**, **11**, and **13**. M06-2X/def2-TZVPP free energies reported in kcal mol⁻¹.

The M06-2X/def2-TZVPP computed ΔG^\ddagger of 31.5 kcal mol⁻¹ for the ring closure of 1,3,5-hexatriene is in good agreement with the experiment value of 29.9 kcal mol⁻¹.³⁸ Unlike the electrocyclization of 1,3,5-hexatriene, the bridged bicyclic trienes **1**, **2**, and **3** shown in Scheme 6.2 undergo spontaneous ring closure upon formation.¹ According to our calculations, the ring closure of bicyclic triene **1** has a ΔG^\ddagger of 21.4 kcal mol⁻¹, roughly 10 kcal mol⁻¹ lower than the ΔG^\ddagger for the ring closure of 1,3,5-hexatriene.³⁸

The effects responsible for the unusual reactivities of these bicyclic trienes were ascertained using the series of model reactions shown in Figure 6.1. The 1,2-disubstituted triene **9** is ~100-fold more reactive (at room temperature) than the unsubstituted triene **7**, because the C2 methyl group destabilizes the *s-trans*, *s-trans* conformer by introducing an allylic clash in this conformer as shown in Figure 6.2. This effect is apparent in all 1,2-disubstituted trienes described here and has also been observed in the intramolecular Diels-Alder reactions of bicyclic 1,3,9-trienes.³⁹

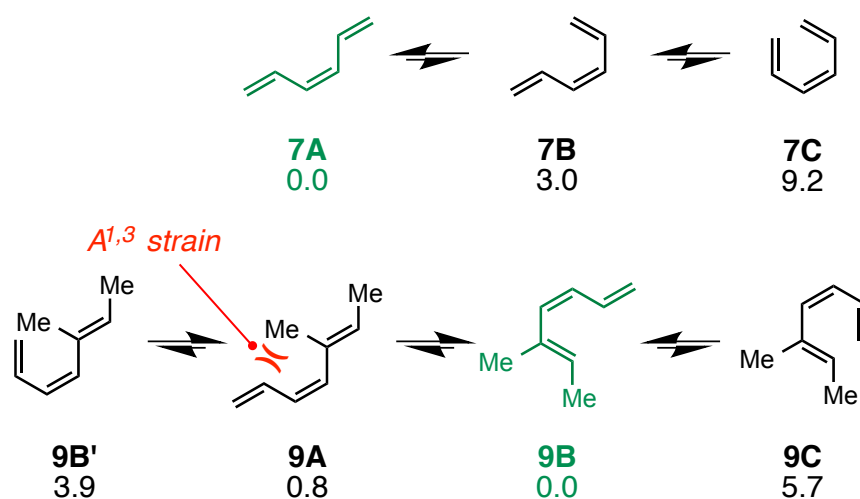


Figure 6.2. Conformational preferences of trienes **7** and **9**. Relative stabilities (ΔG) of various conformers determined using M06-2X/def2-TZVPP. Energy values reported in kcal mol⁻¹.

The difference between the ΔG^\ddagger (ca. 2.8 kcal mol⁻¹) values for the disubstituted trienes **9** and **11** can be attributed to “pre-distortion” of the endocyclic alkene of the norbornenyl substrate;⁴⁰ the strained nature of norbornenyl double bond is well documented, and alkene “pre-distortion” of this sort has been known to contribute to norbornene’s unusual reactivity in (cyclo)additions.³³⁻³⁷ This effect likely also contributes to the enhanced reactivities of trienes **2** and **3**. Lastly, a CH π interaction between the CH bond of the 7-methyl group and the triene π system further lowers the activation barrier for ring closure by 4.2 kcal mol⁻¹ for the 6,7,7

trimethyl derivative **13** relative to the unsubstituted norbornenyl triene **11** (see Figure 6.3). This value is in line with theoretical⁴¹⁻⁴³ and experimental⁴¹ values (ca. 1.0 kcal mol⁻¹ for the CH π interaction found in the benzene–methane dimer);⁴⁴ the *exo* ring closure of triene **2**, which possesses no methyl group on the bridge, has an activation free energy 1 kcal mol⁻¹ higher than that of triene **1**.

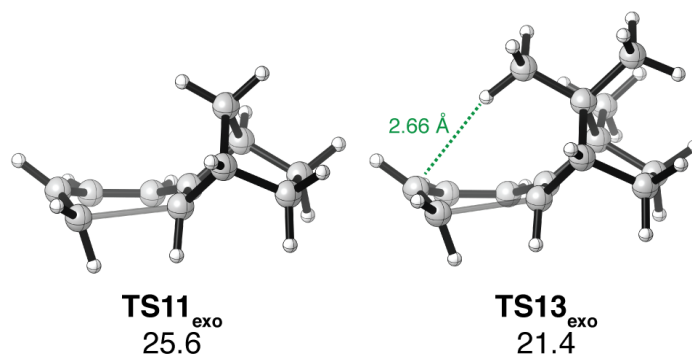


Figure 6.3. Transition structures and ΔG^\ddagger (M06-2X/def2-TZVPP values reported in kcal mol⁻¹) of the *exo* ring closures of trienes **11** and **13**, illustrating the stabilizing CH π interaction responsible for the enhanced reactivity of triene **13** relative to **11**. Energies are M06-2X/def2-TZVPP ΔG^\ddagger reported in kcal mol⁻¹.

Stereoselectivities of the disrotatory ring closures of bridged bicyclic trienes.

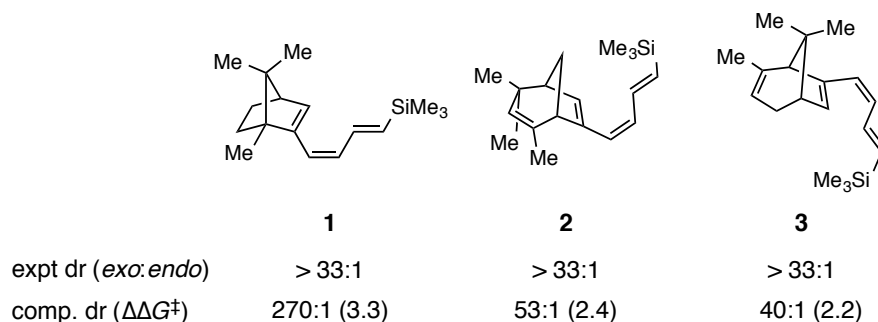


Figure 6.4. Computed and experimental diastereomeric ratios for the ring closures of triene **1-3**. Reactions performed in aqueous THF at a room temperature or under reflux in either THF:H₂O or CH₂Cl₂. Computed diastereomeric ratios determined using the SMD^{THF}/M06-2X/def2-TZVPP model chemistry.

The experimental and computed diastereomeric ratios of the triene electrocyclizations of bicyclic trienes **1**, **2**, and **3** are summarized in Figure 6.4. Theory quantitatively reproduces the *exo* selectivity observed experimentally for the ring closures of **1-3**.

Torsional steering, or minimization of torsional repulsions in transition states, at least partially controls the stereoselectivities of all electrocyclizations described in this report. The *endo* and *exo* transition states for the ring closure of camphor-derived triene **1**, shown in Figure 6.5, illustrate the nature of this effect. The H–C–C–H dihedral shown in the Figure 6.5 is staggered (63°) in **TS1_{exo}** and more eclipsed (21°) in **TS1_{endo}**, leading to increased torsional strain in the *endo* transition state. Based on energy differences of the *endo* and the *exo* transition states of model triene **11**, this effect accounts for roughly half of the 3 kcal mol⁻¹ difference in the free energies of **TS1_{exo}** and **TS1_{endo}**. Thus, a second effect must reinforce the intrinsic *exo* selectivity of the electrocyclizations of these bridged bicyclic trienes. In the case of trienes **1** and **3**, this second effect is a stabilizing CH π interaction (described previously) between the 7-methyl substituent and the triene π system in the *exo* transition state.

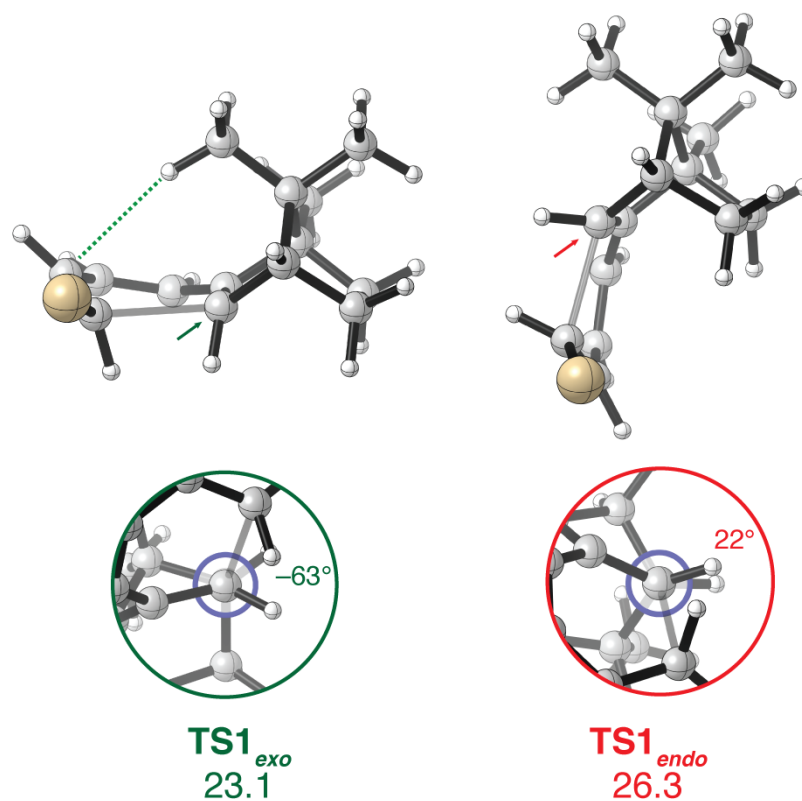


Figure 6.5. Transition structures and ΔG^\ddagger (SMD^{THF}/M06-2X/def2-TZVPP values in kcal mol⁻¹) for the *exo* and *endo* modes of ring closure of bicyclic triene **1**. Methyl groups of the trimethylsilyl substituent are omitted for clarity.

Unlike trienes **1** and **3**, triene **2** is unsubstituted at the bridging carbon; therefore, the CH π interaction described previously cannot act as a stereocontrol element for the electrocyclization of this substrate. Nevertheless, according to our DFT results, the ΔG^\ddagger difference between **TS2_{endo}** and **TS2_{exo}** is 3 kcal mol⁻¹. Interestingly, the barrier for the formation of the *endo* product of **2** is roughly 3 kcal mol⁻¹ higher than the ΔG^\ddagger computed for the *endo* ring closures of bicyclic trienes **1** and **3**, suggesting that a second destabilizing effect present in **TS2_{endo}** is responsible for enhancing *exo* selectivity. Ring closure from the *endo* face is further destabilized by a significant steric clash (shown in Figure 6.6) between the methyl substituent on the bicyclic

skeleton and the hydrogen at the exocyclic terminus of the triene π system, as suggested by West in his initial report.¹ The two clashing hydrogen are separated by only 1.90 Å.

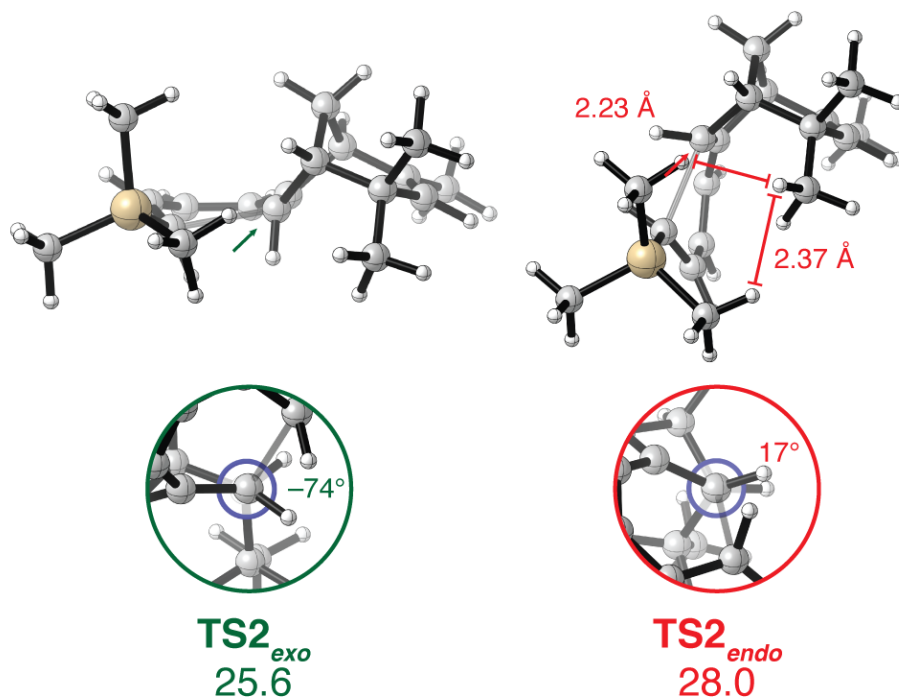


Figure 6.6. Transition structures and ΔG^\ddagger (SMD^{THF}/M06-2X/def2-TZVPP values in kcal mol⁻¹) for the *exo* and *endo* modes of ring closure of bicyclic triene **2**. Methyl groups of trimethylsilyl substituent are shown to illustrate the steric clash that destabilizes the *endo* transition state.

Stereoselectivities of the conrotatory ring closures of bridged bicyclic divinyl ketones.

The computed drs for the Nazarov cyclization of divinyl ketone **4–6** are also in quantitative agreement with experiment. These ring closures were modeled with BF₃, the Lewis acid employed experimentally, coordinated to carbonyl oxygens of the divinyl ketones. Energies are free energies in kcal mol⁻¹.

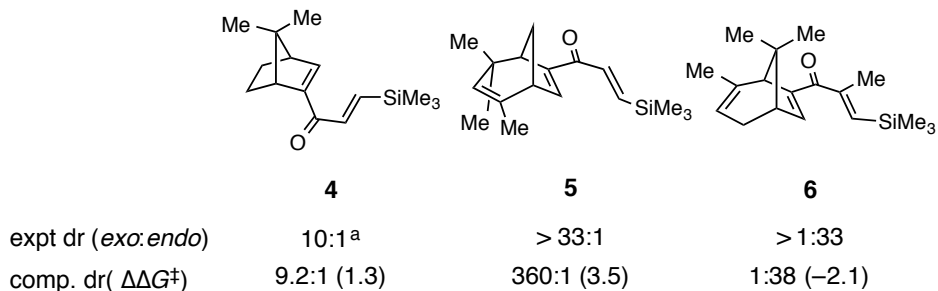


Figure 6.7. Computed and experimental diastereomeric ratios for the ring closures of divinyl ketones **4-6** in dichloromethane. Computed diastereomeric ratios determined using the SMD^{DCM}/M06-2X/def2-TZVPP model chemistry.

The electrocyclic reaction of camphor-derived divinyl ketone **4** ($\Delta\Delta G^\ddagger = 1.3 \text{ kcal mol}^{-1}$) is less selective than the ring closure of triene **1**, because the conrotatory *exo* transition state is not stabilized by a CH π interaction. Unlike the 6-carbon π system of the corresponding triene system, the (formal) pentadienyl reactive array of divinyl ketone **4** adopts an arrangement in which its π density is directed away from the bridging methyl group. Consequently, the selectivity is exclusively determined by torsional effect, which accounts to a $1.1 \text{ kcal mol}^{-1}$ difference in ΔG^\ddagger of the two modes of ring closure (see Figure 6.8).

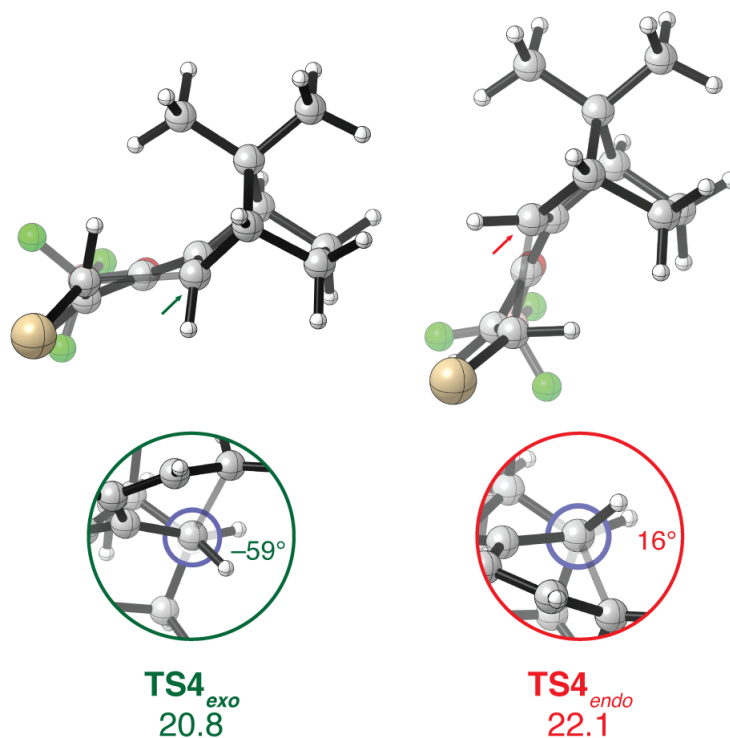


Figure 6.8. Transition structures and ΔG^\ddagger (SMD^{DCM}/M06-2X/def2-TZVPP values in kcal mol⁻¹) for the *exo* and *endo* modes of ring closure of bicyclic divinyl ketone **4**. Methyl groups of the trimethylsilyl substituent are omitted for clarity.

The stereochemical outcome of the Nazarov cyclization of bicyclic divinyl ketone **5** is controlled by the same effects responsible for the ring closure of triene **2**; namely, torsional strain and steric repulsion destabilize the *endo* transition state of this reaction. The steric repulsion between the trimethylsilyl group and the remote bridge of the bicyclic system is diminished in the *endo* transition state of **4** as compared to **TS2_{endo}** due to the decreased steric demand of the 3-carbon unsaturated ketone side-chain relative to the 4-carbon diene side-chain of **1**.

In contrast to the results already described, divinyl ketone **6** undergoes electrocyclicization to form the *endo* product selectively. The transition states for the ring closure of this substrate are shown in Figure 6.9. Computations recapitulate the sense and level of stereoselectivity observed experimentally ($\Delta\Delta G^\ddagger = 2.1$ kcal mol⁻¹). West *et al.* proposed that a through-space orbital

interaction involving the nonconjugated alkene at C5–C6 (labeled in Figure 6.10) and the 4-electron π system stabilizes the *endo* transition state, overriding the intrinsic *exo* selectivity. We find that this through-space interaction is partly responsible for the *endo* selectivity, and this effect is stronger in the *endo* transition state as the π system of the pentadienyl cation is more ideally positioned to interact with the nonconjugated alkene. Computations show that the distance between the interacting carbon atoms (C1 and C6) is 0.15 Å shorter in **TS6_{endo}** than **TS6_{exo}**. Furthermore, the molecular electrostatic potentials (MEPs) show that the nonconjugated alkene is more electron-rich in the *exo* transition structure (more yellow in color) than in the *endo* transition structure (more green in color). Furthermore, the atomic charge on the distal carbon (C2) of the nonconjugated alkene is less negative in **TS6_{endo}** (–0.18e) than in **TS6_{exo}** (–0.31e), also indicative of greater interaction in **TS6_{endo}**. In addition, *endo* selectivity is enhanced by a steric clash that destabilizes the *exo* transition of **6**. A severe clash (1.91 Å) exists between the methyl substituent at bridging carbon and the hydrogen at the exocyclic terminus of the π system (shown in Figure 9). We have examined a model substrate in which the (interacting) nonconjugated alkene has been saturated. For this substrate, *exo* selectivity is observed in support of our hypothesis.

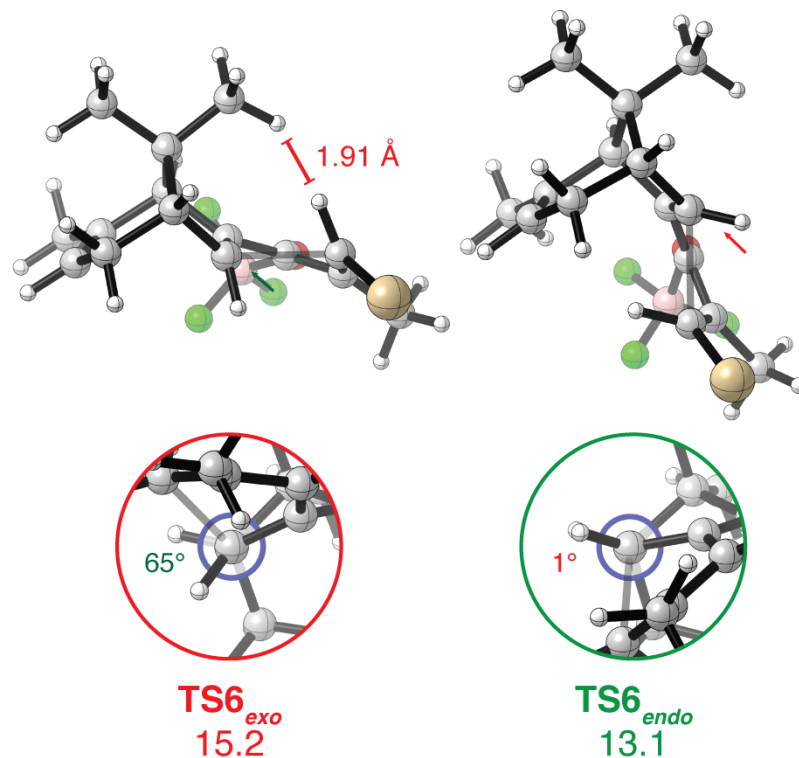


Figure 6.9. Transition structures and ΔG^\ddagger (SMD^{DCM}/M06-2X/def2-TZVPP values in kcal mol⁻¹) for the exo and endo modes of ring closure of bicyclic divinyl ketone **6**. Methyl groups of the trimethylsilyl substituent are omitted for clarity.

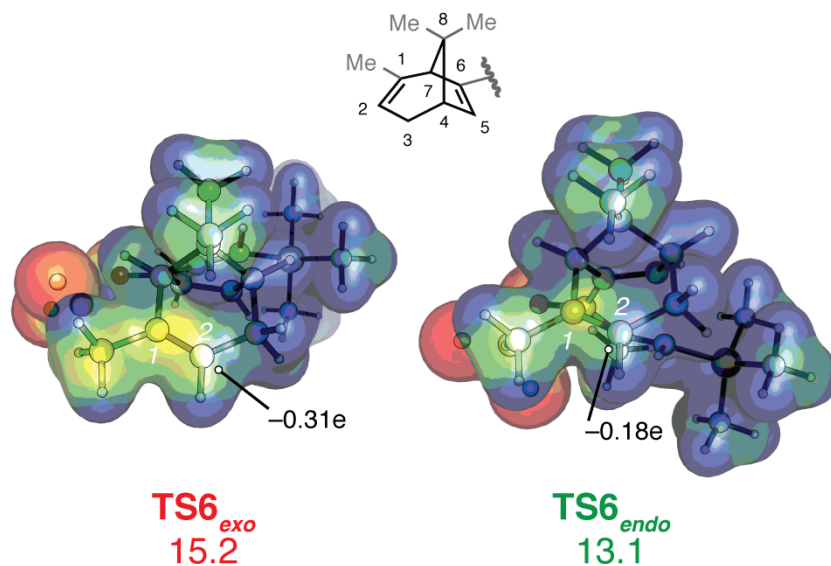


Figure 6.10. Molecular electrostatic potentials (MEPs) for TS6_{endo} and TS6_{exo} and ΔG^\ddagger . Potential ranges from -0.5 au to 0.5 au. CHelpG atomic charges at C2 (the distal carbon of the

nonconjugated alkene) labeled in black. Molecular electrostatic potentials, densities, and ΔG^\ddagger determined using the SMDDCM/M06-2X/def2-TZVPP.

CONCLUSIONS

Substrate preorganization, predistortion, and steric attraction emerge as factors that can promote the electrocyclic reaction of 1,3,5-hexatrienes. Torsional effects alone do not account for the level of selectivity observed for these ring closures; high *exo* selectivity requires the complementary action of a second effect (steric attraction or repulsion). In one system, **6**, through-space interaction of a nonconjugated alkene and steric repulsions reverse the intrinsic *exo* selectivity of Nazarov cyclization.

COMPUTATIONAL METHODS

All quantum mechanical calculations were performed using *Gaussian09*.⁴⁵ Geometry optimizations and frequency calculations were performed with the hybrid meta-GGA density functional M06-2X⁴⁶ and the def2-TZVPP⁴⁷ basis set. The SMD solvation model⁴⁸ was used for the reactions of trienes **1-3** and divinyl ketones **4-6** in THF and CH₂Cl₂, respectively. For all calculations, we employed an “ultrafine” integration grid consisting of 99 radial shells and 590 angular points per shell. Normal mode analysis confirmed all stationary point as either minima or transition states. Unscaled M06-2X/def2-TZVPP frequencies to calculate Helmholtz enthalpies and Gibbs free energies at 25°C and 1 atm. Truhlar’s quasiharmonic approximation was used to correct for errors in the estimation of vibrational entropies due to treatment of low modes (below 100 cm⁻¹) as harmonic oscillations. Molecular electrostatic potentials were rendered using the PyMOL Molecular Graphics System.⁴⁹ Gaussview⁵⁰ and Avogadro^{51,52} were used to construct and visualize structures. Structures were rendered using the CYLview software

AUTHOR CONTRIBUTIONS

A.P. performed the quantum mechanical computations. A.P. and K.N.H. analyzed the resulting data, and A.P, F.G.W., and K.N.H. prepared the manuscript.

ACKNOWLEDGEMENTS

K.N.H and F.G.W. acknowledge the NSF (CHE 105 9084 and CHE 136 1104 to K.N.H.) and the Natural Sciences and Engineering Research Council of Canada (NSERC; Discovery Grant to F.G.W) for funding. A.P. would like to thank the Chemistry-Biology Interface Training Program (T32 GM 008496) and the University of California, Los Angeles, for financial support. Computations were performed using the Hoffman2 cluster at the University of California, Los Angeles as well as the Extreme Science and Engineering Design Environment's (TG CHE 040013N) Gordon and Trestles supercomputers at the San Diego Supercomputing Cluster.

REFERENCES

- (1) Benson, C. L.; West, F. G. *Org. Lett.* **2007**, *9*, 2545.
- (2) Mazzola, R. D.; White, T. D.; Vollmer-Snarr, H. R.; West, F. G. *Org. Lett.* **2005**, *7*, 2799.
- (3) Giese, S.; Mazzola, R. D.; Amann, C. M.; Arif, A. M.; West, F. G. *Angew. Chem. Int. Ed.* **2005**, *44*, 6546.
- (4) Thomas, B. E.; Evanseck, J. D. *Isr. J. Chem.* **1993**, *3*, 287.
- (5) Evanseck, J. D.; Thomas, B. E.; Spellmeyer, D. C.; Houk, K. N. *J. Org. Chem.* **1995**, *60*, 7134.
- (6) Walker, M. J.; Hietbrink, B. N.; Thomas, B. E.; Nakamura, K.; Kallel, E. A.; Houk, K. N. *J. Org. Chem.* **2001**, *66*, 6669.
- (7) Guner, V. A.; Houk, K. N.; Davies, I. W. *J. Org. Chem.* **2004**, *69*, 8024.
- (8) Leach, A. G.; Houk, K. N.; Davies, I. W. *Synthesis* **2005**, *19*, 3463.
- (9) Patel, A.; Barcan, G. A.; Kwon, O.; Houk, K. N. *J. Am. Chem. Soc.* **2013**, *135*, 4878.
- (10) Smith, D. A.; Ulmer, C. W., II. *J. Org. Chem.* **1991**, *56*, 4444.
- (11) Smith, D. A.; Ulmer, C. W., II. *J. Org. Chem.* **1997**, *62*, 5110.
- (12) Smith, D. A.; Ulmer, C. W., II. *Tetrahedron Lett.* **1991**, *32*, 725.
- (13) Cavalli, A.; Masetti, M.; Recanatini, M.; Prandi, C.; Guarna, A.; Occhiato, E. G. *Chem.–Eur. J.* **2006**, *12*, 2836.
- (14) Lemière, G.; Gandon, V.; Cariou, K.; Fukuyama, T.; Dhimane, A.-L.; Fensterbank, L.; Malacria, M. *Org. Lett.* **2007**, *9*, 2207.
- (15) Marcus, A. P.; Lee, A. S.; Davis, R. L.; Tantillo, D. J.; Sarpong, R. *Angew. Chem. Int. Ed.* **2008**, *47*, 6379.

- (16) Lebœuf, D.; Huang, J.; Gandon, V.; Frontier, A. J. *Angew. Chem. Int. Ed.* **2011**, *50*, 10981.
- (17) Faza, O. N.; López, C. S.; Alvarez, R.; de Lera, A. R. *Chemistry* 2004, *10*, 4324.
- (18) Harmata, M.; Schreiner, P. R.; Lee, D. R.; Kirchhoefer, P. K. *J. Am. Chem. Soc.* **2004**, *126*, 10954.
- (19) Shi, F.-Q.; Li, X.; Xia, Y.; Zhang, L.; Yu, Z.-X. *J. Am. Chem. Soc.* **2007**, *129*, 15503.
- (20) Cavalli, A.; Pacetti, A.; Recanatini, M.; Prandi, C.; Scrapi, D.; Occhiato, E. G. *Chem.—Eur. J.* **2008**, *14*, 9292.
- (21) Flynn, B. L.; Manchala, N.; Krenske, E. H. *J. Am. Chem. Soc.* **2013**, *135*, 9156.
- (22) Smith, D. A.; Ulmer, C. W., II. *J. Org. Chem.* **1993**, *58*, 4118.
- (23) Leboeuf, D.; Ciesielski, J.; Gandon, V.; Frontier, A. J. *J. Am. Chem. Soc.* **2012**, *134*, 6296.
- (24) Huang, J.; Lebœuf, D.; Frontier, A. J. *J. Am. Chem. Soc.* **2011**, *133*, 6307.
- (25) Lebœuf, D.; Theiste, E.; Gandon, V.; Daifuku, S. L.; Neidig, M. L.; Frontier, A. J. *Chem.—Eur. J.* **2013**, *19*, 4842.
- (26) Davies, D. I.; Parrott, M. J. *Tetrahedron Lett.* **1972**, *2*, 2719.
- (27) Baldwin, S. W.; Tomesch, J. C. *J. Org. Chem.* **1974**, *39*, 2382.
- (28) Freeman, F. *Chem. Rev.* **1975**, *75*, 439.
- (29) Corey, E. J.; Shibasaki, M.; Nicolaou, K. C.; Malmsten, C. L.; Samuelsson, B. *Tetrahedron Lett.* **1976**, *17*, 737.
- (30) Huisgen, R.; Ooms, P. H. J.; Mingin, M.; Allinger, N. L. *J. Am. Chem. Soc.* **1980**, *102*, 3951.
- (31) Huisgen, R. *Pure Appl. Chem.* **1981**, *53*, 171.

- (32) Allen, A. D.; Tidwell, T. T. *J. Am. Chem. Soc.* **1982**, *104*, 3145.
- (33) Ragué Schleyer, von, P. *J. Am. Chem. Soc.* **1967**, *89*, 701.
- (34) Rondan, N. G.; Paddon-Row, M. N.; Caramella, P.; Mareda, J.; Mueller, P. H.; Houk, K. N. *J. Am. Chem. Soc.* **1982**, *104*, 4974.
- (35) Houk, K. N.; Rondan, N. G.; Brown, F. K.; Jorgensen, W. L.; Madura, J. D.; Spellmeyer, D. C. *J. Am. Chem. Soc.* **1983**, *105*, 5980.
- (36) Lopez, S. A.; Houk, K. N. *J. Org. Chem.* **2013**, *78*, 1778.
- (37) Wang, H.; Houk, K. N. *Chem. Sci.* **2014**, *5*, 462.
- (38) Lewis, K. E.; Steiner, H. *J. Chem. Soc.* **1964**, 3080.
- (39) Krenske, E. H.; Perry, E. W.; Jerome, S. V.; Maimone, T. J.; Baran, P. S.; Houk, K. N. *Org. Lett.* **2012**, *14*, 3016.
- (40) In support of the notion that predistortion of bridged bicyclic alkenes promotes triene ring closures, Magomedov et al. have demonstrated that a norbornenyl divinyl ketone (in the presence of Lewis acid and an amine base) undergoes tautomerization followed by 6π ring closure with greater yield and at lower temperatures than related acyclic or monocyclic substrates. For additional experimental details, see: Magomedov, N. A.; Ruggiero, P. L.; Tang, Y. *Org. Lett.* **2004**, *6*, 3373.
- (41) Shibasaki, K.; Fujii, A.; Mikami, N.; Tsuzuki, S. *J. Phys. Chem. A* **2006**, *110*, 4397.
- (42) Sherrill, C. D.; Takatani, T.; Hohenstein, E. G. *J. Phys. Chem. A* **2009**, *113*, 10146.
- (43) Dinadayalane, T. C.; Paytakov, G.; Leszycynski, J. *J. Mol. Model.* **2013**, *19*, 2855.
- (44) We chose the benzene-methane dimer as a rough measure of the strength of a CH π interaction because of the similarity in shape and size of benzene to the aromatic 6π electron system in the electrocyclization transition states. Differences in the aromaticities of the pericyclic

transition state and benzene have little effect on the strength of π stacking. See: Bloom, J. W. G.; Wheeler, S. E. *Angew. Chem. Int. Ed.* **2011**, *50*, 7847. A similar point could be argued for CH π interactions, as the CH π dimer of ethylene and methane has a gas phase CCSD(T) complete basis set interaction energy of -0.5 kcal mol⁻¹ very similar to the gas phase experimental interaction energy for the benzene-methane dimer of -1.0 kcal mol⁻¹. See a.) ref. 40 b.) Tsuzuki, S.; Honda, K.; Uchimaru, T.; Mikami, M.; Tanabe, K. *J. Phys. Chem. A* **1999**, *103*, 8265.

(45) Frisch, M. J.; Trucks, G. W.; Schlegel, H. B.; Scuseria, G. E.; Robb, M. A.; Cheeseman, J. R.; Scalmani, G.; Barone, V.; Mennucci, B.; Petersson, G. A.; Nakatsuji, H.; Caricato, M.; Li, X.; Hratchian, H. P.; Izmaylov, A. F.; Bloino, J.; Zheng, G.; Sonnenberg, J. L.; Hada, M.; Ehara, M.; Toyota, K.; Fukuda, R.; Hasegawa, J.; Ishida, M.; Nakajima, T.; Honda, Y.; Kitao, O.; Nakai, H.; Vreven, T.; J A Montgomery, J.; Peralta, J. E.; Ogliaro, F.; Bearpark, M.; Heyd, J. J.; Brothers, E.; Kudin, K. N.; Staroverov, V. N.; Kobayashi, R.; Normand, J.; Raghavachari, K.; Rendell, A.; Burant, J. C.; Iyengar, S. S.; Tomasi, J.; Cossi, M.; Rega, N.; Millam, J. M.; Klene, M.; Knox, J. E.; Cross, J. B.; Bakken, V.; Adamo, C.; Jaramillo, J.; Gomperts, R.; Stratmann, R. E.; Yazyev, O.; Austin, A. J.; Cammi, R.; Pomelli, C.; Ochterski, J. W.; Martin, R. L.; Morokuma, K.; Zakrzewski, V. G.; Voth, G. A.; Salvador, P.; Dannenberg, J. J.; Dapprich, S.; Daniels, A. D.; Farkas, Ö.; Foresman, J. B.; Ortiz, J. V.; Cioslowski, J. Gaussian 09, Revision D.01. Gaussian, Inc., Wallingford CT, **2014**.

(46) Zhao, Y.; Truhlar, D. G. *Theor. Chem. Acc.* **2008**, *120*, 215.

(47) Weigend, F.; Ahlrichs, R. *Phys. Chem. Chem. Phys.* **2005**, *7*, 3297.

(48) Marenich, A. V.; Cramer, C. J.; Truhlar, D. G. *J. Phys. Chem. B* **2009**, *113*, 6378.

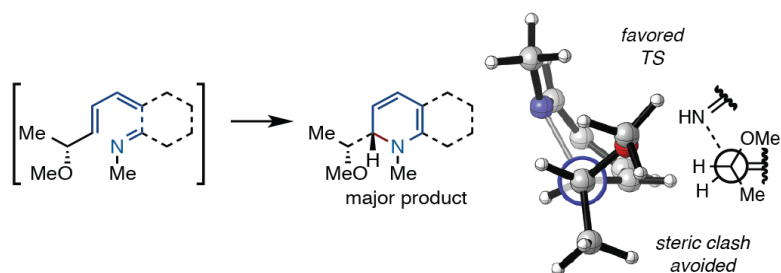
(49) The PyMOL Molecular Graphics System, Version 1.4 Schrödinger, LLC.

- (50) GaussView, Version 5, Dennington, R.; Keith, T.; Millam, J. Semichem Inc., Shawnee Mission KS, **2009**.
- (51) Avogadro: an open-source molecular builder and visualization tool. Version 1.1.1.
<http://avogadro.openmolecules.net/>.
- (52) Hanwell, M. D.; Curtis, D. E.; Lonie, D. C.; Vandermeersch, T.; Zurek, E.; Hutchison, G. *R. J. Cheminform.* 2012, *4*, 1.

Chapter 7

Transition State *Gauche* Effects Control the Torquoselectivities of the Electrocyclizations of Chiral 1-Azatrienes

Patel, A.; West, F. G.; Houk, K. N. *J. Org. Chem.* **2015**, *80*, 2790–2795.



ABSTRACT

Hsung *et al.* have reported a series of torquoselective electrocyclizations of chiral 1-azahexa-1E,3Z,5E-trienes that yield functionalized dihydropyridines. To understand the origins of the torquoselectivities of these azaelectrocyclizations, we modeled these electrocyclic ring closures using the M06-2X density functional. A new stereochemical model that rationalizes the observed 1,2 stereoselection emerges from these computations. This model is an improvement and generalization of the “*inside-alkoxy*” model used to rationalize stereoselectivities of 1,3-dipolar cycloaddition of chiral allyl ethers and emphasizes a stabilizing hyperconjugative effect, which we have termed a transition state *gauche* effect. This stereoelectronic effect controls the conformational preferences at the electrocyclization transition states, and only in one of the allowed, disrotatory electrocyclization transition states is the ideal stereoelectronic arrangement of substituent achieved without the introduction of a steric clash. Computational experiments confirm the role of this effect as a stereodeterminant, since substrates with electropositive groups

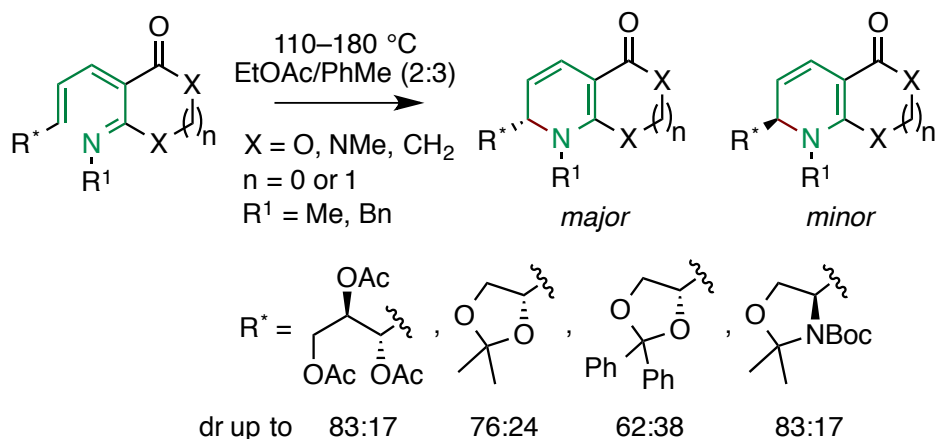
like a silyl substituent and electronegative groups have different conformational preferences at the transition state and undergo ring closure with divergent stereochemical outcomes. This predicted reversal of stereoselectivity for the ring closure of a silyl-substituted azatriene has been demonstrated experimentally.

INTRODUCTION

Hsung *et al.* have demonstrated that an allylic stereocenter can influence the stereochemical outcomes of the disrotatory 6π electrocyclizations of substituted 1-aza-1,3Z,5-hexatrienes (summarized in Scheme 1).¹ Here we report – on the basis M06-2X/6-31+G(d,p) computations – that *gauche* effects present in the electrocyclization transition states determine the preferred mode of disrotatory ring closure for these chiral 1-azatrienes. In short, the forming C–N bond prefers to maintain a *gauche* relationship with the C–O bond at the allylic stereocenter.

Ring closures of azatrienes have been examined by a number of researchers²⁻¹³ and examples of stereoselective azaelectrocyclizations¹⁴⁻²¹ have been reported. Despite the utility of the 6π electrocyclization in natural product synthesis and even in biological contexts (i.e., covalent enzyme inhibition and biolabeling),^{22,23} the origins of the torquoselectivities of these electrocyclizations have yet to be understood. Previous experimental work suggests electrocyclizations of 1-azatrienes are often reversible at elevated temperatures,³ unlike the 6π electrocyclization of 1,3Z,5-hexatriene. However, experiments suggest that azatrienes shown in Scheme 1 undergo irreversible ring closure;¹ hence, the stereoselectivities of these reactions are under kinetic control.

Scheme 1. Torquoselective electrocyclizations of 1-aza-1,3Z,5-hexatrienes



RESULTS AND DISCUSSION

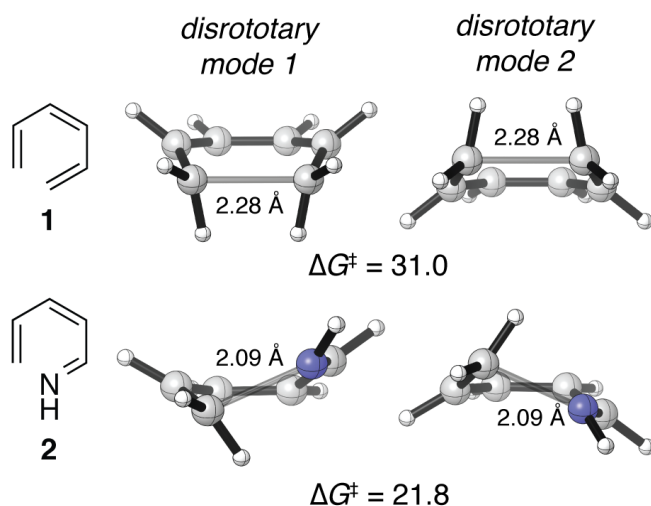
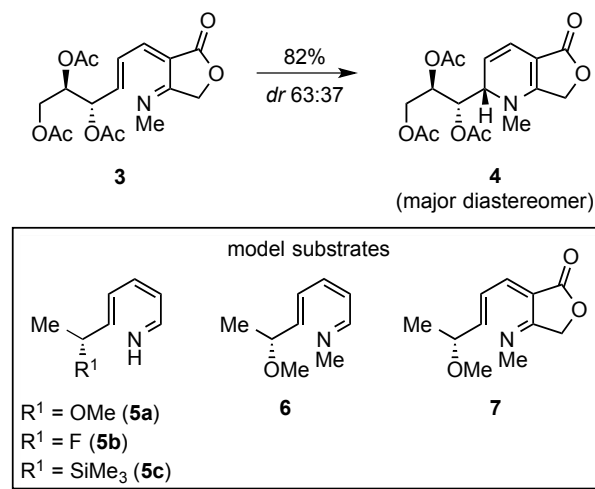


Figure 1. The thermally allowed disrotatory transition structures and activation free energies of the ring closures of 1,3,5-hexatriene and 1-azahexa-1,3,5-triene. Energies are Gibbs free energies in kcal mol⁻¹.

Figure 1 illustrates the allowed disrotatory transition structures of the ring closures of 1,3,5-hexatriene **1** and those of its 1-aza analogue **2**. Whereas the electrocyclic ring closure of 1,3,5-hexatriene proceeds through a C_s symmetric boat-like geometry, the transition structures for the corresponding azaelectrocyclization are of lower symmetry; the structures are distorted such that the nitrogen of the azatriene appears to “approach” the C-terminus of the azatriene from above or below the plane of the terminal double bond. According to our previous work, this distortion

allows the lone pair of the imine nitrogen to overlap with triene π system, stabilizing the transition state. Lone pair conjugation of this sort is largely responsible for $\sim 10^7$ -fold (at 298.15 K, see Figure 1 for free energies of activation) increase in reactivity of 1-azahexa-1,3,5-triene relative to 1,3,5-hexatriene.²⁴

Scheme 2. A representative azaelectrocyclization and model substrates examined computationally.



1-azatriene **3** is representative of the substrates examined by Hsung and coworkers.¹ It features a number of C–C single bonds capable of free rotation; thus, to reduce the number of conformations that needed to be sampled we examined the simplified trienes, **5a-c**, **6**, and **7**, shown in Scheme 2. In all cases, three rotameric transition states were found for each of the disrotatory modes of ring closure (see Figure 2). We labeled these transition states based on the position of the alkoxy substituent with respect the terminal alkene of the azatriene, nomenclature previously used to describe stereoselective additions to alkenes bearing allylic stereocenters.²⁵

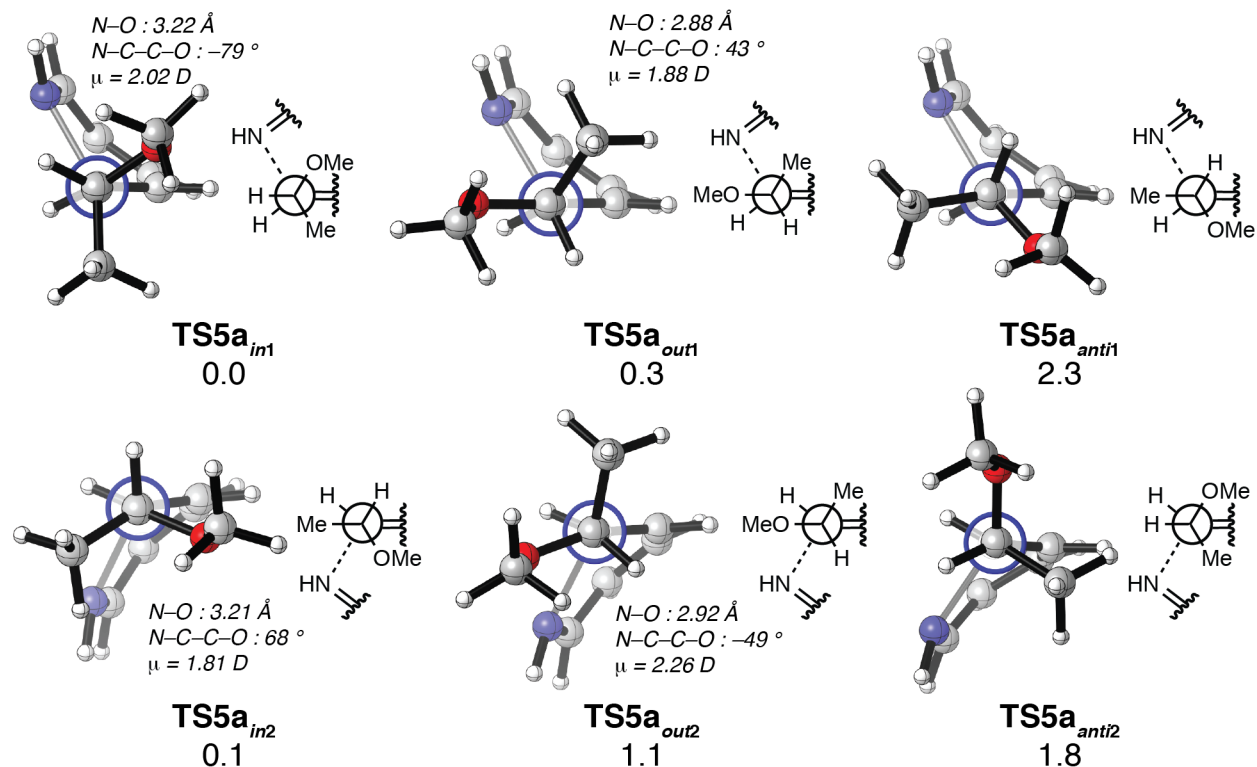
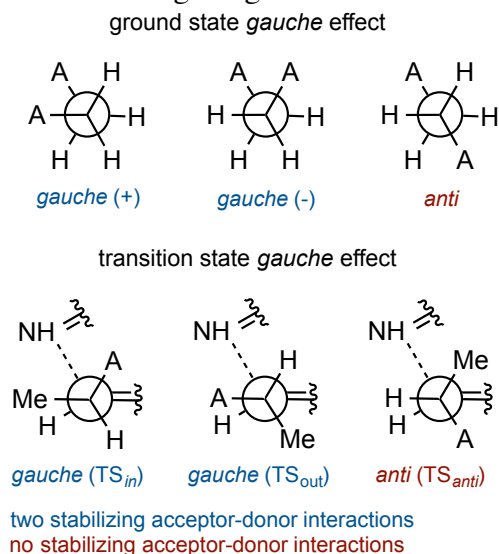


Figure 2. Newman projections of the C5-C6 bond of the M06-2X/6-31+G(d,p)-optimized transition state conformers for the ring closure of **5a**. $\Delta\Delta G^\ddagger$ values are reported in kcal mol⁻¹.

For both disrotatory modes of ring closure of **5a**, the transition states in which the alkoxy substituent in the *inside* position (see Figure 2) are most stable. A *gauche* effect is responsible for this conformational preference. In the **TS5a_{in1}** and **TS5a_{in2}**, the forming C-N bond and the C-O bond between the alkoxy substituent and the allylic stereocenter are antiperiplanar to σ -donating bonds (C-C and C-H bonds, respectively) and *gauche* to one another. The *anti* transition state conformers **TS5a_{anti1}** and **TS5a_{anti2}**, which do not have these favorable donor-acceptor interactions, and are both about 2 kcal mol⁻¹ higher in energy. The *outside*-alkoxy transition states (**TS5a_{out1}** and **TS5a_{out2}**) also have a *gauche* arrangement of the C-O and forming C-N bonds and as a result are more stable than the *anti* transition structures. However, these transition structures are higher in energy than **TS5a_{in1}** and **TS5a_{in2}** due to electrostatic repulsion between the oxygen of the alkoxy group and the azatriene nitrogen. The O-N interatomic

distances are shorter in the outside transition state conformer than the corresponding inside transition structures.

Scheme 3. Newman projections illustrating the ground state and transition state gauche effects.



The *gauche* effect described above differs from a ground state *gauche* effect^{26,27} in that one of the C–X σ acceptors is a bond that is only partially formed in the transition state. For this reason, we have termed this hyperconjugative effect a “transition state *gauche* effect”. For these chiral azatrienes, it is the *gauche* relationship between forming C–N and the vicinal C–X bonds at the allylic position of the triene that is ultimately responsible for stereoselection (Scheme 3). Transition state *gauche* effects of this type are likely general phenomena, and may be responsible for the stereoselectivity of other reactions involving alkenes that possess an allylic σ acceptor. The “inside-alkoxy” effect invoked by Houk^{25,28-31} and others³² to rationalize the stereoselectivities of 1,3-dipolar cycloadditions of nitrones and nitrile oxides and chiral allyl ethers is now recognized to be one case of this more general stereochemical model.

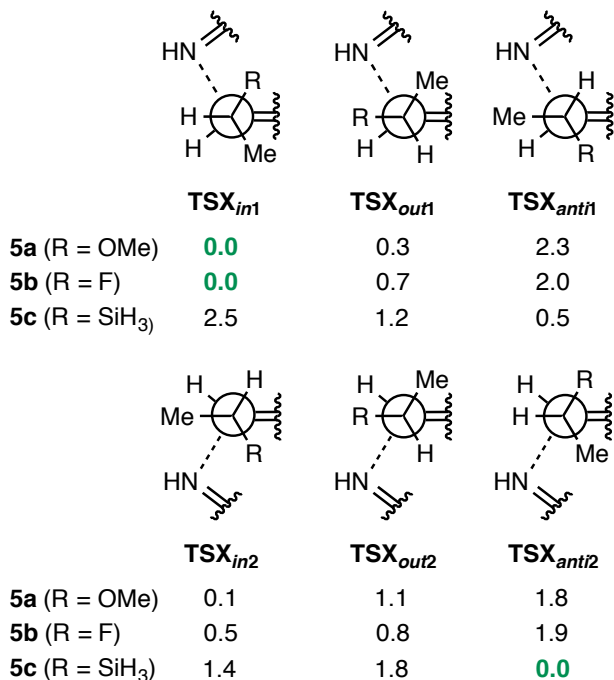


Figure 3. ΔG^\ddagger differences of the M06-2X/6-31+G(d,p) optimized ring closure transition state conformers of **5a-c**. $\Delta\Delta G^\ddagger$ values were determined relative to inside TS_{dis1} for the transition structures of azatrienes **5a** and **5b** and relative to TS_{dis2} for the transition structures of **5c**. Energies are reported in kcal mol⁻¹.

To confirm that these stereoelectronic effects are the principal determinants of the transition state conformational preferences of these azaelectrocyclizations, we also modeled the transition states of related substrates **5b** and **5c**, bearing a fluorine or a silyl substituent at the stereogenic center, respectively. If these effects were important, then **5b** (R = F) should have conformational preferences qualitatively similar to those of **5a** at the transition state. Since the SiMe₃ group is a hyperconjugative donor³³, the *anti* transition state conformers of 1-azatriene **5c** should be the most stable: A good donor (C–Si σ bond) is antiperiplanar to electron-deficient forming C–N bond in the *anti* transition states of **5c**. The $\Delta\Delta G^\ddagger$ of all six transition state conformers of **5a-c** are summarized in Figure 3.

The conformational preferences of the transition states of **5b** are, indeed, similar to those preferences observed for the transition states of **5a**. The *inside* transition states TS5b_{in1} and TS5b_{in2} are most stable, and the *anti* transition states are highest in energy. By contrast, we find

that the *anti* transition state conformers are preferred for the ring closure of **5c** (R = SiMe₃), confirms the nature of C–N forming bond at the transition state as hyperconjugative acceptor. This *anti* preference is related to Cieplak's rationalization regarding the origins of π -facial selectivity of nucleophilic additions to cyclic ketones,^{34,35} and suggests the nature of bond formation in the electrocyclization, a pericyclic process, is fundamentally different from bond formation in a polar reaction (e.g., nucleophilic acyl addition) for which Cieplak's rationale has been criticized.^{36,37}

Experimentally, Hsung et al. have demonstrated that the diastereoselectivities of these azaelectrocyclizations are sensitive to the nature of the N-substituent. To probe this effect, we first examined the transition states conformers of azatriene **6**, bearing a *N*-methyl substituent, and, then, cyclic azatriene **7**. The conformational preferences of **6** remain the same as those found for substrates **5a** and **5b**. According to computations, the two diastereomeric *inside* transition states of azatriene **6** differ in free energy by 1.0 kcal mol⁻¹ and are shown in Figure 4. This difference in ΔG^\ddagger is consistent with the sense and level of diastereoselectivity observed experimentally and is caused by a steric clash that destabilizes **TS6_{in2}**. In **TS6_{in2}**, for the methoxy substituent to occupy its preferred *inside* position, the geminal methyl group must adopt the more sterically demanding *outside* position; whereas, in **TS6_{in1}** the hydrogen occupies the *outside* position when the alkoxy is in the *inside* arrangement. That this steric clash involves the *N*-methyl group explains the substituent's importance in stereinduction.

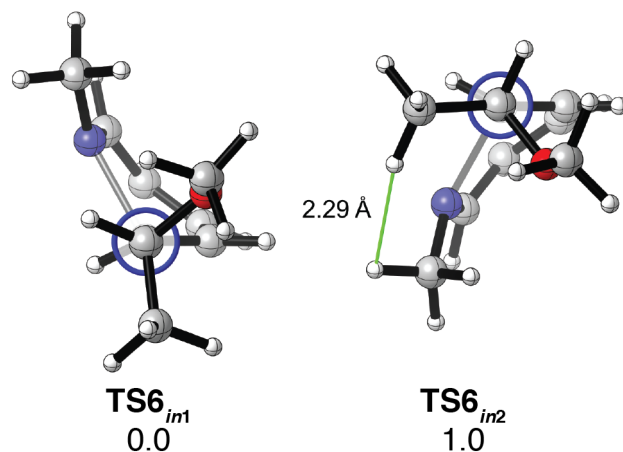


Figure 4. Newman projections of the lowest energy M06-2X/6-31+G(d,p)-optimized 6π electrocyclization transition state conformers of **6**. $\Delta\Delta G^\ddagger$ values are given in kcal mol⁻¹.

We next modelled the ring closure of a cyclic azatriene, compound **7**, (see Figure 5), which more closely resembles the experimental azatriene **4**. The reaction of the cyclic azatriene **7** proceeds with a barrier of almost 18 kcal mol⁻¹ and yields a product that is 16 kcal mol⁻¹ more stable than the reactant. Azatriene **7** is more than 10³-fold more reactive at room temperature ($\Delta\Delta G^\ddagger = 5$ kcal mol⁻¹) than **2a** due to activation by the carbonyl moiety of the lactone and restriction of a rotational degree of freedom by the fused lactone ring. For azatriene **7**, the outside transition states for either mode of ring closure are slightly more stable than the corresponding inside transition states. The subtle change of the conformational preference is due to A^{1,3} strain between the methylene group of the lactone and *N*-methyl of the azatriene in the inside transition state conformers of **7**. Nonetheless, a strong preference for a *gauche* conformation over the *anti* conformation is still predicted. The lowest energy conformers of either mode of disrotation differ by a ΔG^\ddagger of ~ 1 kcal mol⁻¹, consistent with the observed diastereoselectivity for the reaction of **3**.

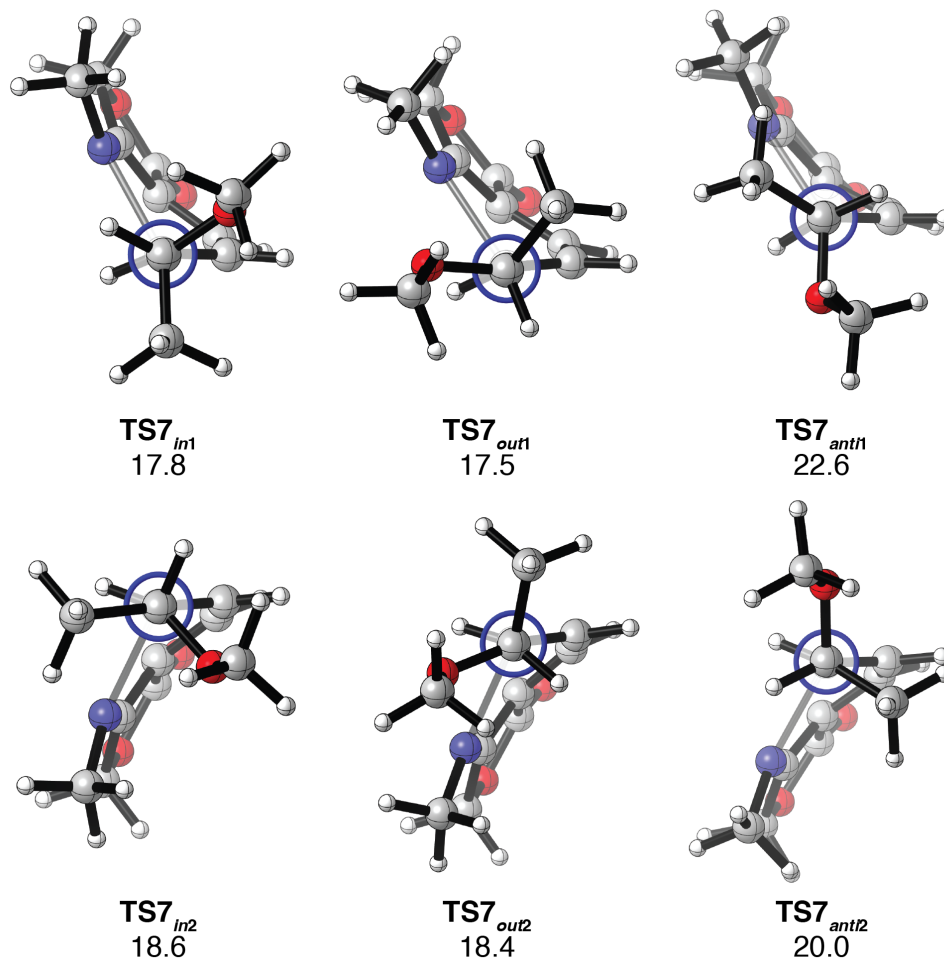
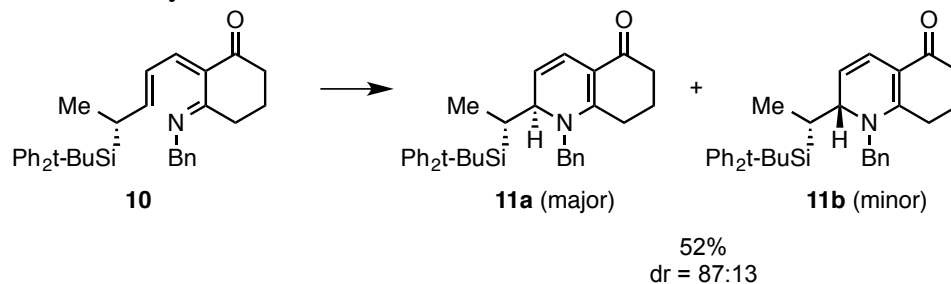


Figure 5. Newman projections of M06-2X/6-31+G(d,p) optimized transition state conformers of the 6π electrocyclicization of azatriene **7**. ΔG^\ddagger are given in kcal mol⁻¹.

Scheme 4. The electrocyclicization of TBPDS-substituted 1-azatriene **10**.³¹



Finally, we return to the silyl derivative **5c**. As discussed above, the silyl group at the allylic position of the azatriene is predicted to reverse the stereoselectivity of the ring closure. This prediction inspired the syntheses and studies of the ring closures of chiral silyl-substituted

1-azatrienes, including, **10** (see Scheme 4). The synthesis of silyl-substituted 1-azatrienes and the scope of the ring closures of these compounds are reported separately.³⁸ The predicted stereochemical outcome is observed experimentally; however, the ring closure of 1-azatriene **10** is reversible at 130°C, and over time the diastereoselectivity of the reaction comes under thermodynamic control. Here we report the origins of the selectivity of the electrocyclicization of **10**, using azatriene **12** as a computational model substrate.

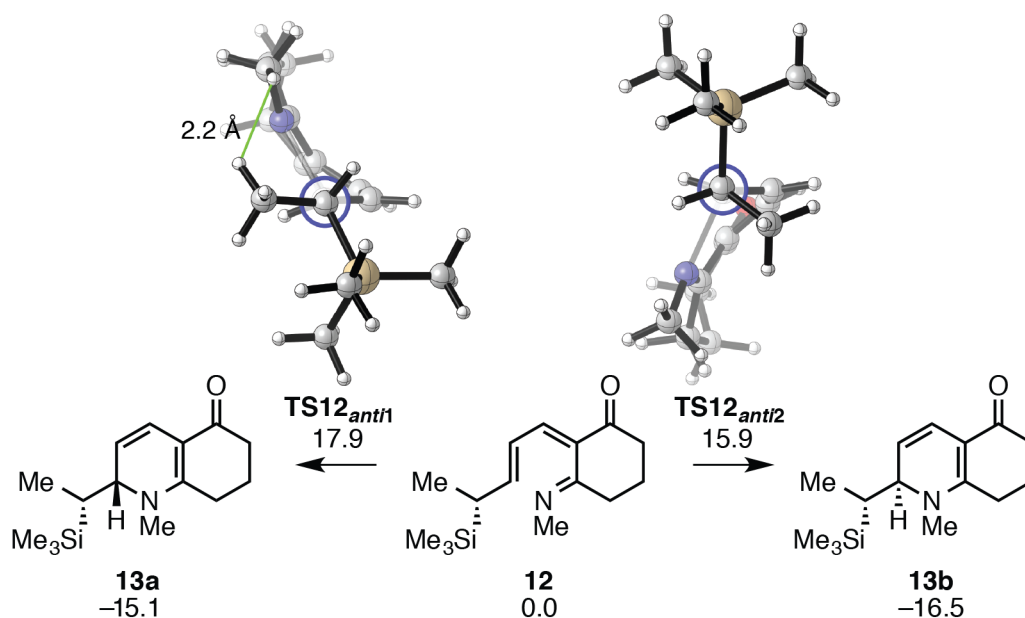


Figure 6. M06-2X/6-31+G(d,p)-optimized transition structures, ΔG^\ddagger , and ΔG_{rxn} for the electrocyclicization of **12**. Reported energies are in kcal mol⁻¹.

Just as is the case for the electrocyclicization of **5c**, the *anti* transition state conformers of the ring closure of **12** are lowest in energy. Hyperconjugative stabilization by interaction of the C–Si σ donor orbital with the antibonding σ orbital of the forming C–N bond is likely reinforced by the steric preference of the silyl group for the *anti* position. Computations of the electrocyclic reaction of **12** are consistent with the experimental stereoselectivity; the computed kinetic product **13b** ($\Delta\Delta G^\ddagger = 2.0$ kcal mol⁻¹) corresponds (in terms of relative stereochemistry) to dihydropyridine **11a**.³¹ The kinetic diastereoselectivity of the azaelectrocyclization of **12** is also

controlled by a steric effect. In **TS12**_{anti1}, which leads to the minor product, the methyl substituent at the α position must adopt the *outside* position in order for the TMS group to occupy the *anti* position. In doing so, this methyl group clashes with the *N*-substituent. This clash is avoided in the favored transition structure **TS12**_{anti2} as the methyl and TMS groups are able to simultaneously occupy the less sterically demanding inside and *anti* positions, respectively.

The equilibration of the two diastereomeric electrocyclization products **13a** and **13b** is observed experimentally, although the major product is still **13b**. The computed $t_{1/2}$ at 130 °C for the ring opening (retroelectrocyclization) of either electrocyclization product is approximately 420 hr, too large a value considering experimental equilibration of the diastereomeric products of electrocyclization occurs within 24 hrs.³⁸ The bulky TBDPS group employed experimentally likely accelerates equilibration by destabilizing the products of the electrocyclic ring closure. In any case, the relative energy differences between two the dihydropyridine products indicate that the thermodynamic product is also the kinetic product **13a**.

CONCLUSIONS

Transition state *gauche* effects explain the observed stereoselectivities of the electrocyclizations of chiral 1-azatrienes bearing α -alkoxy substituents. Computational experiments predict that an allylic fluorine substituent at the allylic position reproduces the experimentally observed stereoselectivity, while a silyl group at the same position changes the preferred transition state conformation and reverses the stereochemical course of the ring closure. The electrocyclization of TBPDS-substituted azatriene **12** confirms this predicted reversal of selectivity. Studies of the generality of the stereochemical influence of α -silyl groups and the synthetic utility of the ring closures of α -silyl azatrienes have been reported separately.³⁸

COMPUTATIONAL METHODS

The DFT computations were performed using *Gaussian09*.³⁹ The M06-2X⁴⁰/6-31+G(d,p) model chemistry was used to optimize the geometries of stationary points and to compute the vibrational frequencies. M06-2X has been demonstrated to reliably reproduce the thermodynamics of π to σ transformations with reasonable accuracy⁴¹ in addition to the kinetics of main group chemistry.⁴² All computations were performed in the gas phase. Normal mode analysis confirmed that the optimized structures of reactants and products were minima (zero imaginary frequencies) and that all optimized transition structures corresponded to first-order saddle points (one imaginary frequency). Thermal corrections were calculated from unscaled M06-2X/6-31+G(d,p) frequencies using the standard state conditions of 1 atm and 298.15 K. Errors in the calculation of vibrational entropy contributions to the free energies by the treatment of low modes as harmonic vibrations was mitigated by raising the frequencies of vibrational modes less than 100 cm^{-1} to exactly 100 cm^{-1} as suggested by Truhlar.^{43,44} Electronic energies were recomputed at the M06-2X/def2-QZVPP^{45,46} level of theory. Reported Gibbs free energies were determined using these electronic energies and thermal corrections determined at the M06-2X/6-31+G(d,p) level. The *Avogadro*^{47,48} and *Gaussview*⁴⁹ software packages were used to build and visualize molecules; the images used in this article were prepared with *CYLVIEW*.⁵⁰ All energies reported are Gibbs free energies in kcal mol^{-1} .

AUTHOR CONTRIBUTIONS

Z-X.M. performed the experiments; Z-X.M. and R.P.H. analyzed the experimental work. A.P. and J.R.V. performed the computations reported herein. A.P and K.N.H. interpreted the computational work. All authors contributed to the writing of this manuscript.

ACKNOWLEDGMENTS

We acknowledge the financial support of the NIH (GM-36700 and CHE-1351104 to K.N.H.) A.P. thanks the Chemical-Biology Interface Training Program for its support (T32 GM 008496). A.P and J.V acknowledge the University of California, Los Angeles and the Amgen Scholars Program, respectively, for financial support. The following computational resources were used in this study: the Hoffman2 cluster at UCLA (IDRE) and the Extreme Science and Engineering Discovery Environment (XSEDE)'s Trestles and Gordon supercomputers (OCI-1053575) at the San Diego Supercomputing Center.

REFERENCES

- (1) Sydorenko, N.; Hsung, R. P.; Vera, E. L. *Org. Lett.* **2006**, *8*, 2611.
- (2) Gilchrist, T. L.; Healy, M. A. M. *Tetrahedron* **1993**, *49*, 2543.
- (3) Maynard, D. F.; Okamura, W. H. *J. Am. Chem. Soc.* **1995**, *60*, 1763.
- (4) Smith, D. A.; Ulmer, C. W., II. *J. Org. Chem.* **1991**, *56*, 4444.
- (5) Beccalli, E. M.; Clerici, F.; Gelmi, M. L. *Tetrahedron* **2000**, *56*, 4817–4821.
- (6) Palacios, F.; Gil, M. J.; de Marigorta, E. M.; Rodríguez, M. *Tetrahedron* **2000**, *56*, 6319.
- (7) Tanaka, K.; Katsumura, S. *J. Synth. Org. Chem. Jpn.* **2005**, *63*, 696.
- (8) Vincze, Z.; Mucsi, Z.; Scheiber, P.; Nemes, P. *Eur. J. Org. Chem.* **2008**, *2008*, 1092.
- (9) Liu, S.; Liebeskind, L. S. *J. Am. Chem. Soc.* **2008**, *130*, 6918.
- (10) Nakamura, I.; Zhang, D.; Terada, M. *J. Am. Chem. Soc.* **2010**, *132*, 7884.
- (11) Nakamura, I.; Zhang, D.; Terada, M. *J. Am. Chem. Soc.* **2011**, *133*, 6862.
- (12) Vincze, Z.; Nemes, P. *Tetrahedron* **2013**, *69*, 6269.
- (13) For a review on aza-electrocyclizations: Okamura, W. H.; de Lera, A. R. In *Comprehensive Organic Synthesis*; Trost, B. M., Fleming, I., Eds.; Paquette, L. A., Vol. Ed.; Pergamon Press: New York, 1991; Vol. 5, pp 699-750.
- (14) Sklenicka, H. M.; Hsung, R. P.; Wei, L.-L.; McLaughlin, M. J.; Gerasyuto, A. I.; Degen, S. *J. Org. Lett.* **2000**, *2*, 1161.
- (15) Tanaka, K.; Mori, H.; Yamamoto, M.; Katsumura, S. *J. Org. Chem.* **2001**, *66*, 3099.
- (16) Tanaka, K.; Katsumura, S. *J. Am. Chem. Soc.* **2002**, *124*, 9660.
- (17) Buchanan, G. S.; Dai, H.; Hsung, R. P.; Gerasyuto, A. I.; Scheinebeck, C. M. *Org. Lett.* **2011**, *13*, 4402.
- (18) Thompson, S.; Coyne, A. G.; Knipe, P. C.; Smith, M. D. *Chem. Soc. Rev.* **2011**, *40*, 4217.

- (19) Sklenicka, H. M.; Hsung, R. P.; McLaughlin, M. J.; Wei, L. I.; Gerasyuto, A. I.; Brennessel, W. B. *J. Am. Chem. Soc.* **2002**, *124*, 10435.
- (20) Tanaka, K.; Kobayashi, T.; Mori, H.; Katsumura, S. *J. Org. Chem.* **2004**, *69*, 5906.
- (21) Liu, X.; Zhang, N.; Yang, J.; Liang, Y.; Zhang, R.; Dong, D. *J. Org. Chem.* **2013**, *78*, 3323.
- (22) Tanaka, K.; Yokoi, S.; Morimoto, K.; Iwata, T.; Nakamoto, Y.; Nakayama, K.; Koyama, K.; Fujiwara, T.; Fukase, K. *Biorg. Med. Chem.* **2012**, *20*, 1865.
- (23) Tanaka, K.; Fukase, K.; Katsumura, S. *Chem. Rec.* **2010**, *10*, 119.
- (24) Walker, M. J.; Hietbrink, B. N.; Thomas, B. E.; Nakamura, K.; Kallel, E. A.; Houk, K. N. *J. Org. Chem.* **2001**, *66*, 6669.
- (25) Houk, K. N.; Moses, S. R.; Wu, Y. D.; Rondan, N. G.; Jager, V.; Schohe, R.; Fronczek, F. R. *J. Am. Chem. Soc.* **1984**, *106*, 3880.
- (26) Wiberg, K. B.; Murcko, M. A.; Laidig, K. E.; MacDougall, P. J. *J. Phys. Chem.* **1990**, *94*, 6956.
- (27) Goodman, L.; Gu, H. B.; Pophristic, V. *J. Phys. Chem. A.* **2005**, *109*, 1223.
- (29) Houk, K. N.; Duh, H. Y.; Wu, Y. D.; Moses, S. R. *J. Am. Chem. Soc.* **1986**, *106*, 2754.
- (29) Raimondi, L.; Wu, Y. D.; Brown, F. K.; Houk, K. N. *Tetrahedron Lett.* **1992**, *33*, 4409.
- (30) Haller, J.; Strassner, T.; Houk, K. N. *J. Am. Chem. Soc.* **1997**, *62*, 8031.
- (31) Haller, J.; Niwayama, S.; How-Yunn Duh, A.; Houk, K. N. *J. Org. Chem.* **1997**, *62*, 5728
- (32) Annunziata, R.; Benaglia, M.; Cinquini, M.; Cozzi, F.; Raimondi, L. *Eur. J. Org. Chem.* **1998**, *1998*, 1823.
- (33) Lambert, J. B.; Zhao, Y.; Emblidge, R. W.; Salvador, L. A.; Liu, X. Y.; So, J. H.; Chelius, E. C. *Acc. Chem. Res.* **1999**, *32*, 183.

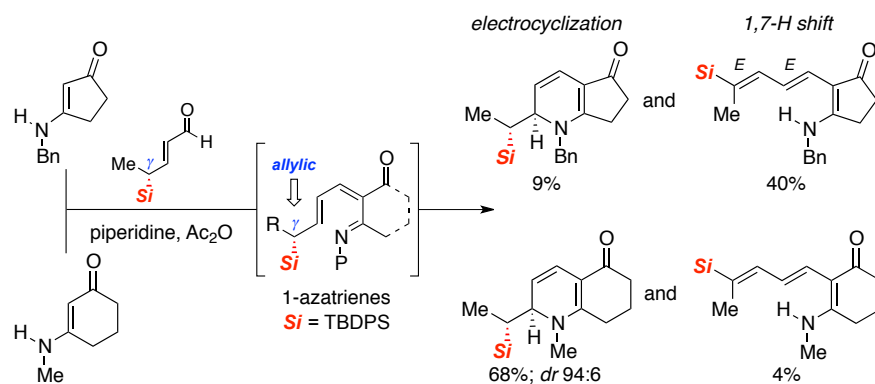
- (34) Cieplak, A. S. *J. Am. Chem. Soc.* **1981**, *103*, 4540.
- (35) Cieplak, A. S.; Tait, B. D.; Johnson, C. R. *J. Am. Chem. Soc.* **1989**, *111*, 8447.
- (36) Wu, Y. D.; Houk, K. N. *J. Am. Chem. Soc.* **1987**, *109*, 908.
- (37) Houk, K. N. *Chem. Rev.* **1976**, *76*, 1.
- (38) Ma, Z.-X.; Patel, A.; Houk, K. N.; Hsung, R. P. *Org. Lett.* **2015**, *17*, 2138.
- (39) Frisch, M. J.; Trucks, G. W.; Schlegel, H. B.; Scuseria, G. E.; Robb, M. A.; Cheeseman, J. R.; Scalmani, G.; Barone, V.; Mennucci, B.; Petersson, G. A.; Nakatsuji, H.; Caricato, M.; Li, X.; Hratchian, H. P.; Izmaylov, A. F.; Bloino, J.; Zheng, G.; Sonnenberg, J. L.; Hada, M.; Ehara, M.; Toyota, K.; Fukuda, R.; Hasegawa, J.; Ishida, M.; Nakajima, T.; Honda, Y.; Kitao, O.; Nakai, H.; Vreven, T.; J A Montgomery, J.; Peralta, J. E.; Ogliaro, F.; Bearpark, M.; Heyd, J. J.; Brothers, E.; Kudin, K. N.; Staroverov, V. N.; Kobayashi, R.; Normand, J.; Raghavachari, K.; Rendell, A.; Burant, J. C.; Iyengar, S. S.; Tomasi, J.; Cossi, M.; Rega, N.; Millam, J. M.; Klene, M.; Knox, J. E.; Cross, J. B.; Bakken, V.; Adamo, C.; Jaramillo, J.; Gomperts, R.; Stratmann, R. E.; Yazyev, O.; Austin, A. J.; Cammi, R.; Pomelli, C.; Ochterski, J. W.; Martin, R. L.; Morokuma, K.; Zakrzewski, V. G.; Voth, G. A.; Salvador, P.; Dannenberg, J. J.; Dapprich, S.; Daniels, A. D.; Farka, Ö.; Foresman, J. B.; Ortiz, J. V.; Cioslowski, J. Gaussian 09, Revision D.01.
- (40) Zhao, Y.; Truhlar, D. G. *Theor. Chem. Acc.* **2008**, *120*, 215.
- (41) Pieniazek, S. N.; Clemente, F. R.; Houk, K. N. *Angew. Chem. Int. Ed.* **2008**, *120*, 7860.
- (42) Zhao, Y.; Truhlar, D. G. *Acc. Chem. Res.* **2008**, *41*, 157.
- (43) Zhao, Y.; Truhlar, D. G. *Phys. Chem. Chem. Phys.* **2008**, *10*, 2813.
- (44) Ribeiro, R. F. R.; Marenich, A. V. A.; Cramer, C. J. C.; Truhlar, D. G. *J. Phys. Chem. B* **2011**, *115*, 14556.

- (45) Weigend, F.; Ahlrichs, R. *Phys. Chem. Chem. Phys.* **2005**, *7*, 3297.
- (46) Weigend, F. *Phys. Chem. Chem. Phys.* **2006**, *8*, 1057.
- (47) Hanwell, M. D.; Curtis, D. E.; Lonie, D. C.; Vandermeersch, T.; Zurek, E.; Hutchison, G. *R. J Cheminform.* **2012**, *4*, 17.
- (48) Avogadro: an open-source molecular builder and visualization tool, version 1.1.1;
<http://avogadro.openmolecules.net/>.
- (49) GaussView, Version 5, Dennington, Roy; Keith, Todd; Millam, John. Semichem Inc., Shawnee Mission, KS, 2009.
- (50) CYLview, 1.0b; Legault, C. Y., Université de Sherbrooke, **2009**
(<http://www.cylview.org>).

Chapter 8

Highly Torquoselective Electrocyclizations and Competing 1,7-Hydrogen Shifts of 1-Azatrienes with Silyl-Substitution at the Allylic Carbon.

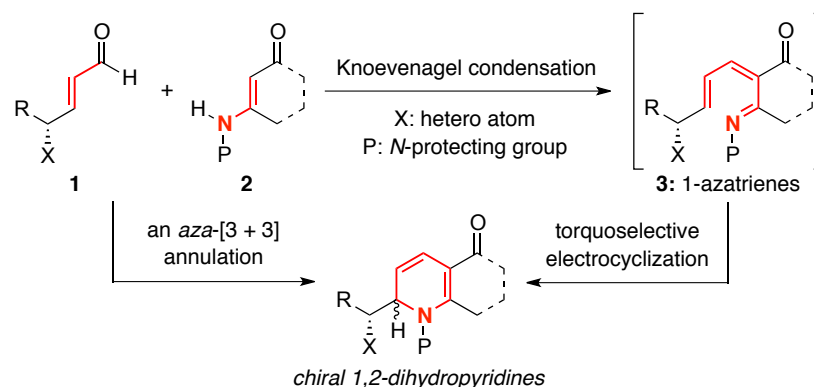
Ma, Z.-X.; Patel, A.; Houk, K. N.; Hsung, R. P. *Org Lett.* **2015**, *17*, 2138–2141.



ABSTRACT

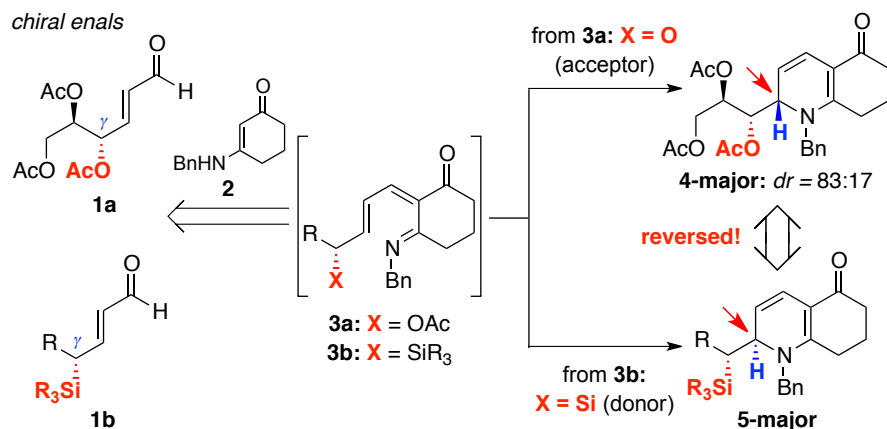
The highly torquoselective electrocyclizations of chiral 1-azatrienes are described. These 1-azatrienes contain an allylic stereocenter that is substituted with a silyl group, and are derived *in situ* from condensation of γ -silyl-substituted enals with vinylogous amides. The ensuing stereoselective ring-closures are part of a tandem sequence that constitutes an aza-[3 + 3] annulation method for constructing 1,2-dihydropyridines. Several mechanisms for the formal 1,7-hydrogen shift of these 1-azatrienes were evaluated computationally.

INTRODUCTION



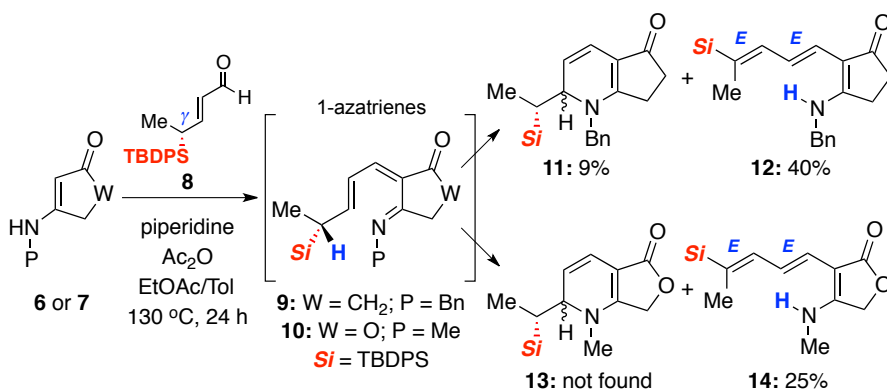
Scheme 8.1. Torquoselective electrocyclizations of 1-azatrienes in aza-[3 + 3] annulations.

Electrocyclizations represent an important pericyclic process in organic synthesis. Our aza-[3 + 3] annulation¹⁻³ methodology involving chiral enals **1** and vinylogous amides **2** is a powerful strategy for total syntheses of alkaloids⁴ and a unique platform for studying the torquoselectivity of electrocyclizations of 1-azatrienes **3**⁵ (Scheme 8.1). Despite its significance in constructing chiral 1,2-dihydropyridines, efforts to develop and understand torquoselective ring-closures of 1-azatrienes such as **3** have lagged behind with the exceptions of Tanaka and Katsumura's elegant work.⁶ Although we have developed highly torquoselective electrocyclizations of a chiral auxiliary substituted 1-azatrienes,⁷ a more general and practical approach employing chiral enals has yielded diastereoselectivity of 83:17 at best (see aza-electrocyclization of **3a** in Scheme 8.2).^{8,9} Recently, our collaborative efforts to understand the origins of the stereoselectivities of a number of pericyclic reactions¹⁰ have led us to model these stereoselective ring closures computationally. A complete stereochemical model for these electrocyclic reactions is still being developed. In the course of our studies, we predicted that the stereochemical outcomes of these electrocyclizations depend on the electronic nature of the allylic substituent X. As shown in Scheme 8.2, if X is a σ donor such as SiR₃ instead of a σ acceptor such as OAc, a reversal of stereoselectivity is predicted (**4** versus **5**). We have now shown that such a reversal occurs and that the electrocyclizations of these silyl-substituted 1-azatrienes are highly torquoselective.



Scheme 8.2. A prediction of reversal of the torquoselectivity.

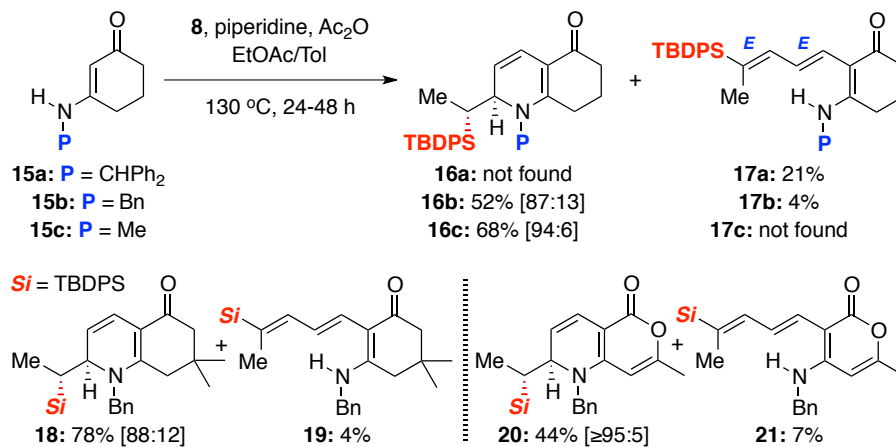
RESULTS AND DISCUSSION



Scheme 8.3. An unexpected competing 1,7-hydrogen shift.

We commenced our investigation by examining aza-[3+3] annulations of vinylogous amides **6** and **7** with silyl-substituted enal **8**^{11,12}, and quickly found that the respective desired aza-annulation products **11/11'** and **13/13'** were minor products (Scheme 8.3). Major products in these reactions were vinyl silanes **12** and **14** from **6** and **7**, respectively. These isomeric vinyl silanes could be formed by a (formal) 1,7-H shift of 1-azatrienes **9** or **10**. Although the competition of a 1,7-H shift with the desired annulation pathway has been documented,¹³ the

isomerizations responsible for the formation of **12** and **14** have never been observed before. The E-configurations of vinyl silanes **12** and **14** were assigned using NOE experiments.



Scheme 8.4. Aza-[3+3] annulations using 6-membered vinylogous amides as annulation partners.

Annulations using 6-membered ring vinylogous amides were more successful. As shown in Scheme 8.4, although the reaction of vinylogous amide **15a** still yielded the 1,7-H shift product (**16a**) as the major product, respective 1-azatrienes from 6-membered ring vinylogous amides **15b** and **15c** predominantly underwent ring-closure in high yields and diastereoselectivity. This is also true in cases of electrocyclizations that led to **18** and **20** with the respective vinyl silanes byproducts **19** and **21** being isolated only in small amounts.

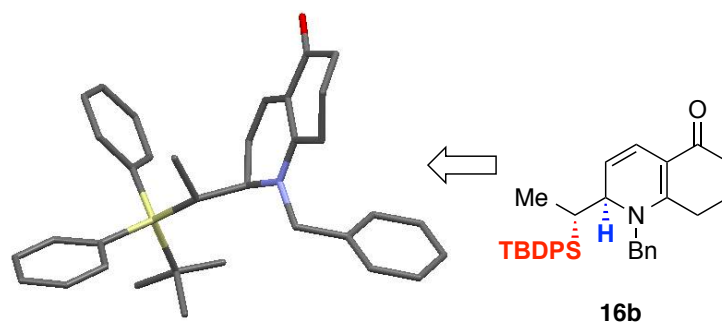


Figure 8.1. X-Ray Structure of 1,2-Dihydropyridine **16b**.

Using the single crystal X-ray structure of **16b**, we were able to unambiguously assigned the stereochemistry of **16b** and confirm the prediction of a complete reversal of selectivity for electrocyclizations of these silyl-substituted 1-azatrienes. The attempted aza-annulations of 1-azatrienes bearing large N-substituent (such as the N-CHPh₂ group of **15a**) would still yield products of 1,7-H shift. This is presumably due to enhanced steric repulsion between the larger N-substituent and the TBDPS group at the electrocyclization transition state. It is noteworthy that in direct contrast, aza-annulations of **15a** with non-silylated chiral enals were feasible and most diastereoselective as demonstrated by **22**.^{8a}

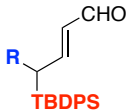
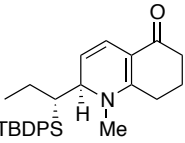
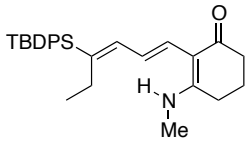
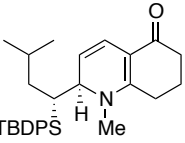
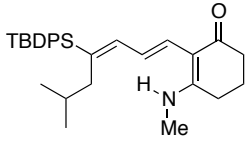
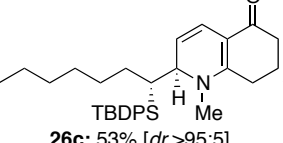
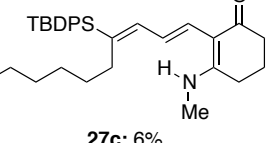
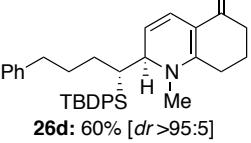
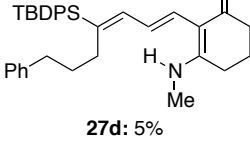
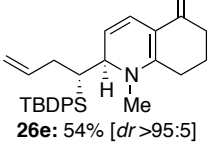
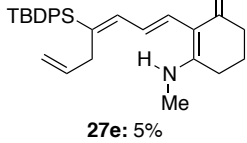
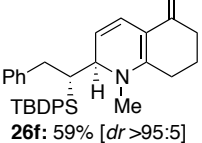
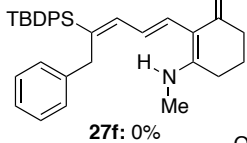
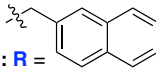
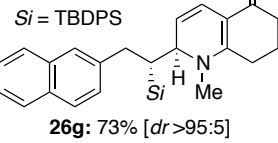
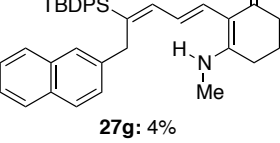
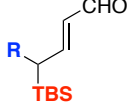
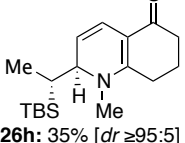
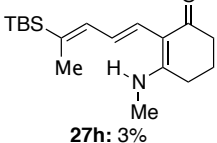
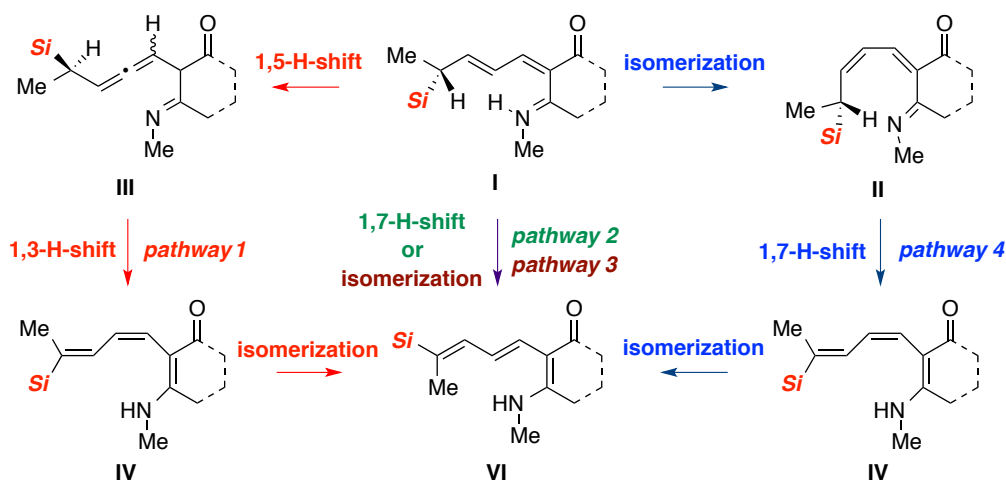
entry	chiral enals	electrocyclization products	1,7-H shift products
1	 25a: R = Et	 26a: 55% [dr 92:8]^{a,b}	 27a: 7%
2	25b: R = <i>i</i>-Bu	 286: 53% [dr >95:5]	 27b: 3%
3	25c: R = <i>n</i>-hex	 26c: 53% [dr >95:5]	 27c: 6%
4	25d: R = Ph(CH₂)₃	 26d: 60% [dr >95:5]	 27d: 5%
5	25e: R = allyl	 26e: 54% [dr >95:5]	 27e: 5%
6	25f: R = Bn	 26f: 59% [dr >95:5]	 27f: 0%
7	 25g: R =	 26g: 73% [dr >95:5]	 27g: 4%
8	 25h: R = Me	 26h: 35% [dr ≥95:5]	 27h: 3%

Table 8.1. A highly torquoselective electrocyclization^{a,b}. All reactions were carried with vinylogous amide **16c** using piperidine and Ac₂O, and reactions were heated at 130 °C for 24 h.
^bAll are isolated yields and dr ratios are determined using ¹H and/or ¹³C NMR.

Table 1.1 illustrates the generality of this stereoselective aza annulation; an array of different silyl-substituted enals **25a-h**, including one substituted with a TBS group, were successfully used as annulation partners. In all cases, the selectivity is very high while the competing 1,7-H shift is by and large mitigated. It is noteworthy that this is the first time a very high level of diastereoselectivity could be achieved in aza-[3 + 3] annulations using acyclic chiral enals.



Scheme 8.5. Potential Mechanism for the Competitive Isomerization

To better understand why 1-azatrienes annulated with 5-membered rings (**9** and **10**), undergo competitive formal 1,7-hydrogen shifts rather than the desired aza-electrocyclizations, we modeled the reaction of truncated 1-azatrienes **28** and **30** (see Figure 8.2) computationally.¹⁵ In Scheme 8.5, a summary of four possible mechanisms by which isomerization may occur is shown. All pathways assume the intermediacy of 1-azatriene **I**, and pathways 1, 2, and 4 feature key steps that are concerted in nature. Consequently, in addition to modeling the electrocyclizations of **28** and **30**, we have also modeled steps of these three pathways. The intermediacy of 1-azatriene **I** in pathway 3, which involves base-mediated proton transfer, has not been modeled; however, such a mechanism is a plausible alternative.

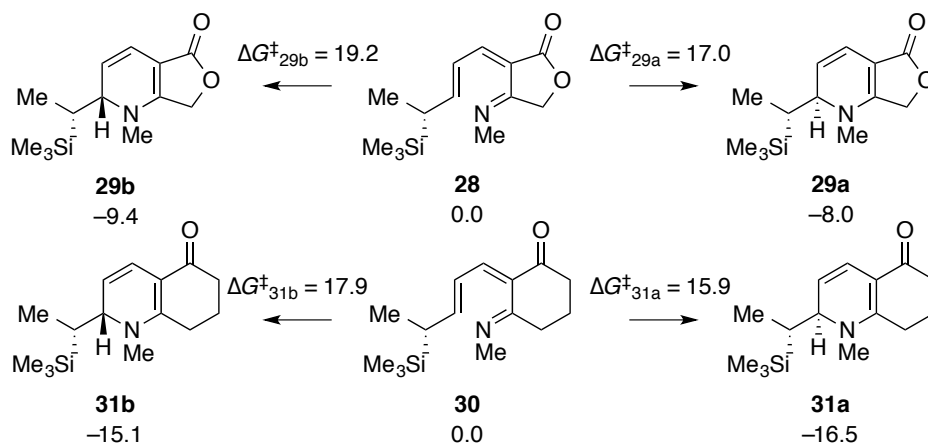


Figure 8.2. Energetics of the electrocyclic ring closures of model 1-azatrienes **28** and **30**. Energies are Gibbs free energies in kcal mol⁻¹ determined at the M062-X/def2-QZVPP//M06-2X/6-31+G(d,p) level.

The energetics of the electrocyclizations of 1-azatrienes **28** and **30** are shown in Figure 8.2. At 130 °C, the aza-electrocyclizations of **28** and **30** are facile reactions ($\Delta G^\ddagger < 20$ kcal mol⁻¹) that under kinetic control stereoselectively yield dihydropiperidines **29a** and **31a**, respectively. Electrocyclization of **30** is, according to theory, only slightly more facile than that of **28**; however, it is significantly more exergonic than the ring-closure of **28** (ca. 8 kcal mol⁻¹).¹⁶

Based on computations, pathways 1 and 2 involving a direct 1,7-hydrogen shift or 1,5-hydrogen shift of 1-azatriene **28**, respectively, are unlikely.¹⁷ These sigmatropic rearrangements feature ΔG^\ddagger of at least 30 kcal mol⁻¹. However, the free energy of activation for the 1,7-hydrogen shift involved in pathway 4 is 17 kcal mol⁻¹. Thus, pathway 4 is a plausible mechanism, so long as the required isomerizations (presumably promoted by base) are facile processes.

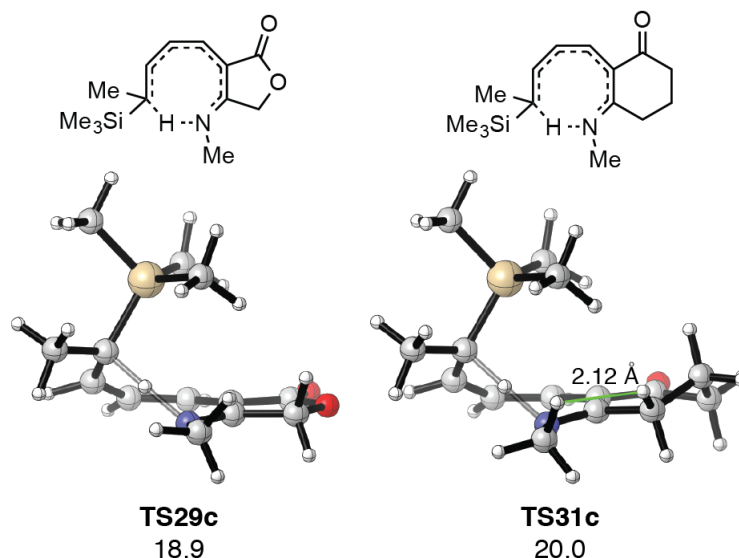


Figure 8.3. M06-2X/6-31+G(d,p) structures of lowest 1,7-hydrogen shift featured in pathway 4. Energies shown are M06-2X/def2-QZVPP//M06-2X/6-31+G(d,p).

Interestingly, the rate of 1,7-hydrogen shift is 100-fold slower ($\Delta\Delta G^\ddagger = 2.7 \text{ kcal mol}^{-1}$) than the ring closure of 1-azatriene **30**. However, for 1-azatriene **28**, these two processes are very similar in activation free energies (Figure 8.3). These difference in reactivity may be (partially) responsible for the distinct product outcomes observed for this pair of azatrienes.

The lowest energy transition structures of the 1,7-hydrogen shift of **II** derived from substrates **28** and **30** (**TS29c** and **TS31c**) are shown in Figure 8.2. **TS31c** is destabilized by $A^{1,3}$ strain between N-methyl substituent and annulated cyclohexanone (see green lines in Figure 8.3). This destabilizing interaction is less severe in **TS29c** featuring the γ -lactone because this moiety, unlike the corresponding cyclohexanone in **TS31c** is planar.

CONCLUSIONS

We have described here a highly torquoselective electrocyclization of a series of novel chiral 1-azatrienes. These 1-azatrienes contain an allylic stereocenter substituted with a silyl

group, and are generated in situ by condensing γ -silyl-substituted enals with vinylogous amides. Theoretical calculations have provided mechanistic insights into a previously unknown competing 1,7-hydrogen shift from the same 1-azatriene intermediate. Efforts to explore synthetic applications of this torquoselective electrocyclization are underway. Full details regarding the stereochemical model that rationalizes the observed torquoselectivities will be reported in due course.

COMPUTATIONAL METHODS

QM computations

All quantum mechanical computations were performed using *Gaussian09*.¹⁵ An ultrafine integration grid consisting of 590 radial shells each with 99 grid points per shell was used. Geometry optimizations and frequency calculations were performed using the M06-2X¹⁶ functional with the 6-31+G(d,p) double- ζ basis set. Normal mode analysis was used to confirm the nature of these stationary points as either minima or transition structures (first-order saddle points). Single point electronic energies were recomputed using the M06-2X/def2-QZVPP¹⁷ level of theory. Zero point energy and thermal corrections were determined using unscaled M06-2X/6-31+G(d,p) frequencies assuming a standard state of 1 atm and 298.15 K. Truhlar's quasiharmonic approximation was employed to mitigate errors in the estimation of molecular vibrational entropies due to the treatment of low frequency vibrational modes as harmonic oscillations.^{18,19} The Gibbs free energies were determined using electronic energies computed at the M06-2X/def2-QZVPP level and zero point energy and thermal corrections determined using M06-2X/6-31+G(d,p). Gaussview²⁰ and Avogadro^{21,22} were used to prepare structures for computational study herein. Images of stationary points were rendered using CYLView.²³

Conformational analysis

The conformers of **31a-c** were sampled using the following protocol. Conformers of these structures were initially sampled using mixed low-mode/ molecular mechanics Monte Carlo (LM/MMMC) simulations.^{24,25} These simulations were performed using Macromodel (V 10.6)²⁶ and Maestro software (V 10.0.013).²⁷ For all simulations, 8,000 Monte Carlo steps were performed; minimizations were performed using the Polak-Ribiere conjugate gradient (PRNG) minimization scheme¹⁴ (5000 cycles) with a gradient-based convergence criterion of 0.0012 kcal mol⁻¹ Å⁻¹ (0.005 kJ mol⁻¹ Å⁻¹). Conformers differing in maximum atomic deviation by at least 0.5 Å were considered unique. Unique structures with energies within 25 kcal mol⁻¹ of the global minimum were included in the conformer library. These structures were re-optimized using M06-2X/6-31+G(d,p). Subsequently, thermal corrections for these minima were determined using M06-2X/6-31+G(d,p) frequency calculations.

AUTHOR CONTRIBUTIONS

Z-X.M. and A.P. have contributed equally to this work. Z-X.M. performed the experiments; Z-X.M. and R.P.H. analyzed the experimental work. A.P. performed the computations reported herein. A.P and K.N.H. interpreted the computational work. All authors contributed to the writing of this manuscript.

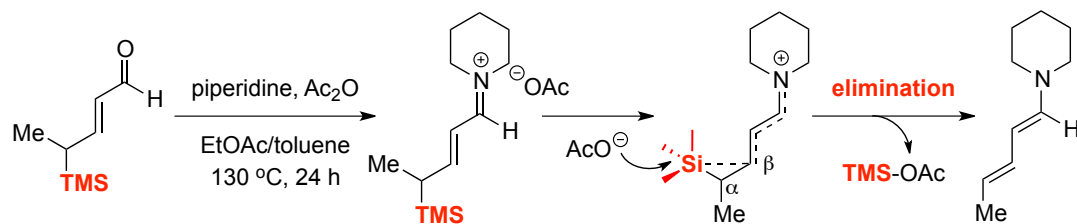
ACKNOWLEDGMENTS

Z-X.M. and A.P. have contributed equally to this work. We thank the NIH (GM-66055 to R.P.H) and NSF (CHE-1059084 and CHE-1361104 to K.N.H.). A.P. thanks the Chemistry-Biology Interface Training Program (NIH Grant T32 GM 008496) for its support and the University of California, Los Angeles (UCLA) for funding. UCLA's Beowulf cluster, Hoffman2, and the Extreme Science and Engineering Discovery Environment's (Grant TG CHE 040013N) Gordon and Trestles supercomputer at the San Diego Supercomputing Center were used to perform computations. We also thank Dr. Victor Young at University of Minnesota for X-ray structural analysis.

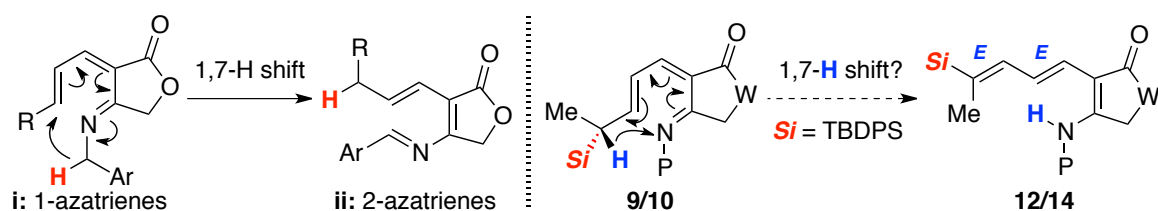
REFERENCES

- (1) For seminal reviews on hetero-[3 + 3] annulations, see: (a) Harrity, J. P. A.; Provoost, O. *Org. Biomol. Chem.* **2005**, *3*, 1349. (b) Hsung, R. P.; Kurdyumov, A. V.; Sydorenko, N. *Eur. J. Org. Chem.* **2005**, *1*, 23.
- (2) For a symposium-in-print devoted to aza-annulations, see: Harrity, J. P. A. *Tetrahedron* **2008**, *64*, Symposium-in-Print No. 133.
- (3) Also see: (a) Tang, Y.; Oppenheimer, J.; Song, Z.; You, L.; Zhang, X.; Hsung, R. P. *Tetrahedron* **2006**, *62*, 10785. (b) Laschat, S.; Dickner, T. *Synthesis* **2000**, *13*, 1781.
- (4) For reviews on applications of aza-[3 + 3] annulation in natural product synthesis, see: (a) Deng, J.; Wang, X.-N.; Hsung, R. P. *In Methods and Applications of Cycloaddition Reactions in Organic Syntheses*; Nishiwaki, N., Ed. Wiley-VCH: 2014; Chapter 12. (b) Buchanan, G. S.; Feltenberger, J. B.; Hsung, R. P. *Curr. Org. Chem.* **2010**, *7*, 363. (c) Gademann, K.; Lawrence, A. K. *Synthesis* **2008**, *2008*, 331. (d) Hsung, R. P.; Cole, K. P. *In Strategies and Tactics in Organic Synthesis*, Harmata, M., Ed.; Elsevier Science: Pergamon Press: Oxford, England, *2004*, *4*, 41.
- (5) For a seminal review, see: Okamura, W. H.; de Lera, A. R. *Comprehensive Organic Synthesis*; Trost, B. M., Fleming, I., Eds.; Paquette, L. A., Volume Ed.; Pergamon Press: New York, 1991; *5*, 699.
- (6) For recent elegant accounts on stereoselective ring-closure of 1-azatrienes, see: (a) Tanaka, K.; Katsumura, S. *J. Am. Chem. Soc.* **2002**, *124*, 9660. (b) Tanaka, K.; Mori, H.; Yamamoto, M.; Katsumura, S. *J. Org. Chem.* **2001**, *66*, 3099. (c) Tanaka, K.; Kobayashi, T.; Mori, H.; Katsumura S. *J. Org. Chem.* **2004**, *69*, 5906

- (7) (a) Sklenicka, H. M.; Hsung, R. P.; Wei, L.-L.; McLaughlin, M. J.; Gerasyuto, A. I.; Degen, S. J.; Mulder, J. A. *Org. Lett.* **2000**, *2*, 1161. (b) Sklenicka, H. M.; Hsung, R. P.; McLaughlin, M. J.; Wei, L.-L.; Gerasyuto, A. I.; Brennessel, W. W. *J. Am. Chem. Soc.* **2002**, *124*, 10435.
- (8) (a) Sydorenko, N.; Hsung, R. P.; Vera, E. L. *Org. Lett.* **2006**, *8*, 2611. (b) Ghosh, S. K.; Buchanan, G. S.; Long, Q. A.; Wei, Y.; Al-Rashid, Z. F.; Sklenicka, H. M.; Hsung, R. P. *Tetrahedron* **2008**, *63*, 883.
- (9) For the use of chiral cycloalkylidene aldehydes, see: McLaughlin, M. J.; Hsung, R. P.; Cole, K. C.; Hahn, J. M.; Wang, J. *Org. Lett.* **2002**, *4*, 2017.
- (10) (a) Wang, X.-N.; Krenske, E. H.; Johnston, R. C.; Houk, K. N.; Hsung, R. P. *J. Am. Chem. Soc.* **2014**, *136*, 9802. (b) Du, Y.; Krenske, E. H.; Antoline, J. E.; Lohse, A. G.; Houk, K. N.; Hsung, R. P. *J. Org. Chem.* **2013**, *78*, 1753. (c) Krenske, E. K.; He, S.-Z.; Huang, J.; Du, Y.; Houk, K. N.; Hsung, R. P. *J. Am. Chem. Soc.* **2013**, *135*, 5242. (d) Antoline, J. E.; Krenske, E. H.; Lohse, A. G.; Houk, K. N.; Hsung, R. P. *J. Am. Chem. Soc.* **2011**, *133*, 14443. (e) Krenske, E. H.; Houk, K. N.; Lohse, A. G.; Antoline, J. E.; Hsung, R. P. *Chem. Sci.* **2010**, *1*, 387. (f) Lohse, A. G.; Krenske, E. H.; Antoline, J. E.; Houk, K. N.; Hsung, R. P. *Org. Lett.* **2010**, *12*, 5506.
- (11) See Supporting Information.
- (12) We used TBDPS-substituted enals, because we failed in our initial attempts of using TMS-substituted enals. Peterson-like elimination of TMS group was observed instead of the desired ring closure. We attempted reactions of enals substituted with silyl groups of intermediate sizes (Ph₃Si and Ph₂MeSi). However, synthesis of these enals proved difficult.



(13) A 1,7-H shift of 1-azatriene **i** was also observed, giving 2-azatriene **ii**. This shift is quite distinct from the rearrangement of **9** to **12** or **10** to **14**. See: Sydorenko, N.; Hsung R. P.; Darwish, O. S.; Hahn, J. M.; Liu, J. J. *Org. Chem.* **2004**, *69*, 6732.



(14) Azatrienes **28** and **30** (see Figure 8.2) are truncated model substrates featuring a TMS substituent instead of the bulky TBDPS group.

(15) Gaussian 09, Revision D.01, Frisch, M. J.; Trucks, G. W.; Schlegel, H. B.; Scuseria, G. E.; Robb, M. A.; Cheeseman, J. R.; Scalmani, G.; Barone, V.; Mennucci, B.; Petersson, G. A.; Nakatsuji, H.; Caricato, M.; Li, X.; Hratchian, H. P.; Izmaylov, A. F.; Bloino, J.; Zheng, G.; Sonnenberg, J. L.; Hada, M.; Ehara, M.; Toyota, K.; Fukuda, R.; Hasegawa, J.; Ishida, M.; Nakajima, T.; Honda, Y.; Kitao, O.; Nakai, H.; Vreven, T.; Montgomery, J. A., Jr.; Peralta, J. E.; Ogliaro, F.; Bearpark, M.; Heyd, J. J.; Brothers, E.; Kudin, K. N.; Staroverov, V. N.; Kobayashi, R.; Normand, J.; Raghavachari, K.; Rendell, A.; Burant, J. C.; Iyengar, S. S.; Tomasi, J.; Cossi, M.; Rega, N.; Millam, M. J.; Klene, M.; Knox, J. E.; Cross, J. B.; Bakken, V.; Adamo, C.; Jaramillo, J.; Gomperts, R.; Stratmann, R. E.; Yazyev, O.; Austin, A. J.; Cammi, R.; Pomelli, C.; Ochterski, J. W.; Martin, R. L.; Morokuma, K.; Zakrzewski, V. G.; Voth, G. A.; Salvador, P.;

- Dannenberg, J. J.; Dapprich, S.; Daniels, A. D.; Farkas, Ö.; Foresman, J. B.; Ortiz, J. V.; Cioslowski, J.; Fox, D. J. Gaussian, Inc., Wallingford CT, 2009.
- (16) Zhao, Y.; Truhlar, D. G. *Theor. Chem. Account.* **2008**, *120*, 215.
- (17) Weigend, F.; Ahlrichs, R. *Phys. Chem. Chem. Phys.* **2005**, *7*, 3297.
- (18) Zhao, Y.; Truhlar, D. G. *Phys. Chem. Chem. Phys.* **2008**, *10*, 2813.
- (19) Ribeiro, R. F. R.; Marenich, A. V. A.; Cramer, C. J. C.; Truhlar, D. G. D. *J Phys Chem B* **2011**, *115*, 14556.
- (20) GaussView, Version 5, Dennington, R.; Keith, T.; Millam, J. Semichem Inc., Shawnee Mission KS, **2009**.
- (21) Hanwell, M. D.; Curtis, D. E.; Lonie, D. C.; Vandermeersch, T.; Zurek, E.; Hutchison, G. R. *J Cheminform.* **2012**, *4*, 17.
- (22) Avogadro: an open-source molecular builder and visualization tool. Version 1.0.1. <http://avogadro.openmolecules.net/>.
- (23) CYLview, 1.0b; Legault, C. Y., Université de Sherbrooke, **2009** (<http://www.cylview.org>).
- (24) Kolossvary, I.; Guida, W. C. *J. Am. Chem. Soc.* **1996**, *118*, 5011.
- (25) Kolossvary, I.; Guida, W. C. *J. Comput. Chem.* **1999**, *20*, 1671.
- (26) Schrödinger Release 2014-4: MacroModel, version 10.6, Schrödinger, LLC, New York, NY, **2014**.
- (27) Schrödinger Release 2014-4: Maestro, version 10.0.013, Schrödinger, LLC, New York, NY, **2014**.
- (28) Polak, E.; Ribiere, G. *Francaise Informat. Recherche Operationelle, Serie Rouge.* **1969**, *16*, 35.